Proton conducting polymer electrolytes for CO sensors

Submitted for the degree of
Doctor of Philosophy

April 2001

By

Yaser Abu-Lebdeh

BSc, MSc, GRSC, MCIC

University Of Southampton
Faculty Of Science
Department of Chemistry

UNIVERSITY OF SOUTHAMPTON
FACULTY OF SCIENCE
DEPARTMENT OF CHEMISTRY
DOCTOR OF PHILOSOPHY

PROTON CONDUCTING POLYMER ELECTROLYTES FOR CO SENSORS

Yaser Abu-lebdeh

ABSTRACT

Commercially available CO sensors suffer from many drawbacks most important of all is the dependence of their performance on changes in humidity. The objective of this work is to develop a non-aqueous proton conducting polymer to overcome such a problem.

A novel ionic liquid consisted of a mixture of imidazole and imidazolium bis-(triflouromethanesulphonyl imide) solids, IMI. The liquid was introduced into poly(vinyledenefluoride), PVdF, Poly(vinyledenefluoride-co-hexafluoropropylene), PVdF-HFP, poly(epichlorohydrin-co-ethyleneoxide), PEE and a blend of poly(methylmethacrylate), PMMA and PVdF-HFP polymeric hosts in order to obtain homogeneous films. Compatibility of the polymer hosts with IMI was first addressed. PEE and the (PMMA/PVdF-HFP) blend gave homogenous films whereas IMI mixtures with PVdF or PVdF-HFP were phase segregated. The latter became homogenous upon addition of propylene carbonate, PC. Conductivity of the films were studied as a function of IMI content, where a linear behaviour was observed between the logarithm of the conductivity versus the IMI content. A percolation threshold was proposed to explain the observed break point in the conductivity dependence of the PVdF-HFP:IMI films. XRD, TGA and DSC were used to characterise the films.

A planar amperometric CO sensor was fabricated using a IMI:PC:PVdF-HFP film. The sensor showed no response without being pre-equilibrated with water. The sensor response and t_{90} were found to be dependent on the CO concentration and relative humidity. Cyclic Voltammograms were performed on a Pt electrode in a IMI:PC solution. It was concluded that water was very crucial for the CO oxidation.

A new gap electrode method was developed to measure the conductivity of the films. The results showed that uncontrollable variations in either the polymer conductivity or the geometry or both have made it difficult to fit the systematic variation to the theoretical model. Nevertheless, acceptable conductivity values were obtained for the polymers by a combined normalization/iteration method. The technique should therefore be generally applicable given better control of polymer uniformity and thickness.

Table of contents

Chapter four

Chapter five

Chapter six

Acknowledgements

My sincere thanks are due to Dr John Owen for his considerable help during the preparation of this thesis and throughout the project. I thank him for his patience especially at the times where my alarm o'clock had failed to set off in the morning.

I would like also to thank the present and past members of the solid state electrochemistry group for making my time enjoyable. Special thanks to Thierry, Girts, Emmanuelle, Phil, the Australian Skunk, for proof reading the thesis. Ashraf and Mmdouh for their encouregment.

I would like to thank City Technology Ltd for the financial support and the British government for the Overseas Research Scheme Award.

Yaser Abu-Lebdeh

بسم الله الرحمن الرحيم

أهدي هذه الرساله الى .....

روح الوالد رحمه الله
أمي الحنونه
أخواني و أخواتي.

و... الى وطني الجريح .

To the memory of my father, to my mother, to the rest of my family

and to my homeland, Palestine.

List of abbreviations

a^*	The molecular diameter
AC	Alternating current
b	The length of an electrode in the gap cell
C	Capacitance
c_i	The molar concentration of *i* ions
D	Diffusion coefficient
DC	Direct current
DSC	Differential Scanning Calorimetry
E	Potential
g	A geometric factor
G	Conductance
I	Current
K	Cell constant
K_{sim}	Simulated cell constant

L	Polymer film thickness
M	Geometrical modulus
P(v)	The probability of observing the free volume
q_i	The charge of one mole of *i* ions.
R	Resistance
R	The gas constant
t_{90}	The response time for 90% of a sensor signal.
T_s	Reference temperature.
T_g	Glass transition temperature.
TGA	Thermogravimetric analysis
u	The thermal velocity of a molecule
u_i	The electrical mobility of the ions under the applied electric field.
v_f	The average free volume per molecule
V_M	The molar volume
w	The width of a gap in the gap cell

XRD	X-ray diffraction
Y	Admittance
Y'	Real part of admittance
Y''	Imaginary part of admittance
Z	Impedance
Z'	Real part of impedance
Z''	Imaginary part of impedance
γ	Lagrange parameter
α	The thermal expansion coefficient of the free volume
σ	Conductivity

List of chemical abbreviations

APEO	Amorphous poly(ethylene oxide)
BL	γ-butyrolactone
CO	Carbon monoxide gas
DMF	Dimethylformamide
EC	Ethylenecarbonate
EMIBF4	1-ethyl-3-methyl imidazolium tetrafluoroborate
IMI	a 1:1 molar ratio ionic liquid of imidazole and imidazolium (bistrifluoromethane sulphonyl)imide.
LiPUS	Lithium poly(ureasulphonyl imide)
NAFION ®	A perfluoropolyelectrolyte with the following structure $(C_2F_4)x(C_2F_3)y\text{-}(OCF_3F_6)OC_2F_4SO_3H$
PC	Propylenecarbonate
PDMSO	Poly(dimethylsiloxane)
PEE	Poly(epichlorohydrin-co-ethylene oxide)
PEG_{400}	Poly(ethylene glycole)
PEI	Poly(ethylene imine)
PEO	Poly(ethylene oxide)
PEU	Poly(ether urethane)
Poly(HEMA)	Pol(hexaethylmethyacrylate)

PPO	Poly(propylene oxide)
PTFE	Poly(tetrafluoroethylene)
PVC	Poly(vinyl chloride)
PVdF	Poly(vinyledenefluouride)
PVdF-HFP	Poly(vinyledenefluouride-co-hexafluoropropylene)
THF	Tetrahydrofuran

Chapter One

Introduction

General introduction

Polymers have always been thought of as insulators. It was not until 1978 that this view was changed by two new developments one of which was the fortuitous discovery that poly(acetylene) can be made into an electrical conductor by doping with iodine.[1,2] The other was the realization by Armand of the potential applications of polymer-salt complexes.[3-6] This had opened a new area of research and development.

There are two types of conducting polymers: electronically conducting and ionically conducting polymers, or what is to be known later as polymer electrolytes. The first type consists of a chemically or electrochemically treated polymer having conjugated double bonds that allow for the movement of electrons along the polymer chain. The main use of this type is as an electrode material for light emitting diodes and sensors.[7] Examples are poly(acetylene), poly(pyrrole) and poly(thiophene). The second consists of salt dissolved in a polymer with a solvating group, this type will be discussed in depth in the following section.

Power sources for electronic devices like mobile phones, portable computers, and electric vehicles have created a huge demand for solid state electrolyte materials with high performances for batteries, supercapacitors and other energy storage

devices. The state-of-the-art development in this area of research is to produce all-solid-state devices, where the anode, electrolyte and the cathode are solids. Such devices are commercially available or still under high-level R&D, *e.g.*, all-plastic devices.[8]

CO sensors based on Polymer electrolytes offer a good alternative to the traditional acid electrolyte-based sensors. They eliminate the difficulties in handling the acid and its evaporation, both of which reduce the lifetime of the sensor. The polymer electrolyte, on the other hand, is easy to fabricate and reduces the size of the sensor.

For a polymer electrolyte to be used in a CO sensor it should have the following properties:

1 High proton conductivity.
2 High permeability to the reactant and product gases in cases where they are required to diffuse through the electrolyte.
3 Independence of permeability and conductivity with water content.
4 Chemical inertness.

1.1 Ionically conducting Polymers

1.1.1 Polymer electrolytes

Polymers with high ionic conductivity such as ion exchangers have been known for some time. The evaporation of solvents at high temperatures and the consequent decrease in the conductivity have been a major drawback in their application and therefore alternatives have been sought.

Solvent-free electrolyes were first reported by P. Wright in 1973,[9,10] when introduced alkali-metal salt into poly(ether) polymers like poly(ethylene oxide), PEO, and poly(propylene oxide), PPO. Five years later M. Armand realised their

potential application in applied electrochemistry, mainly in lithium polymeric batteries.[3]

Pure PEO is a partially crystalline polymer with a appreciable amount of amorphous regions. When alkali metal salts are added, *e.g.*, $Li^+:X^-$ (where X^- can be perchlorate, triflate, .. *etc*) they dissolve in the amorphous region at low salt levels and form crystalline PEO:salt complexes. It is now generally believed that the conductivity occurs in the amorphous part of the structure where the metal ion co-ordinates with oxygen atoms from the PEO chains. The major part of the conduction process occurs in the elastomeric regions where the cation mobility is assisted by the movement of the chains to maintain the co-ordination number of Li^+ at a stable value of three or four. (*i.e.* number of oxygen atoms around the Li^+ ion).[11-14]

The conductivity of a polymer electrolyte can be enhanced by increasing the mobility of the polymer host. This has opened a new area of research, mainly focussing on modifying the polyether archeticture (*e.g.*, using comb branched polyphosphazene) or finding an alternative binding site in the chain like in the case of poly(ethylene imine), PEI, where nitrogen works in a similar way to oxygen.

1.1.2 Polymeric Gel Electrolytes based on the salt/solvent/polymer system

Because of the difficulty in obtaining polymer electrolytes with applicable room temperature conductivities with poly(ether)/salt systems, alternatives were sought. [15] One way to prepare polymer electrolytes with higher performances is to immobilise a liquid electrolyte, *i.e.*, salt/solvent, in a polar polymeric matrix. In the polymer-solvent-salt system, the main role of the polymer is to provide a host matrix for the liquid although the liquid sometimes plasticizes the polymer chains. [16-20] Examples are poly(vinylidenefluoride), PVdF, Poly(acrylonitrile), PAN and Poly(methyl methacrylate), PMMA. The polar solvent should have a high dielectric constant or high donor number to be able to dissociate the salt into free ions, and a low viscosity to form an easy conduction paths. Examples are shown in table 1.1[21]

Table 1.1: Physical properties for many solvents used in polymer gels

Solvent	Dielectric constant at 25 °C	Viscosity cP
DMF	36.7	0.80
PC	64.4	2.51
EC	89	1.90
BL	39.1	1.75
H_2O	78.5	1.00
PEG_{400}	5	3.00

Many polymer gel electrolytes were prepared using mainly lithium salts. By carefully choosing the polymer, the solvent and the ratio of the two to the lithium salt, *e.g.*, 9.13 % PAN: 84.87% PC: 6% $LiBF_4$ by weight, conductivity values approaching those of the liquids, ~ 1 mS/cm, were obtained. [22]

In spite of the good conductivities obtained with such polymer electrolytes, they still suffered from many drawbacks:

1 Subsequent evaporation of the solvent.
2 Poor mechanical properties at high levels of plasticization.
3 Reactivity of the polar solvent with lithium when used in a lithium battery.

1.1.3 Polymeric Gel Electrolytes based on the molten salt/polymer (ionic liquid/polymer) system

In cases where the salt itself is a liquid, *i.e.,* it is a room temperature molten salt or ionic liquid, no solvent is needed to form a homogeneous polymeric film with the

salt.[23] Herein the molten salt will be introduced as a plasticizer of the polymeric matrix and will conduct ions without necessarily coupling with the polymer chains.

Many salts were prepared for this purpose. Carlin *et al* [24,25] used an N,N'-alkyl imidazolium-based salts in which they incorporated in PVdF-HFP. The resultant gels could be made into films with room temperature conductivities reaching ~1 mS/cm. The conductivity was still one order of magnitude lower than that of the neat liquid. Watanabe *et al* [26] prepared an N-alkyl pyridinum molten salt and incorporated it in its polymeric analogue. The room temperature conductivity of the film with the highest content, which was still free-standing (90% salt content), was one order of magnitude lower than that of the neat liquid. Murray *et al* [27] also made a pyridinum molten salt and incorporated it into poly(dimethylsiloxane), PDMSO, as a host. They obtained similar room temperature conductivity values for both the polymer and the neat molten salt.

In another work, Watanabe *et al* [28] prepared a Li-based molten salt which they incorporated into PAN. The films obtained had room temperature conductivities one to two orders of magnitudes lower than that of the molten salt.

Angell [29] prepared LiI/$LiClO_4$ molten salt and its PPO polymer films. A one order of magnitude decrease in conductivity was observed between the neat liquid and the highest salt content, free standing rubbery film. In his work Angell tried to address the problem of the low conductivity of poly(ether)/LiX complexes. He argued that the conductivity was low due to the strong coupling between the polymer repeating units and the lithium cation where the escape time of the ions is slower than the chains segmental motion. To overcome the problem he introduced a new concept, which he called polymer-in-salt, where a polymer is added to a molten salt in small amounts to give films with ionic conductivity decoupled from the segmental motion of the polymeric chains. He also suggested that the molten salt should have low melting point. Based on that principle many polymer electrolytes were reported by Angell *et al*,[30] Frorsyth *et al*, [31] Watanbe *et al*, [32] and Ohno *et al*. [33]

The results of their studies are summarized in table (1.2):

Table (1.2) Summary of the highest conducting polymer-in-salt films.

polymer	salt	Salt/polymer ratio	Conductivity S/cm	Reference
LiPUS	$AlCl_3/LiAlCl_3$	20 % molar $AlCl_3$	10^{-3}	30
PAN	$LiCF_3SO_3$	75% w.t.	10^{-6}	31
Poly(HEMA)	$EMIBF_4$	50% molar ratio	10^{-3}	32
PEO ended with lithium sulphonyl amide	$LiClO_4$	50% molar ratio	10^{-4}	33

Carlin [25] has summarized the main advantages of ionic liquid electrolytes by:

1- High ionic conductivity.
2- Wide electrochemical windows.
3- Negligible volatility.
4- Non-flammability.
5- High thermal stability.
6- Sub-ambient temperature operation.

1.1.4 Polymeric proton conductors

Proton conducting polymer electrolytes have many potential applications in batteries, sensors, smart windows and fuel cells. NAFION, the most studied of all, showed high conductivity as a proton conductor reaching $2x10^{-2}$ S/cm at room temperature and exhibited good mechanical strength. [34] Those good properties have

been hampered by the later realisation of the dependence of its performance on the solvating state of its sulphonic groups.

As an alternative, anhydrous proton conducting polymer electrolytes were formed by mixing polymers bearing basic sites, e.g., polyimide,[35] polyimine[36] or polyether[37] with strong acids like H_3PO_4 or H_2SO_4. Lassegues reviewed the properties of those polymer systems,[38] (Table 1.3). In spite of the room temperature conductivities reaching $1x10^{-2}$ S/cm, they suffered from poor chemical and thermal stabilities. The former was due to the degradation of the polymeric host by the strong acid and the latter was due to the dehydration of the polymer films at higher temperatures. Nylon 6-10 has been used to overcome the former problem because of its resistance to strong acids,[39]

1.1.5 Proton conductors based on Imidazole

1.1.5.1 Introduction

Imidazole, a heterocyclic compound is a good example of a compound which has two nitrogen atoms which would conduct protons in a similar way as water by the Grotthus mechanism (see figure (1.1)).[46,47] This property of imidazole is advantageous in proton reactions in a way similar to water, phosphoric acid and sulphamide.[48] Imidazole, in this respect is a good candidate for supporting proton conductivity at ambient temperatures independent of the relative humidity.

Table1.3: Properties of some proton conducting polymer electrolytes based on strong acid/basic polymer. Where x is the molar ratio of the acid to the repeating unit of the polymer.[38]

Polymer	Tg /°C	Acid concentration		Ref
Weakly basic polymers, low pK				
Poly(ethylene oxide), PEO	-67	H_3PO_4	0<x<2	37
Poly(vinyl alcohol), PVA	58-85	H_3PO_4/H_2O	-	40
Intermediately basic polymers, moderate pK				
Poly(acrylimide), Paam	165-188	H_3PO_4 H_2SO_4	0.6<x<2 0.6<x<2	41,35
Poly(vinylpyrrolidone), PVP	175	H_3PO_4 H_2SO_4	0.5<x<8 1<x<3	42
Strongly basic polymers, high pK				
Poly(2-vinylpyridene), P_2VP	104	H_3PO_4 H_2SO_4	0.5<x<3 0.5<x<3	43
Poly(4-vinylpyridene), P_4VP	104	H_3PO_4	0.5<x<3	43
Linear Poly(ethyleneimine), LPEI	-23.5	H_3PO_4 H_2SO_4	0<x<1 0<x<1	26
Branched Poly(ethyleneimine), BPEI	-43	H_3PO_4 H_2SO_4 HCl	0<x<3 0<x<3 0<x<0.8	40
Poly(aminosilicates)aminosils	-53	$HClO_4$	0<x<0.3	44

Most research on proton conducting materials focuses on oxygen atom containing compounds, whereas the nitrogen atom is known to act in a similar way as a proton acceptor and its protonated form as a proton donor.[45]

The conductivity of pure imidazole was studied by Kawada *et al.* [49] and a moderate proton conductivity was found. They suggested Grotthuss mechanism, see next section, for the proton conductivity arising from the self-dissociation of imidazole. Casciola *et al* [50,51] intercalated imidazole and other heterocyclic compounds in α-zirconium hydrogen phosphate (α-$Zr(HPO_4)_2.H_2O$). The reported conductivities were relatively low, about $1.9x10^{-7}$ S/cm at 120 °C. The Grotthus mechanism was suggested for the proton conductivity of the intercalated compounds.

Kreuer *et al* [52] studied the conductivity of imidazole:sulphuric acid and imidazole:sulphanilic acid mixtures at 373 and 343K, respectively. They observed a maximum in the conductivity within the 50-100% molar percent of added imidazole region; the increase on adding imidazole was attributed to the formation of new proton defects such as the imidazolium ion, whereas the decrease was attributed to the geometric constrains applied by the addition of the acid. They also studied imidazole-incorporated sulphonated polyetherketone polymers in different concentrations. Conductivities of 10^{-4}-10^{-2} S/cm within the temperature range 25-200 °C were obtained. This conductivity increased with an increase of imidazole concentration. Their diffusion coefficient measurements supported a Grotthuss mechanism (see below). Recently *Meyer et al* [53] prepared poly(4-vinyl-imidazole), in which imidazole is bound to the polymer backbone suppressing any vehicular mechanism. However, the polymer showed low conductivity even at higher protonation levels. Ohns *et al* [54] prepared poly(2-vinyl-imidazole) then they neutralized the imidazolium ring with HBF_4. They obtained very low room temperature conductivities reaching $2x10^{-9}$ S/cm.

1.1.5.2 Grotthus mechanism

The high proton conductivity in water has been explained by the Grotthus. Agmon [55] reviewed the subject area. He argued that such a mechanism occurs on a microscopic scale and its exact nature is still controversial.

In essence, the mechanism involves proton hopping from a water molecule to its nearest neighbour, followed by the right reorientation to allow for the second proton-hopping step. The process involves H-bonds forming and breaking within and in the periphery of the conducting region. Figure (1.1) shows a suggested Grotthus mechanism in imidazole.

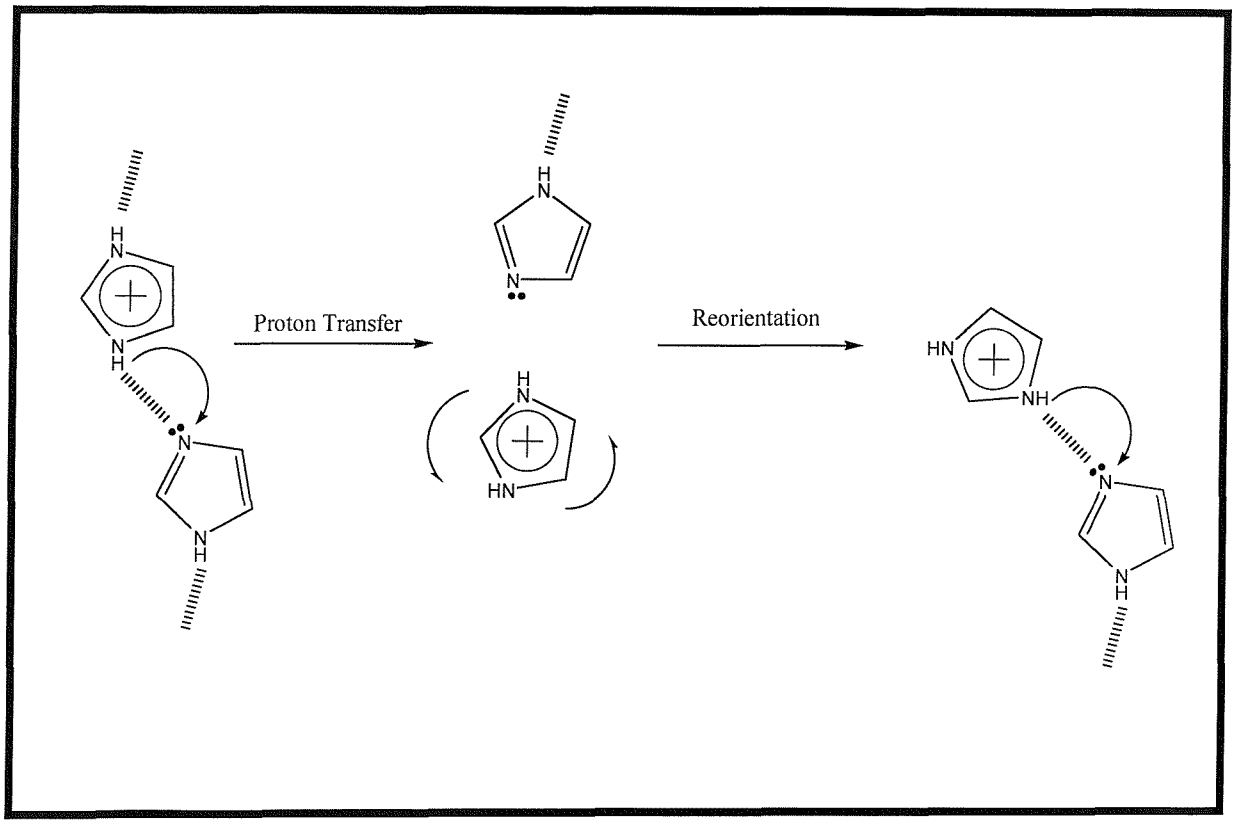

Figure (1.1) Possible Grotthus-type mechanism in imidazole

1.1.6 Polymer hosts used in this work

1.1.6.1 Poly(vinylidenefluoride), PVdF

Poly(vinyledenefluoride), PVdF, $(-CH_2CF_2-)_n$, is a highly crystalline polymer with a high dielectric constant (7.2). It contains both amorphous and crystalline regions.[56] The amorphous regions are able to trap large amount of liquid electrolytes and the crystalline regions provide good mechanical properties. It has a glass transition temperature of -40 °C. Because of its high dipole moment it was used as a polymer stiffener in many polymeric gel electrolytes especially for lithium salts in many solvents. Films with good conductivities were obtained depending on the composition.

The high crystallinity of PVdF can be reduced by copolymerizing vinyledene fluoride with a hexafluoropropylene monomer. The copolymer of the two, may be written, Poly(vinylidene fluoride-co-hexafluoropropylene, PVdF-HFP, or $(-CH_2CF_2-)_n(-CF_2CF(CF_3)-)_m$. This has the same bi-phasic structure as PVdF with lower crystallinity and a higher content of the amorphous phase. It has been tried for a Li^+ ion conducting polymer electrolyte and conductivities reaching 1 mS/cm were reported.[57]

1.1.6.2 Poly(epichlorohydrin-co-ethylene oxide), PEE

Poly(epichlorohydrin-co-ethylene oxide) is a copolymer of epichlorohdrin and ethylene oxide, $(-O-CH_2CH(CH_2Cl)-)_n(-O-CH_2CH_2-)_m$. The CH_2Cl side groups in the chain have the effect of reducing the crystallinity in the polymer in comparison to PEO. It is an elastomer with a glass transition temperature of –40 °C. Silva *et al* [58] made films using PEE and $LiClO_4$ without the need for a solvent. They obtained thermal and electrochemically stable films with room temperature conductivities *ca.* 10^{-5} S/cm at O/Li ratio of 6, where O/Li ratio is the molar ratio of the O atoms in the monomeric unit to the number of moles of lithium ions. De Paoli *et al* [59] also used

PEE for a lithium salt and obtained similar conductivities. Kohjiva *et al* [60] used the epichlorohydrin homopolymer with the lithium salt and they reported very low conductivities of $2x10^{-9}$ S/cm O/Li ratio of 33.

1.1.6.3 Polymer Blends

One of the main drawbacks of salt/solvent/polymer electrolytes was the poor mechanical properties of the films at high levels of plasticization, see section 1.2. To overcome the problem, polymer blends were suggested as an alternative polymeric host. A polymer blend is a mixture of two polymers compatible on the molecular level giving properties that lying between those of the two polymers. It usually has good mechanical properties and in cases where one of the polymers is semi-crystalline an extra mechanical integrity is obtained.[61,62]

The improvement in the mechanical properties arises from the fact that the plasticizer is miscible with one of the polymers, say pol_1, leading to a dual-phase structure, where one of the polymers absorbs the liquid electrolyte, $poly_1$/liquid phase, and the second, say $poly_2$ works as a polymeric matrix, $poly_1/poly_2$ phase.

Matsumoto [63] used a blend of two block copolymers of Poly (acrylonitrile-ω-butadiene), NBR, and poly(styrene-co-butadiene), SBR with $LiClO_4$ salt in γ-butyrolactone, γ-BL and 1,2-dimethoxyethane, DME. The resultant films were mechanically strong with conductivities reaching $\sim10^{-3}$ S/cm at liquid contents above 40 w.t. %.

Oh and Kim [64] used a blend of PVdF-HFP and P(MMA-co-AC), Poly(methyl methacrylate-co-vinyl acetate) for a $LiClO_4$/(PC/EC) liquid electrolyte. The resultant gel films showed conductivities above 1 mS/cm and good electrochemical stability. A dual phase structure was suggested for the films by observing two glass transition temperatures in the DSC curves.

Other polymer blends like PVC/PMMA for a $LiCF_3SO_3$ salt in a mixture of EC and PC were reported. [65] The conductivity of the prepared films was found to be dependant on the PVC/PMMA ratio and the liquid content. Such behavior was explained in terms of the morphology of the films

1.2 Conductivity

1.2.1 Introduction

Conductivity can be defined as the movement of a charge in response to an applied electric field.[66] In liquid electrolytes the charge is an ion and it is called ionic conductivity, whereas in metals it is the electron, and it is called electronic conductivity. The conductivity involves all the charged mobile species in the electrolyte, *e.g.*, anions, cations, ionic clusters.

The specific conductivity of an electrolyte is given by :

$$\sigma = \sum_i qc_i u_i \qquad \mathbf{1}$$

Where:

q: is the charge of one mole of ions *i*.

c_i: is the molar concentration of ions *i*.

u_i: is the electrical mobility of the ions under the applied electric field.

1.2.2 Conductivity mechanism in polymer electrolytes

The microscopic motion of elastic polymers is liquid-like more than solid-like, thus the theory of ionic mobility in liquids can be applied to polymers as well.[67] The free volume theory developed by Cohen and Turnbull [68] is the simplest approach to explain the conductivity in polymers.

The theory suggests that the structural units of soft matter cannot align themselves to form a close-packed structure thus leaving a fraction of space vacant, called the free volume, v. Below Tg these vacancies are stationary but above Tg, chain flexibility increases as result of the allowed rotation of chain bonds. The main assumption of the theory is that diffusion is not an activated process but a result of the re-distribution of the free volume where ions can have a long-range diffusion. The contribution of a molecule with thermal velocity, u, to the diffusion coefficient is then:

$$D(v) = ga(v)\ u \qquad \mathbf{2}$$

Where g is a geometric factor and $a(v)$ is the cage diameter. $D(v)$ has no contribution unless the free volume exceeds a critical value, v^*, so that

$$D = \int_{v^*}^{\infty} D(v)p(v)dv \qquad \mathbf{3}$$

Where $P(v)$ is the probability of observing the free volume, which is equal to

$$p(v) = \frac{\gamma}{v_f}\exp(-\gamma\frac{v^*}{v_f}) \qquad \mathbf{4}$$

Where v_f is the average free volume per molecule and γ is a lagrange parameter. By substituting equations (2) and (4) into (3) followed by integration, the following equation for the diffusion coefficient can be obtained:

$$D = ga^*\ u\exp(-\gamma v^*\ /v_f) \qquad \mathbf{5}$$

Where a* is the molecular diameter. To expand v_f around a reference temperature, T_0, where the excess free volume disappears over the range T to T_0 the following equation was obtained:

$$v_f = \alpha \overline{v_M}\left[T - T_o\right] \qquad \mathbf{6}$$

Where v_M is the molar volume and α is the thermal expansion coefficient of the free volume. Substituting equation (6) into equation (5) the following expression for the diffusion coefficient is obtained:

$$D = ga^{*}u \exp\left[-\frac{\gamma v^{*}}{\alpha \overline{v_M}\,(T - T_o)}\right] \qquad \mathbf{7}$$

Using Nernst-Einstein equation and other treatments the following equation, which is known as the VTF equation, was derived for the conductivity. [69]

$$\sigma = \sigma_0 \exp\left(-\frac{B}{R(T - T_o)}\right) \qquad \mathbf{8}$$

Where B and σ_0 are parameters where σ_0 contains $T^{-1/2}$. It is worth mentioning that B here cannot be interpreted as an activation term.

1.2.3 Concentration-dependence of ionic conductivity

In a poly(ether):salt system the relationship between conductivity and salt concentration follows a shape as illustrated in figure (1.2).[70-72] At low concentrations the conductivity increases with the salt content as it is only controlled by the number of charge carriers. As concentration increases the conductivity goes through a maximum, this may be ascribed to either an increase in the viscosity, which arises from the formation of cross-links between ions and polymer chains, which in turns stiffen the chains and increases its T_g or the formation of ion-pairs or less mobile ion aggregates.

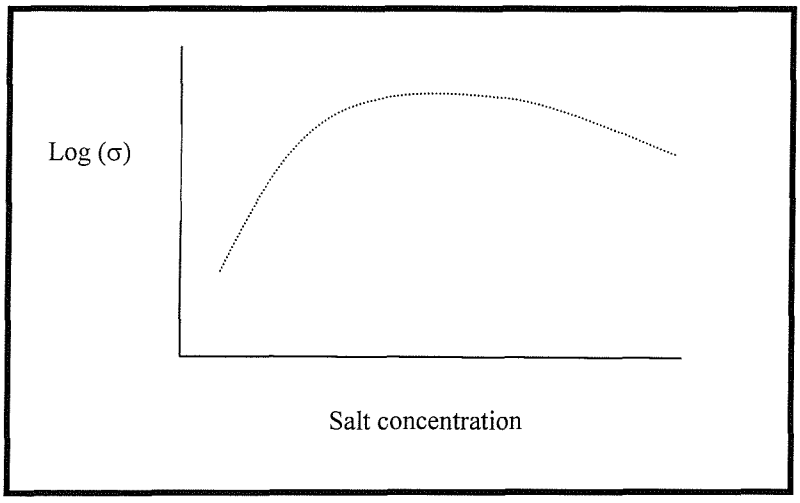

Figure (1.2) A schematic plot of ionic conductivity as a function of concentration for poly(ether):salt systems.

In a polymer/salt/solvent gel electrolyte Watanabe [73] and coworkers reported that at a fixed salt/solvent ratio, log (σ) increases linearly with the proportion of the liquid

electrolyte suggesting a composition independence of conductivity. This was observed for PAN/$LiClO_4$ in PC or EC films at $LiClO_4$/PC ratios of 0.5 and 2.

Tsunemi *et al* [74] reported a critical ratio of 1.6:1 of $LiClO_4$/PC where the conductivity of PVdF/$LiClO_4$/PC films levels off at high concentrations for electrolytes It has also been reported that the solvent's viscosity and dielectric constant have a profound effect on the conductivity. In polymer systems a distinction has been made between a macroscopic and a microscopic viscosity. Both are controlled by the properties of the solvent

In an ionic liquid-polymer gel electrolyte, the conductivity is also found to increase linearly with the liquid content reaching values of the neat liquid at very high content. [20] This behavior has been explained by the fact that the liquids are highly conductive themselves and addition of the polymer to the liquid results in an increase in the macroscopic viscosity without affecting the viscosity of the microscopic liquid domains. In contrast to the polymer/salt solvent system the polymer works here as a stiffener and has no role in the conduction pathway.

In Angell's system,[75] the conductivity reaches a maximum at low salt contents but it increases linearly to reach values of the neat liquid at higher contents. This was thought to be because at high concentrations, lithium is free of its coupling with the polymer chains and behaves as a true liquid-polymer system or what he called a polymer-in-salt system.

1.2.4 Temperature-dependence of ionic conductivity

For most solid electrolytes the Arrhenius equation is used to relate the conductivity to temperature.[76,77] However, Armand found that amorphous polymer electrolytes are best to be treated by the VTF equation .[78]

For most polymer electrolytes the temperature-conductivity data follows either a VTF throughout the temperature range or an Arrhenius at low temperatures and VTF at higher ones, or Arrhenius with two activation energies. Another equation which has been employed in the analysis of log(σ)-T curves, especially at temperature range within the vicinity of T_g, is the WLF equation below.

$$\log \sigma_T = -\frac{C_1(T - T_s)}{C_2 + (T - T_s)} \qquad \mathbf{9}$$

Where C_1, C_2 are arbitrary constants and T_s is a reference temperature. The WLF becomes equivalent to the VTF equation after few mathematical treatments.

1.3 AC-complex impedance spectroscopy

1.3.1 Theory

AC technique is a popular method to determine the conductivity of polymer electrolytes.[79-85] In an AC experiment a sinusoidal voltage, E, is applied to a sample of polymer electrolyte and the sinusoidal current, I, is determined. They are out of phase by an angle θ as shown below:

$$E = \Delta E \sin(\omega t) \qquad \mathbf{10}$$

$$I = \Delta I \sin(\omega t + \theta) \qquad \mathbf{11}$$

Where ω is the angular frequency, equal to $2.\pi.f$, where f is the sinusoidal frequency measured in Hz.

The ratio of the voltage to the current is measured to give the impedance, Z, in ohms. Impedance is a complex property, *i.e,* it has a real part, Z', and an imaginary part, Z'' which all are given below:

$$|Z| = \Delta E/\Delta I \qquad \textbf{12}$$

$$Z' = |Z| \cos\theta \qquad \textbf{13}$$

$$Z'' = -|Z| \sin\theta \qquad \textbf{14}$$

Admittance is simply the inverse of impedance and the following equations can be used to convert from impedance to admittance:

$$Y^* = Y' + jY'' = \frac{1}{Z' + jZ''} \qquad \textbf{15}$$

$$Y' = \frac{Z'}{Z'^2 + Z''^2} \qquad \textbf{16}$$

$$Y'' = \frac{-Z''}{Z'^2 + Z''^2} \qquad \textbf{17}$$

Impedance spectroscopy is the measurement of impedance as a function of frequency, which can be displayed in the form of Z' and Z'' as a function of angular frequency in what is called a complex impedance plot as shown in figure (1.3) below.

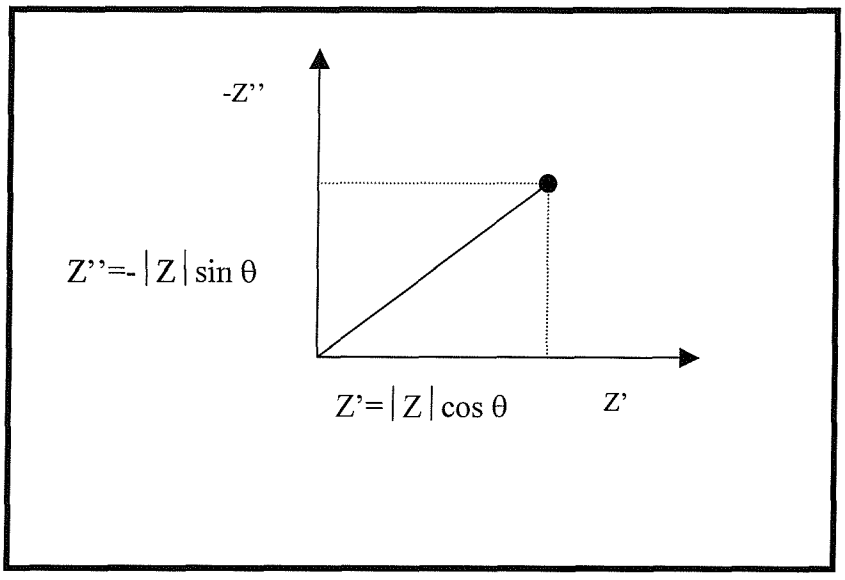

Figure (1.3): A schematic representation of a complex impedance plot for a single frequency.

Another way to represent the impedance response of the system is by plotting the individual impedance of each component against the frequency as shown in figure (1.4)[86]

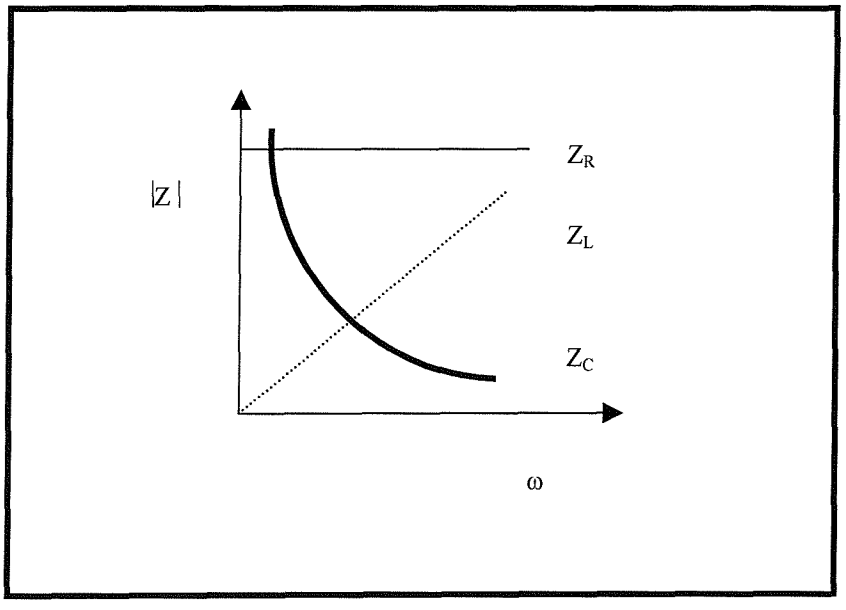

Figure (1.4): A schematic representation of a plot of the contribution of the impedance of a capacitor, Z_C, a resistor, Z_R, and an inductor, Z_L. to the total impedance against frequency.

1.3.2 AC plots and equivalent circuits

To interpret the complex impedance plot, a theoretical model in a form of an equivalent circuit of resistors and capacitors has to be established to represent the polarization and the charge resistance within the real cell. [87]

For a resistor, E is always in phase with I, *i.e*, $\theta = 0$ and the magnitude of the impedance is the value of the resistance, $|Z| = R$, which is independent of the frequency. The impedance is represented in the plot by a point at a distance R along the real axis, figure (1.5A). For a capacitor, the voltage lags behind the current by 90 °, *i.e.*, $\theta = -\pi/2$ and the magnitude of the impedance is frequency dependent and $|Z| = 1/\omega C$ where C is the capacitance, in the complex plot the impedance is a vertical spike coincident with the imaginary axis, figure (1.5B).

For a capacitor and a resistance connected in series, the individual impedances are directly additive and $Z_{total} = R - j/\omega C$. In the plot this is represented as a vertical spike displaced by a distance R along the real axis, figure (1.5C). However, for a parallel combination of a resistance and a capacitor Z_{total} is equal to:

$$Z_{total} = \frac{1}{\frac{1}{R} + j\omega C} = R\left[\frac{1}{1+(\omega CR)^2}\right] - jR\left[\frac{\omega RC}{1+(\omega RC)^2}\right] \qquad \textbf{18}$$

This shows a semicircle in the complex plot, figure (1.5D) with a distance R and a maximum in the imaginary part at a frequency ω_{max}, where the following relation applies:

$$\omega_{max} R C = 1 \qquad \textbf{19}$$

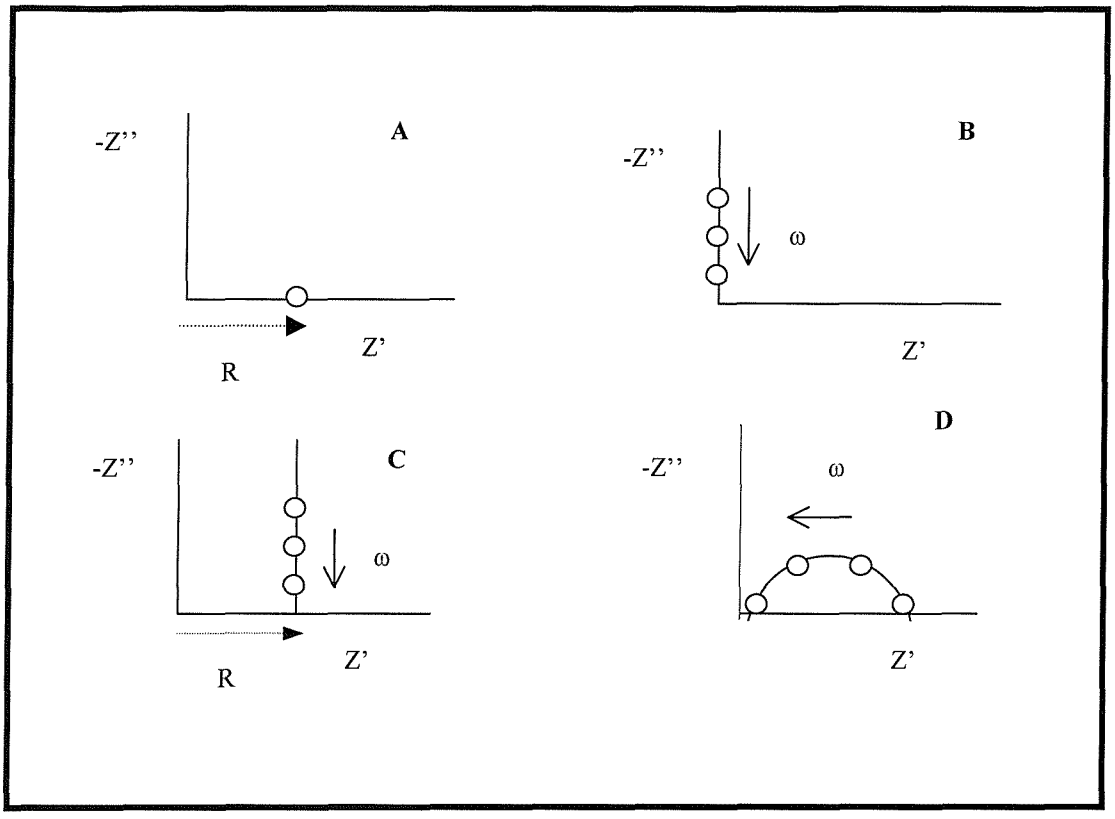

Figure (1.5): A schematic representation of the response of (A) a resistor, (B) a capacitor, (C) a resistor in series with a capacitor, (D) a resistor in parallel with a capacitor.

For a polymer electrolyte sandwiched between two blocking electrodes, no ionic species can go in or out of the polymer bulk. When an AC voltage is applied and the frequency is varied, the electrodes become oppositely charged and ions will accumulate on the surface forming a parallel-plate capacitor with a capacitance, C_e, (typically 10-50x10^{-6} F/cm^2) the alternating field will also causes ions to move in the bulk material against a resistance, R (typically 10^2-10^8 Ωcm). Moreover, a small capacitance, typically 10^{-12} F/cm arises due to the polarization of immobile polymer chains, C_b . The whole response of the cell is shown in figure (1.6). In practice the

plot looks more complicated; the semi-circle is broadened due to the phase-inhomogeneity of the bulk material; the spur appears with angles less than 90°.

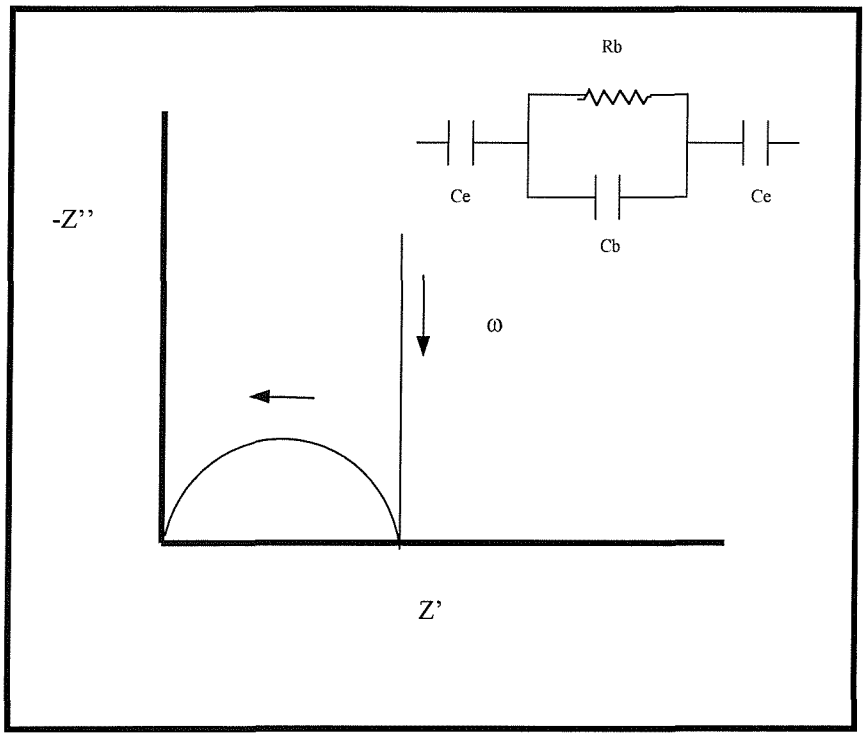

Figure (1.6): A schematic representation of a complex impedance plot for a polymer electrolyte/blocking electrode cell. The equivalent cell is also shown.

1.4 Amperometric CO sensors:

1.4.1 Introduction:

Carbon monoxide is a poisonous, odourless gas. It is blamed for many deaths especially in winter months when temperature and relative humidity are low. Commercial CO sensors include tin oxide and electrochemical sensors. Electrochemical sensors are based on sulphuric acid as an electrolyte and the majority to detect CO amperometrically.

CO sensors usually consist of a three-electrode-cell with reference (RE), counter (CE) and working electrodes (WE). [88,89] It has been proposed that the sensor signal originates from the oxidation reaction of CO at the working electrode as:

$$CO + H_2O \rightarrow CO_2 + 2H^+ + 2e^- \qquad \mathbf{20}$$

and the reduction of oxygen at the counter electrode as:

$$2H^+ + \tfrac{1}{2} O_2 + 2e^- \rightarrow H_2O \qquad \mathbf{21}$$

The overall reaction is therefore:

$$CO + \tfrac{1}{2} O_2 \rightarrow CO_2 \qquad \mathbf{22}$$

Some researchers showed evidence that the CO oxidation rate is first order with respect to both water and CO concentrations, *i.e.*, it is a second order reaction as follows: [90]

$$\text{oxidation rate} = k\,[CO]\,[H_2O] \qquad \mathbf{23}$$

Others, [91] have favored a second order reaction with respect to water concentration.

1.4.2 Polymer electrolytes for CO sensor:

Perfluorosulfonate ionomers, the most studied proton conducting polymers, are believed to have the best chemical and physical properties to be used as in a CO sensor. NAFION ®, one member of that family, has been employed for such properties. It showed good conductivity, but it was dependent on changes in relative humidity. One approach to overcome this problem was to apply a water

reservoir in the sensor to keep the polymer wet at all times. [92] Another approach was to use an indirect compensation method for the humidity effect by using a second cell to determine the polymer permeability by measuring an oxygen reduction current. [93]

1.4.3 Mechanism of CO oxidation on Platinum:

Much of the research on CO oxidation on platinum has been done in acidic aqueous medium.[94-98] The exact course of the oxidation mechanism is still controversial. [99] The most accepted view that the oxidation takes place between neighboring adsorbed CO and adsorbed OH species on the surface of platinum. The formation of the adsorbed OH species is potential dependant and results from the dissociation of water.

The following mechanism has been proposed for the oxidation in acidic solutions,

$$H_2O + * = OH_{ads} + H^+ + e^- \qquad \textbf{24}$$

$$CO + OH_{ad} = CO_2 + H^+ + e^- + 2* \qquad \textbf{25}$$

Where (*) represents a free site on the surface of platinum.

It is well established now that at high CO coverages, CO is adsorbed in the on-top sites of the platinum surface, while the adsorption site for OH species is still controversial.

The region where the oxidation reaction takes place is believed to be a three–phase interface, where Pt, CO and the acidic solution coexist as depicted in the black area in figure (1.7). This thinly wetted region is maximized by using a gas-diffusion electrode, a Pt powder mixed with PTFE. In the case of a solid polymer electrolyte a good contact has to be made between the polymer film and the Pt. The role of water

is also important here to make such contact even stronger and for the reaction to go faster.

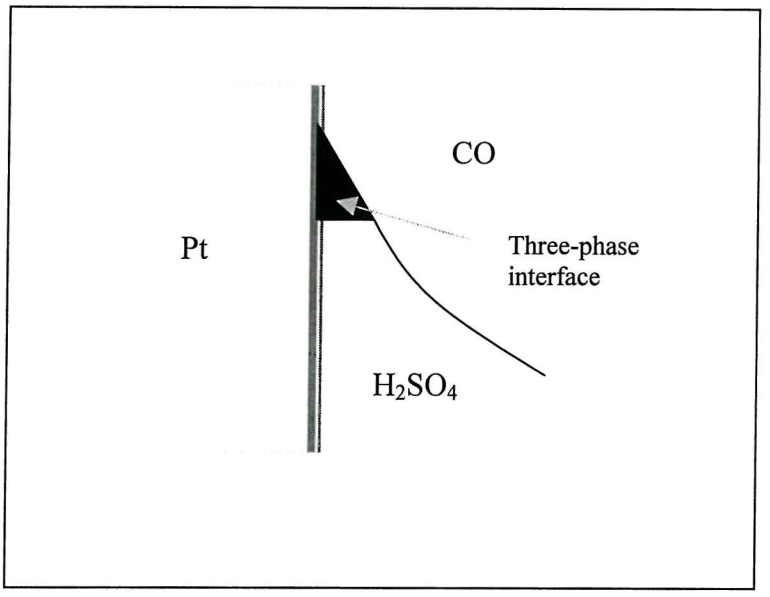

Figure (1.7) A schematic diagram for the three-phase interface region in the oxidation of CO on Pt in acidic solution.

1.4.4 Sensor design

Sensors incorporating solid polymer electrolytes have been made in a planar geometry. The most common one, which was adopted by Yasuda, [100-103] who had the three electrodes on one substrate and the polymer was deposited on the top. Van der Wal [92] used the same method of fabrication as Yasuda but with different shapes

of the electrodes, figure (1.8). This sensor design has been adopted in this work for its simplicity.

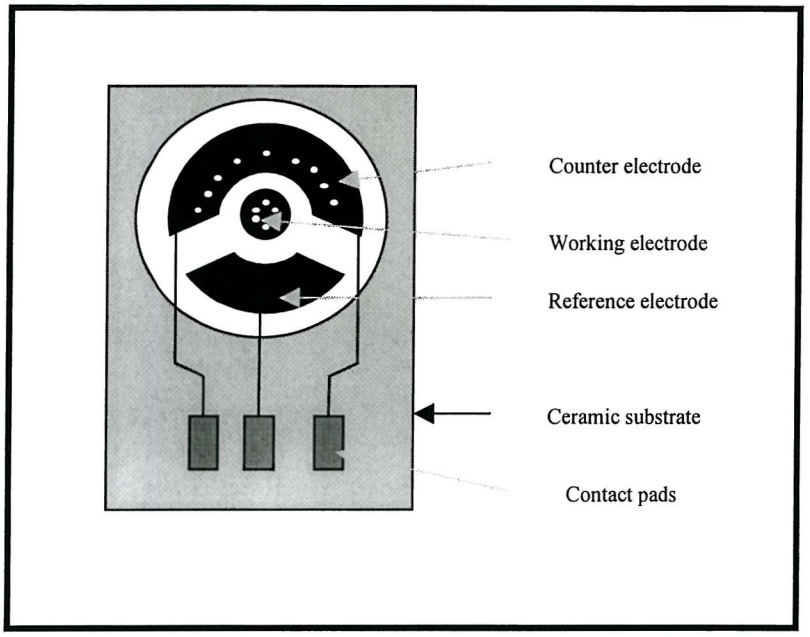

Figure (1.8): A schematic diagram of the planar CO sensor used by Van der Wal.

1.5 Gap electrode cell

1.5.1 Introduction

The currently used method for measuring the conductivity of polymers consists of sandwiching a polymer film between two blocking platinum electrodes. The method involves measurement of the thickness of the film, which is usually accompanied by a large error.

The gap method involves the deposition of a thin polymer film on two thin electrodes separated by a gap of known width. By measuring the resistance of the film for different gaps, this allows the elimination of the cell constant from the equation and the film thickness is no longer required to measure the conductivity.

There are two electrode geometries of the gap cell as can be shown in figure (1.9)

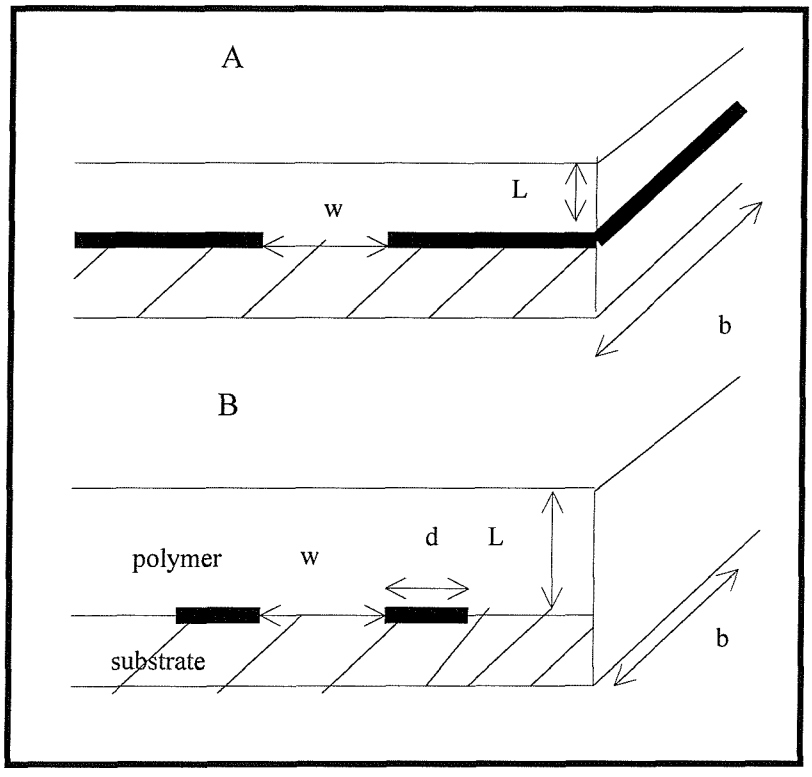

Figure (1.9) A schematic diagram of semi-infinite electrodes (A), and coplanar thin electrodes, (B).

1.5.2 Semi-infinite electrodes

This consists of two semi-infinite thin electrodes with a separation of w and a length b, where b>>w.

The electric field at the plane bi-secting the electrodes has been determined by Schwartz-Christoffel transformation leading to the following equation [104-106]

$$E_{(\chi,0)} = \frac{V}{L\pi} / \sqrt{(\chi^2 + w^2/4L^2} \qquad \textbf{26}$$

Where V is the voltage applied across the electrodes and χ is the dimensionless distance parameter (x/L); where x is the distance in the film

The total current passing between the electrodes is given by:

$$I = b\int_0^1 \sigma E.dx \qquad \textbf{27}$$

By substituting in equation 27 for x= χ L we have

$$I = bL\int_0^1 \sigma E(\chi,0).d\chi \qquad \textbf{28}$$

The conductance, G, is equal to I/V, and can be given by:

$$G = \frac{bL}{V}\int_0^1 \sigma E(\chi,0).d\chi \qquad \textbf{29}$$

By integrating the product of the local conductivity and the electrical field over a closed surface between χ=0 to 1, conductance can be calculated from the geometry as:

$$G = \frac{\sigma b}{\pi} \ln\left[\frac{1+\sqrt{1+w^2/4L^2}}{w/2L}\right] \qquad \textbf{30}$$

The cell constant, K, which is equal to σ/G, can be given by

$$K = \frac{\pi}{b \ln\left(\frac{1+\sqrt{1+W^2/4L^2}}{w/2l}\right)} \qquad \textbf{31}$$

When w<<L, and comparing the cell constants for two gaps, σ can be calculated by:

$$\sigma = \frac{\pi}{b \ln\left(\frac{w2}{w1}\right)}(G_1 - G_2) \qquad \textbf{32}$$

1.5.3 Coplanar thin electrodes

In this case the electrodes are finite coplanar of width, d. The conformal transformation gives the electric field as:

$$E_a(\chi,0) = \frac{V}{2A^*L^2} \frac{1}{\sqrt{([\chi^2 + w^2/4L^2][M^2\chi^2 + w^2/4L^2])}} \qquad \textbf{33}$$

Where M is the geometrical modulus:

$$M = \frac{w}{w+2d} \qquad \textbf{34}$$

And the constant A^* is the complete elliptic integral of the first kind.

$$A^* = \frac{2}{w}\int_0^1 \frac{dt^*}{\sqrt{([1-t^{*2}][1-M^2t^{*2}])}} \qquad \textbf{35}$$

The conductance is given by:

$$G = \frac{\sigma b}{2A^*L}\int_0^1 \frac{d\chi}{\sqrt{([\chi^2 + w^2/4L^2][M^2\chi^2 + w^2/4L^2]}} \qquad \textbf{36}$$

The principle of the gap technique has been employed in Biochemistry for making biosensors.[107] In a biosensor an interdigitated gold microelectrodes were used, figure (1.10). Using a standard solution with a known conductivity, *e.g.*, 0.1 M KCl, the concentration of a biomolecule was measured either by a DC or an AC method.

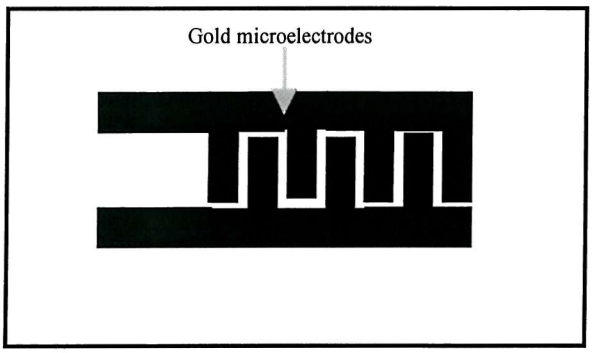

Figure (1.10) A schematic diagram of interdigitated electrodes device used as a bio-sensor.

Owen and Ismail [108,109] prepared a gap cell and have tested it on aPEO/$LiClO_4$ polymer electrolytes. They summarized the advantages of the gap electrode cell in terms of its relief of the following problems with cylindrical cell:

1- Difficulty in calculating the cell constant to an accuracy better than 5%.
2- Difficulty in equilibrating the sample with a surrounding atmosphere.
3- Requirement of a large amount of the polymer sample.
4- Difficulty in dealing with irregularly-shaped samples.

In their work they observed a Warburg impedance at low frequencies which they attributed to a cell geometry which contained a transmission line effect. However, they still observed a high frequency semi-circle which could be extrapolated to get a value for the resistance. They used equation (32) to measure the conductivity of the polymer electrolyte using the resistance values obtained from two gap widths.

This work

The objectives of this work were:

1-To develop a novel solid polymer electrolyte, that is unaffected by reasonable change in humidity when used in a CO sensor. For this purpose a novel molten salt based on imidazole, IMI, was prepared in which its proton conductivity does not depend on the presence of water. Many polymeric hosts were tried for the IMI. The prepared films have been characterized and their conductivities were measured.

2-To investigate the use of one of the prepared films in a CO sensor and measure the response as a function of CO concentration and relative humidities. Also to investigate the CO oxidation on a Pt electrode in IMI:PC and H_2SO_4 solutions under dry and ambient conditions.

3-To develop a new technique for conductivity measurements of polymer electrolytes based on the gap electrode method.

References

1 C. Chiang, W. Park, J. Heeger, H. Shirakawa, E. Louis and A. MacDiarmid, *J. Chem. Phys.*, **69 (11)** (1978) 5098.

2 W. Feast, in "Handbook of conducting polymers", Ed. By T. Skotheim and M. Dekker, New York, 1986, vol. 1, P. 1.

3 M. Armand, J. Chebagno and M. Duclot, *Second Int. Conf. On solid electrolytes*, St Andrews, 1978, P 65.

4 M. Armand, J. Chebagno and M. Duclot, in " Fast ionic transport in solids", Ed. by P. Vashista, J. Munday and G. Shenoy, Elsevier, New York, 1979, P. 131.

5 M. Armand and M. Duclot, *Eur. Pat.*, 78 32976, 1984.

6 M. Armand, *Solid State Ionics*, **9-10** (1983) 754.

7 "The electrochemistry of Novel Materials", Ed. By J. Lipkowski and P. Ross, VCH, New York, 1994, P. 85.

8 G. Appetecchi, S. Panero, E. Spila and B. Scrosati, *J. App. Electrochem.*, **28** (1998) 1299.

9 D. Fenton, J. Parker and P. Wright, *Polymer*, **14** (1973) 589.

10 P.V. Wright, *Br. Polym. J.*, 7 (1975) 319.

11 P. Bruce and C. Vincent, *J. Chem. Soc. Faraday Trans.*, **89(17)** 1993, 3187.

12 D. Baril, C. Michot and M. Armand, *Solid State Ionics*, **94** (1997) 35.

13 M. Armand, *Solid State Ionics*, **69** (1994) 309.

14 K. West, Report of the solid state electrochemistry group, The Technical University of Denmark, 1989, P. 103.

15 J. Cowie in "Polymer electrolyte reviews 1", Ed. By J. MacCallum and C. Vincent, Elsevier, London, 1987, chapter 4, P 69.

16 D. Fauteux, in "Polymer electrolyte reviews 2", Ed. By J. MacCallum and C. Vincent, Elsevier, London, 1989, chapter 4. P 121.

17 M. Alamgir and K. Abraham, in " Lithium Batteries", Ed. By G. Pistoia, Elsevier, Amsterdam, 1994. P.93.

18 G. Appetecchi, F. Croce and B. Scrosati, *J. Power Sources,* **66** (1997) 77.

19 G. Dautzenberg, F. Croce S. Passerini and B. Scrosati, *Chem. Mat.,* **6** (1994) 538.

20 G. Appetecchi, F. Croce, G. Dautzenberg, S. Passerini and B. Scrosati, *Electrochemica Acta.,* **39** (1994) 2187.

21 Ref. 15, P. 97.

22 G. Nagasubramanian, A. Attia and G. Halpert, *J. Appl. Electochem.*, **24** (1994) 298.

23 M. Armand, *Extended abstracts of the 3rd international symposium on new materials for electrochemical systems*. Montreal, 1999, P. 5.

24 J. Fuller, A. Breda, R. Carlin, *J. Electrochem. Society*, **144(4)** (1997) 3881

25 J. Fuller, A. Breda, R. Carlin, *J. Electroanal. Chem.*, **459** (1998) 29.

26 M. Watanabe, S. Yamada and N. Ogata, *Electrochemica Acta*, **13-14(40)** (1995) 2285.

27 R. Pyati and R. Murray, *J. Electrochem. Society*, **143(2)** (1996) 401.

28 M. Watanabe and T. Mizumura. *Solid State Ionics*, **86-88** (1996) 353.

29 C. Angell, C. Liu and E. Sanchez, *Nature*, **362** (1993) 137.

30 S. Zhang, Z. Chang, K. Xu and C. Angell, *Electrochimica Acta.*, **45(8-9)**, (2000) 1229.

31 M. Forsyth, D. MacFarlane and A. Hill, *Electrochimica Acta.*, **45(8-9)**, (2000) 1243.

32 A. Noda and M. Watanabe, *Electrochimica Acta.*, **45(8-9)**, (2000) 1265.

33 Y.Tominaga, N. Takizawa and H. Ohno, *Electrochemica Acta.*, **45(8-9)**, (2000) 1285.

34 V. Zea, C. Poinsignon and M. Armand, *J. Mater. Chem.*, **7(9)** (1997) 1677.

35 J. Lassegues, B. Desbat, O. Tringuet, F. Cruegge and C. Poinsignon, *Solid State Ionics*, **35** (1989) 17.

36 M. Daniel, B. Desbat, F. Cruegge, O. Tringuet and J.C. Lassegues, *Solid State Ionics*, **28-30** (1988) 637.

37 P. Donoso, W. Gorecki, C. Berthier, F. Defendem, C. Poinsignon and M. Armand, *Solid State Ionics*, **28-30** (1988) 969.

38 J. Lassegues, in "Proton conductors: Solids, membranes and gels-matereials and devices", Ed. By P. Colomban, Cambridge University Press, Cambridge 1992, Ch. 20.

39 J. Grondin, D. Rroctriguez and J. Lassegues, *Solid State Ionics*, **77** (1995) 70.

40 S. Petty-Weeks, J. Zupacic and J. Swedo, *Solid State Ionic*, **31** (1988) 117-125.

41 D. Rodriguez, C. Jegat, O. Tringuet, J. Grondin and J. Lassegues, *Solid State Ionics*, **61** (1993) 195.

42 F. Defendini, PhD thesis, University Of Grenoble, France 1987.

43 O. Tringuet, PhD thesis, Bordeaux University, France 1990.

44 Y. Charbouillot, D. Ravaine, M. Armand and C. Poinsignon, *J. Non-Cryst. Solids*, **103** (1988) 325.

45 K. Kreuer, *Solid State Ionics*, **97** (1997) 55.

46 K. Kreuer, *Solid State Ionics*, **97** (1997) 1-15.

47 K. Kreuer, A. Fuchs, M. Ise, M. Spaeth and J. Maier, *Electrochemica Acta*, **(43)10-11** (1998) 1281.

48 V. Bermudez, C. Poinsignon and M. Armand, *J. Mater. Chem.*, **7(9)** (1997) 1677.

49 A. Kawada, A. McGhie and M. Labes, *J. Chem. Phys.*, **52** (1970) 3121.

50 M. Casciola, U Costantino and A. Calevi, *Solid State Ionics*, **61** (1993) 245.

51 M. Casciola, S. Chieli, U. Costantino and A. Peraio, *Solid State Ionics*, **46** (1991) 53.

52 K. Kreuer, A. Fuchs, M. Ise, M. Spaeth, J. Maier. *Electrochimica Acta*, **43 (10-11)** (1998) 1281.

53 U. Meister, M. Ise, K. Kreuer and W. Meyer, *Extended abstracts of the 12th international coonference on solid state ionics*, Halkidiki 1999, P 429.

54 E. Tsuchido, H. Ohno, K. Tsunemi and N. Kbayaski, *Solid State Ionics*, **11** (1983) 227.

55 N. Agmon, *Solid State Ionics*, **244** (1995) 456.

56 "Speciality Polymers", Ed. By R. Dyson, Blackie Ac. and Prof., UK, 1992, P.106.

57 J. Tarascon, A. Gozdz, C. Schmutz, F. Skokooli and P. Warren, *Solid State Ionics*, **86-88** (1996) 49.

58 G. Silva, N. Lemes, C. Fonseca and M. De Poli, *Solid State Ionics*, **93** (1997) 105.

59 E. Duek, M. De Paoli and M. Mastragostino, *Chem. Mater*, **5** (1993) 650.

60 S. Kohjiva, T. Horiuchi and S. Yamashita, *Solid State Ionics*, **37** (1992) 1721

61 T. Kwei and T. Wang, in "Polymer Blends", Ed. By D. Paul and S. Newman, Academic Press, London, 1987, volume 1.

62 M. Matsumoto, T. Ichino, J. Rutt and S. Nishi, *J. Electrochem. Soc.*, **141** (1994) 1989.

63 M. Matsumoto, *Polymer*, **36** (16) (1995) 3243.

64 B. Oh and Y. Kim, *Solid State Ionics* **124** (1999) 83.

65 H. Rhoo, H. Kim, J. Park and T. Hwang, *Electrochemica Acta,* **24(10)** (1997) 1571.

66 P. Atkins, Physical chemistry, Oxford University Press, Fifth edition, 1994, P 834.

67 J. Owen, in *"ion conducting polymer"*, Ed. By R. G. Linford, Elsevier, London, (1987) chapter 3.

68 M. H. Cohen and D. Turnbull, *J. Chem. Phys.*, **31**, (1959), 1164.

69 J. Souquet, M. Duclot and M. Levy, *Solid State Ionics*, **85** (1996) 149.

70 "Solid Polymer Electrolytes", Ed. By Fiona Gray, VCH Publishers, London, 1991, P. 85.

71 P. Hall, G. Davies, J. McIntyre, I.Ward, D. Bannister and K. Le Brocq. *Polym. Commun.*, **27** (1986) 98.

72 M. Watanabe, J. Ikeda and I. Shinohara, *Polym. J.*, **15** (1983) 65.

73 M. Watanabe, M. Kanba, K. Nagaoka and I. Shinoltara, I. *Poly. Sci., Polym. Phys. Ed.*, **21** 939 (1983).

74 E. Tsunemi, H. Ohno and E. Tsuchida, *Electrochimica Acta*, **28** (1983) 833.

75 S. Zhang, Z. Chang and C. Angell, *Electrochimica Acta*, **45** (2000) 1229.

76 D. Baril, C. Michot, M. Armand, *Solid State Ionics*, **94** (1997) 35.

77 ref. 15, P. 185.

78 M. Armand. J. Chabagno and M. Duclot, in "Fast ion transport in solids". Ed. By P. Vashisa, J. Munday and G. Shenoy, Elsevier/North Holland, New York, 1979, P. 131.

79 J. R. MacDonald, in *"Impedance Spectroscopy"*, John Wiley, London, (1987).

80 I. Oslen, J. Barker and R. Koksbang, *Solid State Ionics*, **83** (1996) 125.

81 C. Hunter, D. Sinclair, A. West and A. Hooper, *Journal of Power Sources*, **24** (1988) 157.

82 A. Bard and L. Faulkner, "Electrochemical Methods", John Wiley and Sons, 1980, P. 316.

83 "The CRC Handbook of Electrochemistry", Ed. By H. Bouwmeester and P. Gelling , 1997, P.63.

84 W. Baochen, F. Li and P. Xinsheng, *Solid State Ionics*, **48** (1991) 203.

85 A. Kuffman, in *"Understanding Electrochemical Cells"*, Schlumberger Electronics (UK), Technical report number 017/85, (1985).

86 "Electrochemical Supercapacitors", Ed. By B. Conway, Kluwer Academic/Plenum Publishers, New York, 1999, P. 489.

87 Ref. 15, Chapter 8, P. 237.

88 H. Yan and C. Liu, *Sensors and Actuators*, **B17** (1994) 165.

89 A. Yasuda, N. Yamaga, K. Doi and T. Fujioka, *Sensors and Actuators* **B21** (1994) 229.

90 S. Lee, A. Cocco, D. Keyvani and G. Maclay, *J. Electrochem. Soc.*, **142 (1)** 1995 157.

91 L. E. Lemoine, Department of Chemistry, University of Southampton, MPhil thesis 1997.

92 P. Van Der Wal, N. De Rooij and Koudelka-Hep, *Sensors and Actuators*, ***B 35-36*** (1996) 119.

93 P. Neuzil, D. Kayvani and G. Maclay, *extended abstract of the sixth international meeting on chemical sensors*, Garthersburg-USA, 1996.

94 "Encyclopedia of Electrochemistry of the Elements", Ed. By A. Bard, Marcel Dekker Inc., New York, 1976, vol 7, P. 182.

95 S. Gilman, *J. Phys. Chem.*, **71 (13)** (1967) 4331.

96 S. Gilman, *J. Phys. Chem.*, **70 (9)** (1966) 2880.

97 S. Gilman, *J. Phys. Chem.*, **68 (1)** (1964) 70.

98 R. Bellows, E. Marucchi and D. Buckley, *Ind. Eng. Chem. Res,* **35** (1996) 1235.

99 M. Koper, A. Jansen, A. Santen, J. Lukkien and P. Hilbers, *J. Phys. Chem.*, **109 (14)** (1998) 6051.

100 A. Yasuda, N. Yamaga, K. Doi and T. Fujioka, *Sensors and Actuators*, B **21** (1994) 229.

101 A. Yasuda, K. Doi, N. Yamaga, T. Fujioka and S. Kusanagi, *J. Electrochem. Soc.*, **139(11)** (1992) 3224.

102 A. Yasuda, N. Yamaga, K. Doi, T. Fujioka and S. Kusanagi, *J. Electrochem. Soc.*, **139(4)** (1992) 1091.

103 T. Otagawa, M. Madou, S. Wing, J. Rich-Alexander, S. Kusanagi, T. Fujioka and A. Yasuda, , *Sensors and Actuators*, B **1** (1990) 319.

104 J. Gardner, *Semincond. Sci. Technol.*, **4** (1989) 345.

105 J. Gardner, *Sensors and Actuators*, **18** (1989) 373

106 J. Gardner, P. Bartlett and K. Pratt, *IEE proc. Circuits devices sys.*, **5** (1995) 321.

107 "Biosensors", Ed. By E. Hall, Open University Press, London, 1990, P.336

108 I. Ismail and J. Owen, *Solid State Ionics*, **85** (1996) 163.

109 I. Ismail, Ph.D thesis, University Of Southampton, 1996. P 63.

Chapter Two

Experimental work and techniques

2.1 Preparation of IMI and IMI:PC liquids

IMI liquid which is a mixture of imidazole and imidazolium bis-(trifluoromethanesulphonyl) imide, was prepared by adding a 2:1 molar quantity of imidazole, Aldrich, to bis-(trifluoromethanesulphonyl) imide, Fluka. The exothermic reaction of the two solids gave a yellowish liquid, which was dried *in vacuo* overnight. IMI:PC solutions were prepared by adding the appropriate amount of IMI to PC, Aldrich. IMI dissolved rapidly in PC in all proportions.

2.2 Preparation of the Polymeric gel electrolytes

2.2.1 PVdF and PVdF-HFP: IMI:PC films

PVdF and PVdF-HFP were ordered from Solvay Ltd, UK, and were used as received. The appropriate amounts of PVdF or PVdF-HFP, IMI and PC, 1 g in total, were added to a small glass vial. The three components were mixed manually and an off-white paste was obtained. 4 ml of THF, Aldrich, was added to the paste The viscous cloudy solution was heated gently using a heat gun for 2 minutes until it turned transparent. The solution was then poured into a Petri dish. The films were left to dry at ambient conditions for 4 h and further dried *in*

vacuo for 12 h at room temperature. The films were weighed before and after drying.

2.2.2 PEE:IMI films

PEE, was supplied by Zeon chemicals, USA, and was used as received. A weighed amount of PEE was dissolved in 10 ml THF and left to stir for 24 hours for complete solubility. Then the appropriate amount of IMI was added, 1 g in total, to the solution. The polymer solution was left to homogenise for 10 hours and then was poured into a Petri dish. The films were left to dry at ambient conditions and further dried *in vacuo* for 12 hours. The films were weighed before and after drying.

2.2.3 PMMA/PVdF-HFP:IMI films

The appropriate amounts of PVdF-HFP, PMMA, Aldrich, and IMI were added to a small vial, 1g in total. The ratio of PVdF-HFP to PMMA was 1:1 by weight. Mixture of the three gave a white paste. 4 ml of THF was added to the vial and the mixture was left to dissolve for 4 hours. The clear solution was then poured into a Petri dish and transparent films were obtained. The films were dried as in the previous section.

2.3 Conductivity measurements

2.3.1 Liquid cell

The conductivity of liquid samples was measured using a cell with a design as shown in figure 2.1. The cell consists of two platinum wires fitted into a test tube filled with a liquid sample. The cell was calibrated by a 0.1 M KCl solution before each experiment. The resistances of the KCl solution and the liquid were obtained using an HP frequency analyser to sweep the frequency from 5 Hz to

100 kHz with an amplitude of 10 mV. The conductivity of the liquid , σ_L, was obtained using:

$$\sigma_L = \frac{\sigma_{KCl} . R_{KCl}}{R_L}$$

Where R_L and R_{KCl} are the resistances, obtained from the complex impedance plot, of the liquid sample and the KCl solution, respectively. σ_{KCl} is the conductivity of the 0.1 M KCl solution, which is equal to 1.29×10^{-2} S/cm.

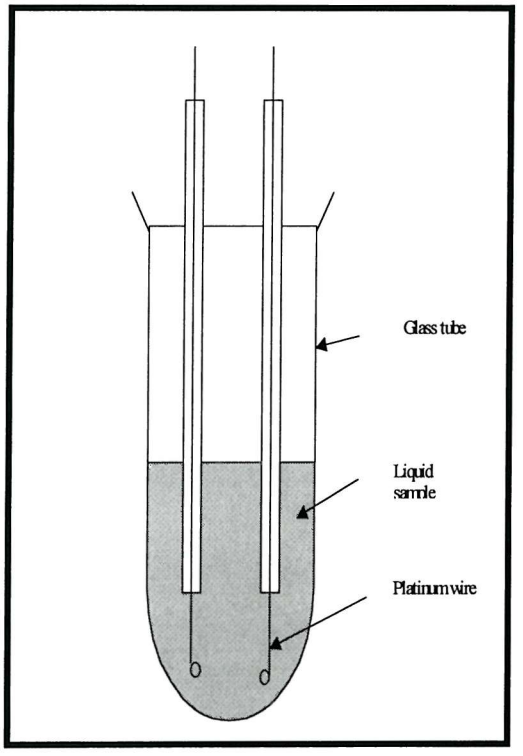

Figure (2.1) Conductivity cell for measuring the ionic conductivity of liquids.

2.3.2 Polymer cell

In order to measure the conductivity of the polymers, films with a typical thickness of 0.10-0.50 mm (± 0.01) were prepared as described in section 2.2. In the case of the PEE-IMI polymers the films were not free standing but could be shaped into circular discs to fit into the cylindrical cell.

2.3.2.1 Cylindrical cell

Figure (2.2) shows a cylindrical cell that was used to measure the ionic conductivity of the films. [1] The cell was assembled inside a glove box with water content less than 5 ppm. Samples were sandwiched between the two Alumina-polished stainless steel blocking electrodes in a Buchi tube. The tube was taken out of the box and fitted into a Buchi furnace supplied with an Argon flow. HP frequency analyser was used to sweep the frequency from 5 Hz to 13 MHz with an amplitude of 100 mV. The obtained complex impedance plot was fitted, using in-house written software, to obtain values of the resistance.[2] The samples were submitted to heating between room temperature and 75°C and about 30 minutes were allowed for thermal equilibration at each temperature. The temperature was controlled with K-type thermocouple connected to a digital thermometer. A travelling microscope was used to monitor the thickness of the film at each temperature.

The conductivity of a polymer film, σ, was obtained using:

$$\sigma = \frac{L}{A} \cdot \frac{1}{R}$$

Where:

L: is the thickness of the film, in centimeters, as measured by the travelling microscope.

A: is the area of one of the stainless steel electrodes, which is equal to 0.625 cm^2.

R: is the resistance, in ohms, as obtained from the complex impedance plot.

Figure (2.3) depicts a typical complex impedance plot of a polymer sample. It shows a semi-circle and a spur. The resistance of the sample is the value at which the low-frequency end of the semi-circle crosses the x-axis. In cases where the semicircle did not cross the axis an extrapolation was made.

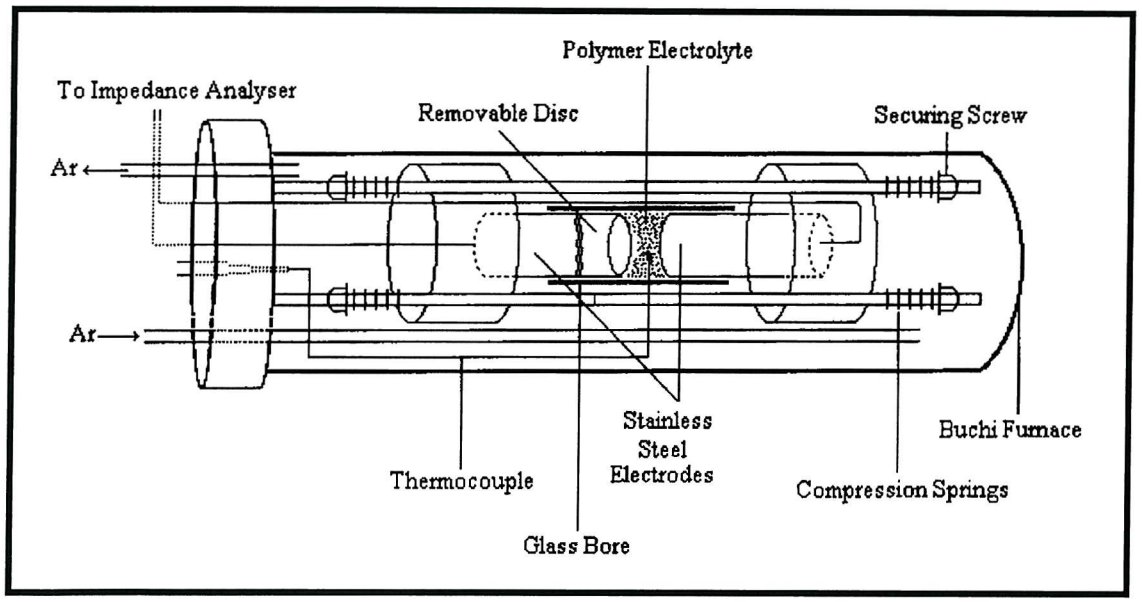

Figure (2.2) A schematic diagram of the design of the cylindrical cell.

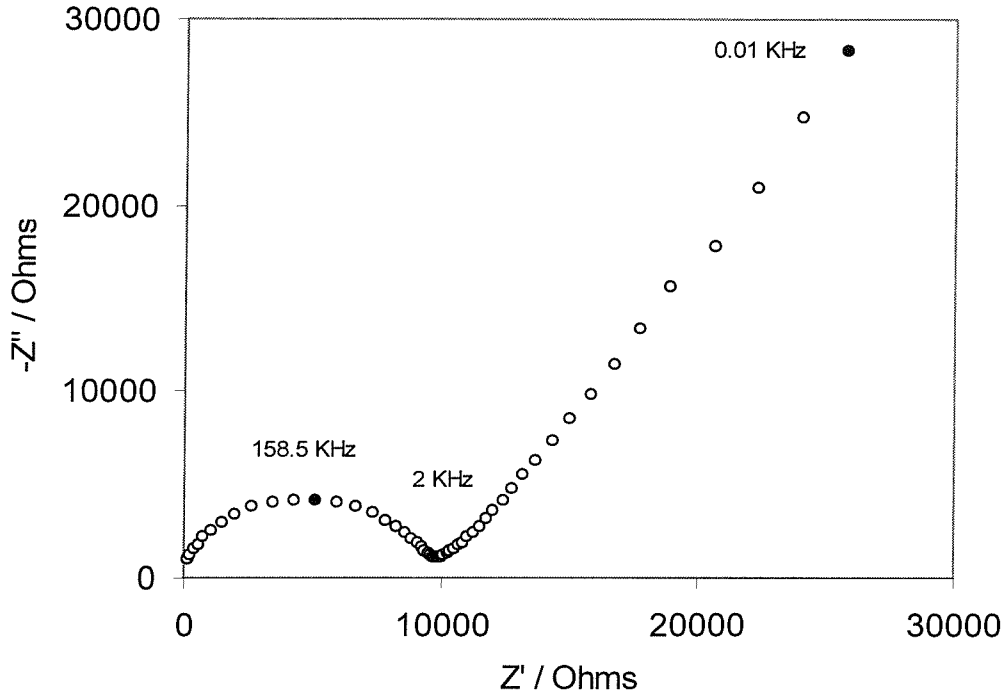

Figure (2.3) A complex impedance plot of a 30% (1.2 M IMI:PC):PVdF-HFP polymer gel sample in a cylindrical cell obtained at room temperature. The film thickness is 0.031 cm.

2.3.2.2 Gap cell

Figure (2.4) shows a schematic diagram of design of the two gap cell, fabricated by University of Warwick, [3] which were used in this work. A gap cell consisted of an array of seven pairs of thin platinum electrodes deposited on an insulating substrate, silicon nitride. Each pair the two electrodes are separated by a gap, the value of which was varied by 5, 10, 20, 50, 100 and 200 microns.

The two gap cells differ only in the arrangement of the electrode pairs within the 1 mm^2 region of the device. For the GC 160 design the pairs were placed in an overall rectangular shape whereas in the case of the GC 161 they were arranged in a circle. The latter has the advantage of obtaining a more uniform coverage of the films on the electrode pairs.

Each gap cell had eight pins; six of them to make the measurements, the seventh was for the interdigitated microelectrode array, which is not going to be used here and the eighth was the common.

For the purpose of obtaining the conductivity of a polymer film, a few drops of the polymer solution (5 w.t. %) was placed gently, using a pipette, on the 1mm^2 region of the cell. The cell was left at ambient conditions to allow for the solvent to evaporate and then fitted to a standard ribbon cable, which was soldered on a copper holder. The whole cell was then fitted inside a Buchi tube/furnace, similar to the cylindrical cell. The same drying procedure was also applied.

In the case of the KCl solutions a small amount of the solution was poured into a vial, then the 1mm^2 region of the gap cell was immersed vertically into the solution.

In the case of the NAFION solution (Aldrich, 5% in water and low aliphatic alcohols). For each deposition of the polymer the gap cell was taken out of the Buchi furnace and a drop of the NAFION solution was applied, then the cell was left to dry at ambient conditions for one hour and then put back into the Buchi furnace. The sample was then dried at 60 °C for a further hour under the flow of 48%-humidified Argon.

The HP analyser was used to obtain the complex impedance or admittance plot of each pair against the common. The frequency was swept from 5 Hz to 100 kHz with an amplitude of 50 mV.

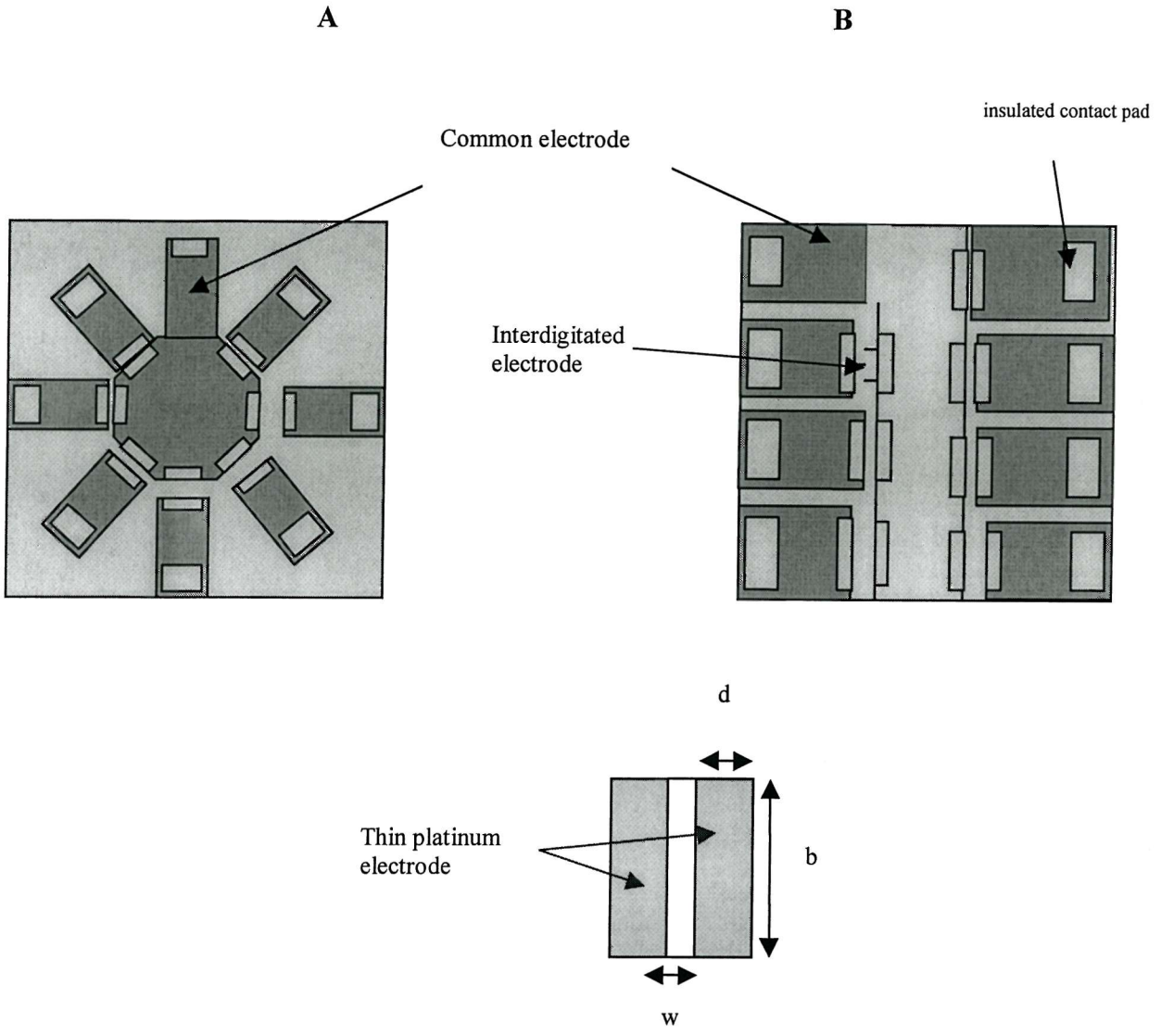

Figure (2.4) A schematic diagram of the design of the two gap cells, (A) GC 161, (B) GC 160. The diagram shows the 1 mm^2 region of the cells.

2.4 Differential Scanning Calorimetry, DSC

2.4.1 Background

DSC is part of a group of thermal techniques in which a physical property of a substance is measured as a function of temperature. [4] In a DSC experiment the heat required to maintain the temperature of the sample holder similar to a

reference material inside a furnace. A DSC curve represents the change in the heat capacity over the experimental temperature change.

In polymers, the three most studied parameters are glass transition temperature, T_g, melting temperature, T_m and the degradation temperature T_d. Figure (2.5) below depicts these three transitions. DSC was used in this work to determine the T_g and $T_{m,,}$ if any, of the polymer films.

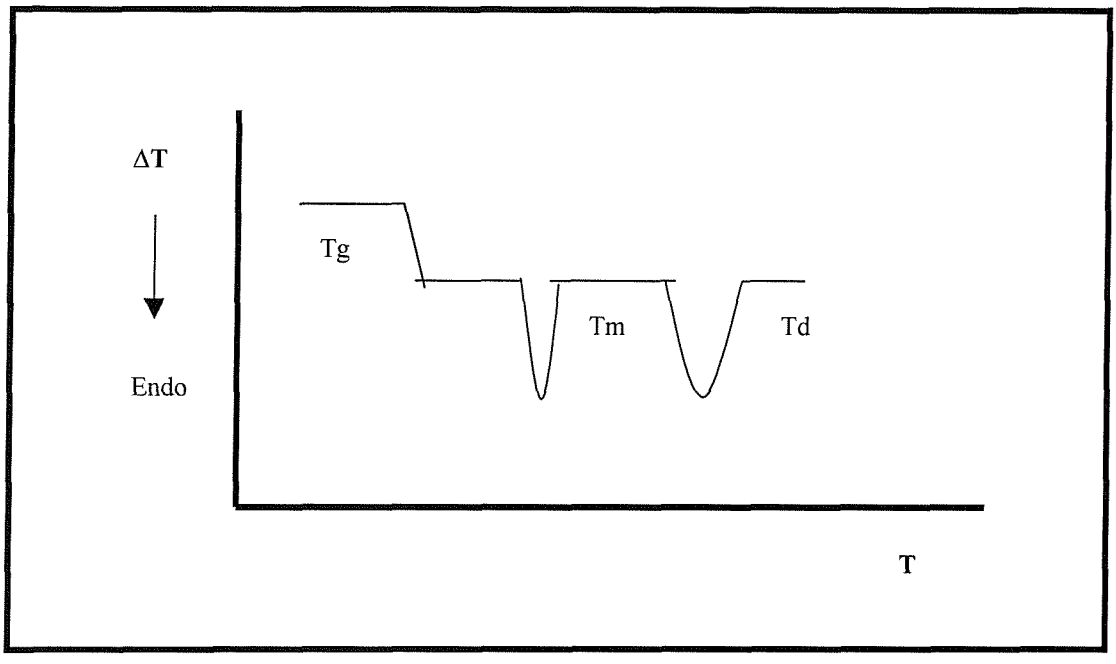

Figure (2.5) A schematic diagram of a DSC curve of a polymer sample showing the three most studied transitions; T_g, T_m and T_d.

2.4.2 Experimental procedure

DSC experiments were carried out on a Seiko SSC/5200 instrument. Measurements were performed by heating the sample first to 150 °C to make it homogeneous and well dispersed in the Al pan. The sample was then cooled down to –100 °C and heated up again to 150 °C under nitrogen gas flow. The scan rate was 10 °C/min.

2.5 Thermogravimetric Analysis, TGA

2.5.1 Theory

In a TGA experiment the mass of a substance is measured as a function of temperature. [5] This is usually associated with a chemical change. In polymers, TGA is mainly used to determine the amount of additives or moisture and also to check the thermal stability. Figure (2.6) below shows a typical TGA curve.

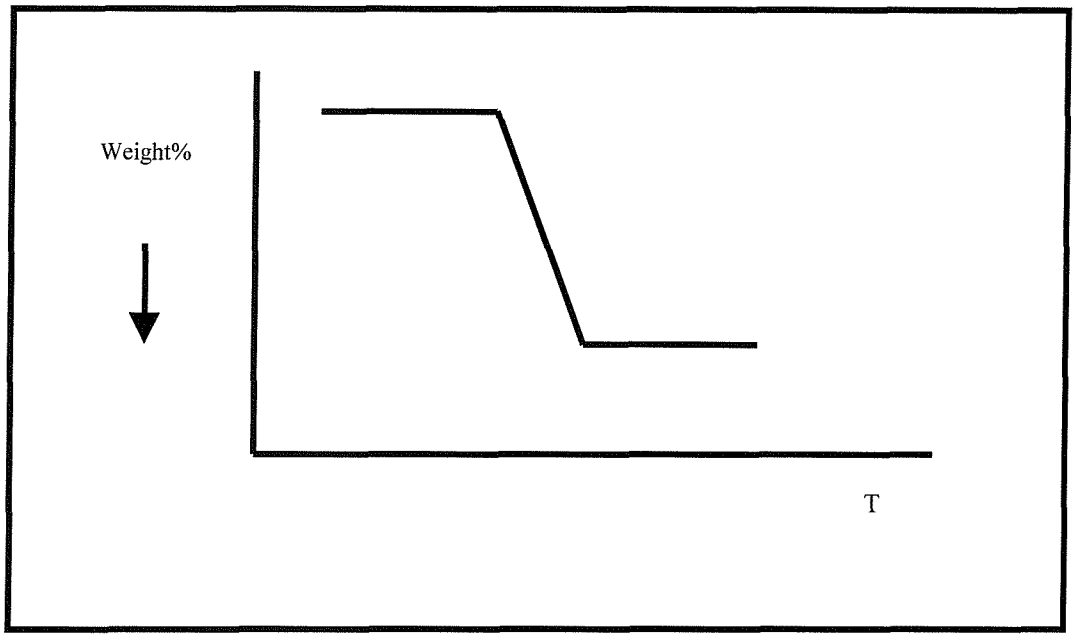

Figure (2.6) A typical TGA curve showing the mass loss as a function of temperature.

2.5.2 Experimental procedure

TGA experiments were performed using a TG/TDA 220 instrument to heat the sample from 25 to 600 °C under air flow with a heating rate of 10 °C /min.

2.6 X-Ray Diffracion

2.6.1 Background

XRD method is a powerful technique for determining the structure of polymers. [6] Any polymer sample with some degree of order is considered to be a two-phase system; crystalline phase and amorphous phase. The XRD pattern of such a system consists of a diffuse hallow due to the amorphous phase and a sharp maxima resulting from the crystalline portion of the sample. Figure (2.7) shows a typical XRD diffraction pattern of a semi-crystalline polymer sample.

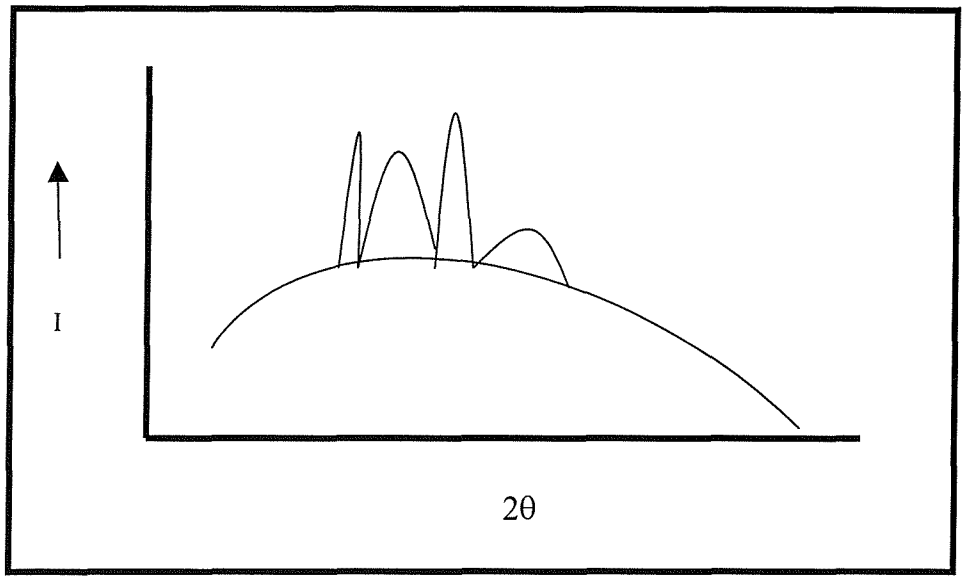

Figure (2.7) A schematic diagram of an XRD pattern of a semi-crystalline polymer sample.

2.6.2 Experimental procedure

Powder X-ray patterns were obtained using a Siemens D5000 (Cu-Kα, λ=0.15418 mm) diffractometer. Samples for analysis were prepared by cutting a piece of a film in a circular shape. The sample was then placed on a plastic holder and loaded to the diffractometer.

2.7 Infrared spectroscopy:

Infrared spectra were recorded on a computer interfaced FTIR system in the range between 4000-500 cm^{-1}. The IR of the films was taken by sandwiching a polymer film bewteen two KCl plates.

2.8 CO sensor

The sensor body (the electrodes on the substrate) was supplied by City Technology Ltd. The substrate was a ceramic chip with a thickness of 0.635 mm. The three electrodes were made of Teflon bonded platinum black. [7] The working and the counter electrodes were situated on the part of the sensor with laser-drilled holes to allow gas diffusion to the electrode/electrolyte interface. The working and the counter electrodes had 27 and 20 holes respectively. The working electrode was shaped in a circle with an area of 7.6 mm^2 whereas the counter and the reference electrodes were shaped as crescents with areas of 14.0 and 5.2 mm^2 respectively. A thin polymer film of EF1, see chapter three, was cast on the electrodes. After allowing for the solvent to evaporate, a glass slide was mounted on the sensor as shown in figure (2.8).

The working and the reference electrodes were short-circuited and the sensor was left in a dessicator containing a beaker full of water. The sensor was then placed in glass housing and exposed to gas as shown in the schematic diagram of figure (2.9). The computer-controlled system allows for the variation of CO concentration between 0-1000 ppm with a constant gas flow of 200 cm^3/min. The sensor was connected to a potentiostat, Citystat supplied by City Technology. The gas flow and its composition were controlled by two mass flow meters. The gas was humidified by bubbling it through a flask filled with a saturated solution of a salt to give the desired humidity. The humidity of the saturated salts were checked by placing a beaker filled with the solution along with a domestic-humidity meter in a desicator for two days. The obtained humidities of the salts were are shown in table 2.1

Table 2.1: Measured relative humidities of of the saturated salts used in the sensor measurements.

Saturated salt	Stated relative humidity[8]	Measured relative humidity
$CaCl_2.6H_2O$	32	42
$Ca(NO_3)_2.4H_2O$	51	48
KBr	84	70

.

The pre-equilibration with water was needed because preliminary experiments on the sensor showed that the sensor has no response at all relative humidities except at 100 % where it showed a background current of only 0.3 nA. This suggests that the polymer film was too dry to supply the water required for the oxidation of CO to take place.

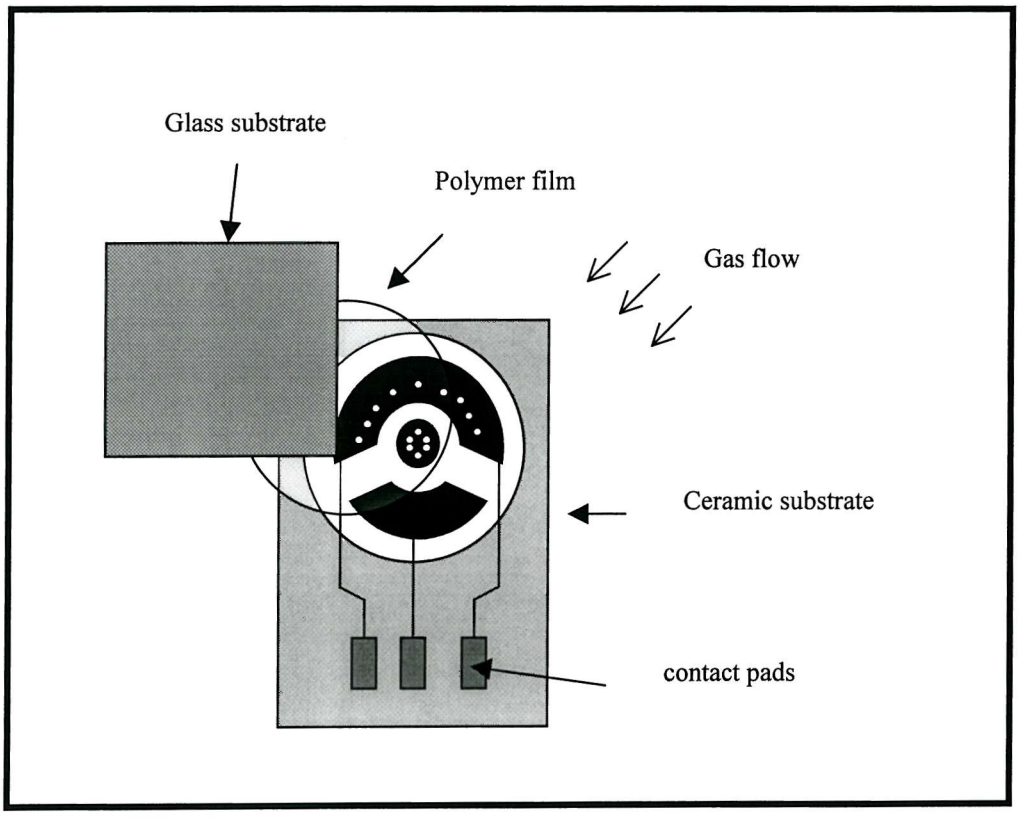

Figure (2.8) A schematic diagram of the fabrication of a planar CO sensor.

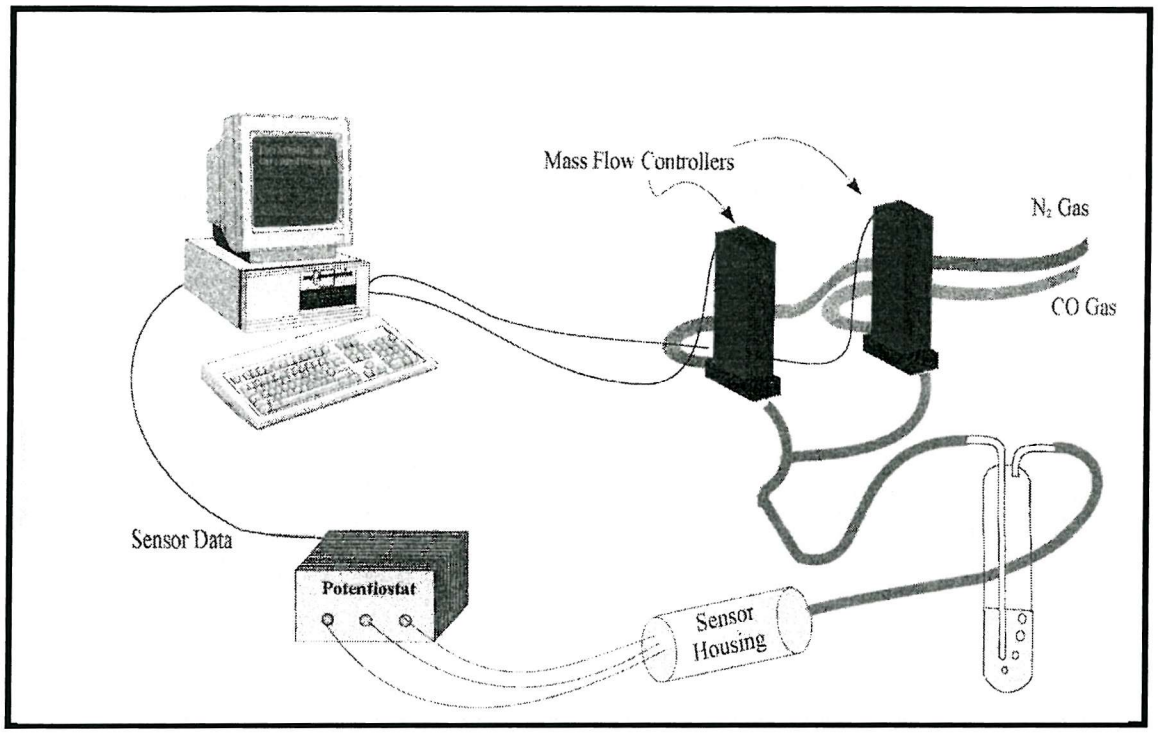

Figure (2.9): A schematic diagram of the rig used to test the sensor.

2.9 Cyclic voltammetry

Cyclic voltammograms at a Pt electrode were obtained using a conventional three-electrode-cell. A Pt electrode with a 0.5 mm diameter was used, the electrode was polished each time before use with 1 and 0.05 μm Alumina. The counter electrode was a Pt gauze while the reference electrode was a saturated calomel electrode. The potential was ramped using a Sycopel potentiostat. For the experiment with 0.2 M IMI:PC electrolyte the cell was assembled inside the glove box and then was taken out to obtain the voltammograms.

Cyclic voltammograms at the gap cell were taken in a similar cell. In this case the device worked as the working electrode and used a Pt gauze counter electrode and a saturated mercury sulphate electrode (MSE) as the reference electrode. The cell was purged with argon for half an hour and the cyclic voltmmograms were obtained using a home-built potentiostat.

References

1 E. Linden and J. Owen, *British Polymer Journal*, **20** (1988) 237.

2 "Polymer electrolyte reviews 1", Ed. By J. MacCallum and C. Vincent, Elsevier, London, 1987, P 250.

3 The devices were ordered from Warwick Center for Microtechnology, University of Warwick.

4 "Polymer synthesis and characterization", By S. Sandler, W. Karo, J. Bonesteel and E. Pearce, Academic Press 1998, London, P. 120

5 Ref.. 4, P. 108.

6 Ref. 4, P. 107.

7 K. P. Van Der Wal, N. De Rooij and M. Koudelka. *Sensors and Actuators B*, **35-36** (1996) 119.

8 The handbook of chemistry and physics, 70th Edition, CEC press 1989-1999, P E-43.

Chapter Three

Results and discussion

Preparation and characterisation of imidazole-based polymers

3.1 Compatability and stability of the polymer films

3.1.1 PVdF:IMI:PC and PVdF-HFP:IMI polymers

PVdF and PVdF-HFP were first investigated as polymeric host matrices for IMI liquid. Polymer films incorporating either of the two polymers and IMI have been prepared over a large composition range. The films were visually opaque. However investigation under the Optical Microscope reveals microscopic phase segregation as can be seen in figure (3.1A).

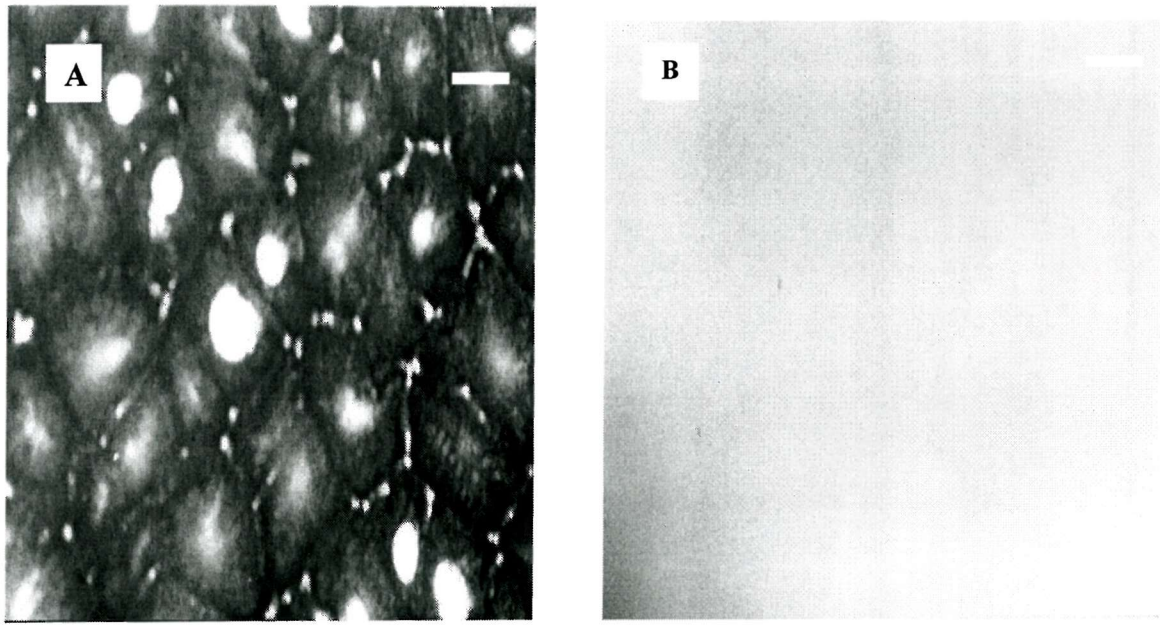

Figure (3.1) Optical microscopy pictures of (A): a PVdF-HFP;IMI film and (B): a PVdF-HFP:IMI:PC film. The white bar in the figure corresponds to 50 μm.

This observation suggests that IMI is insoluble in either of the polymer hosts. Therefore a solvent should be used to aid miscibility between IMI and the polymeric matrix. The solvent should have the following characteristics:

1 Compatibility with both IMI and PVdF-HFP.
2 High boiling point, high dielectric constant and low viscosity.
3 Good electrochemical properties, *e.g.*, wide electrochemical window.

One of the non-aqueous solvents that was found to satisfy all of these conditions is Propylene carbonate, PC. Due to the lower crystallinity of PVdF-HFP as compared with PVdF, it was used to make the films. Films incorporating IMI, PC and PVdF-HFP were transparent and homogeneous as shown in figure (3.1B). Initial investigations indicated that the properties of the films were highly dependent on the ratio of the three components. Films of various PVdF-HFP:IMI:PC compositions were prepared to optimise the amount of PC needed for dimensional stability and homogeneity of the films. The results are shown in terms of a composition diagram in figure (3.2). The black circles in the triangle emphasises compositions where the films are homogeneous and dimensionally stable. It is observed from the diagram that the amount of PC added to polymer is critical. Adding less than 7.5 w.t.% gave inhomogenous films, red circle, whereas adding more than 45 w.t.% gave fragile films, white circle. From the diagram we can also notice that when less than 30 w.t.% of the polymer host was added fragile films were obtained, blue circle.

In salt/solvent/polymer systems composition diagrams [1] are not common and very few have been reported. Previous studies on ionic liquid/polymer systems have focused on matching ionic liquids with suitably miscible commercial polymers. Wherever ionic liquid/polymer incompatibility was found alternative polymer hosts were sought. An alternative approach was taken for solving the miscibility problem in which a co-solvent was added to the system. The need for a composition diagram arises in order to work as a guide in preparing films with the best compromise of mechanical strength, homogeneity and ionic conductivity.

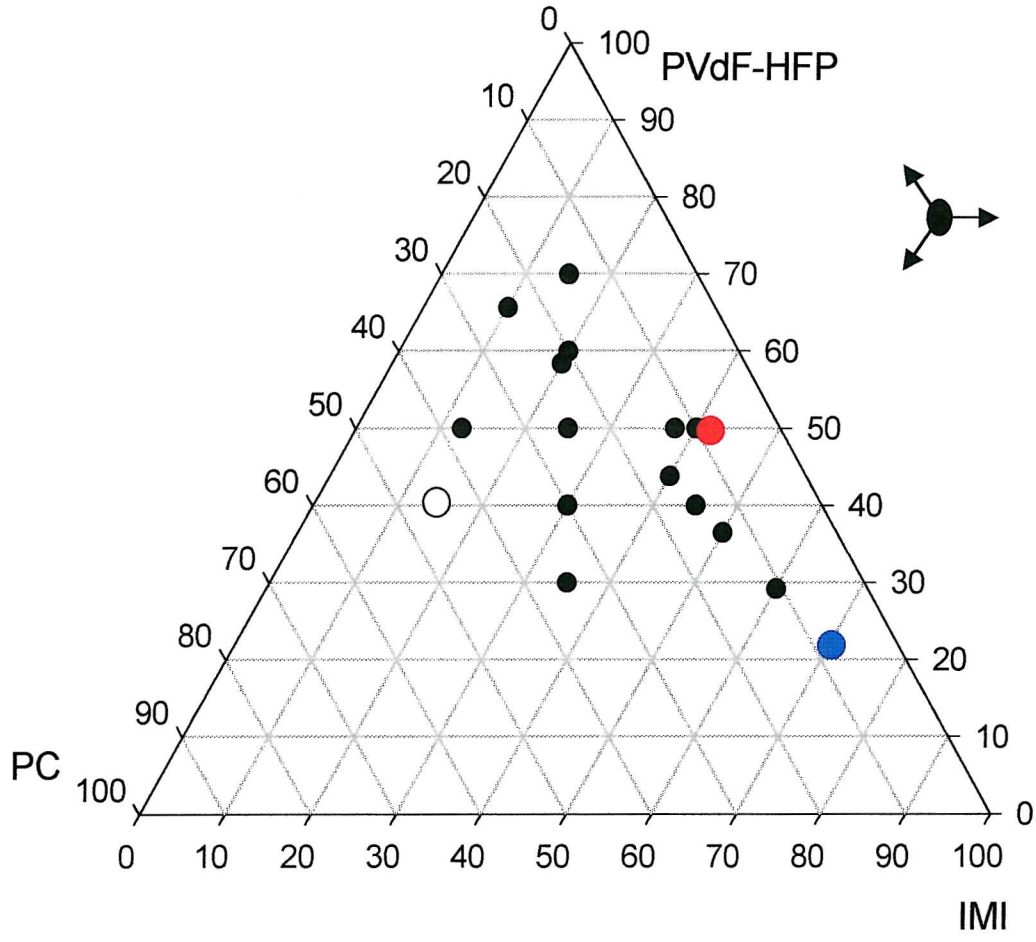

Figure (3.2) Composition diagram of polymer films containing PVdF-HFP, PC and IMI. The intercept of the gridlines with the axis represents a polymer film with the corresponding weight percent of each component. Black circles represent films which are homogeneous and dimensionally stable. The red circle is an inhomogeneouse film. Blue and white circles are fragile films.

3.1.2 PEE:IMI polymer films

It has been shown in the previous section that polymer films incorporating PVdF-HFP and IMI could not be made without use of to a co-solvent. This presents a problem due to the eventual evaporation of PC from the films and the consequent deterioration in their properties. Other hosts were sought and one alternative was PEE.

Many films with various PEE:IMI content have been prepared. The addition of IMI did not appreciably change the appearance of the PEE from which it was concluded that the two components were mutually compatible. This has also been confirmed by the optical microscope. Films with IMI content between 5-40 % were elastic and rubbery with good mechanical strength, whereas films with higher content were viscous liquids. This is obviously due to an increase in the mobility of the chains arising from the plasticising effect of IMI on the polymer matrix.

3.1.3 IMI: (PMMA:PVdF-HFP) polymer films

Although PEE:IMI films were homogeneous and gave good conductivities as will be discussed later the films were not free standing at film thicknesses less than 100 micrometer as required for the conductivity measurements. An alternative host with good mechanical strength was subsequently sought. Polymer blends are known to give films with high strength [2] and so a blend of PMMA:PVdF-HFP was chosen to make films containing IMI.

Polymer films composed of IMI and PMMA only were prepared in many proportions and found to be homogeneous. As discussed earlier, IMI is insoluble in PVdF-HFP. This was advantageous when using a polymer blend as a polymeric host. Here IMI is miscible in PMMA to form a continuous phase and immiscible in PVdF-HFP. The result is another phase of PMMA:PVdF-HFP that provides the required mechanical strength.

Polymer films incorporating IMI:(PMMA:PVdF-HFP) were prepared in different ratios. The resulting films were highly transparent in appearance with mechanical strength highly dependent on the amount of IMI, as observed in table (3.1).

Table (3.1): Mechanical strength of various IMI:(PMMA:PVdF-HFP) films.

IMI content / w.t. %	Mechanical strength
21	Stiff-rubbery
33	Stiff-rubbery
40	Rubbery
60	Rubbery-like
71	Liquid-like
80	Liquid-like
90	Liquid-like

3.2 Conductivity of the polymer films and the liquids

3.2.1 Conductivity studies on the liquids

The room temperature conductivity of IMI was measured using the liquid cell shown in figure (2.1). It was found to be 5.0×10^{-3} S/cm. It was also measured for various IMI:PC solutions as a function of concentration and the results are shown in figure (3.3). The conductivity of the solutions increased with the increase in concentration. A maximum value was reached at 1.4 M solution. The occurrence of a maximum in the conductivity-concentration plots of concentrated solutions is a normal behaviour. [3] As at the dilute end, the conductivity increases due to the introduction of the charge carriers, then shows

a maximum and decreases afterward. The decrease is expected since the conductivity is a product of the number of charge carriers and mobility. At high solution concentrations the increase in the number of charge carriers is counterbalanced by the decrease in their mobility. Such decrease could be ascribed to an increase in viscosity or to the formation of less mobile higher ion aggregates. [4]

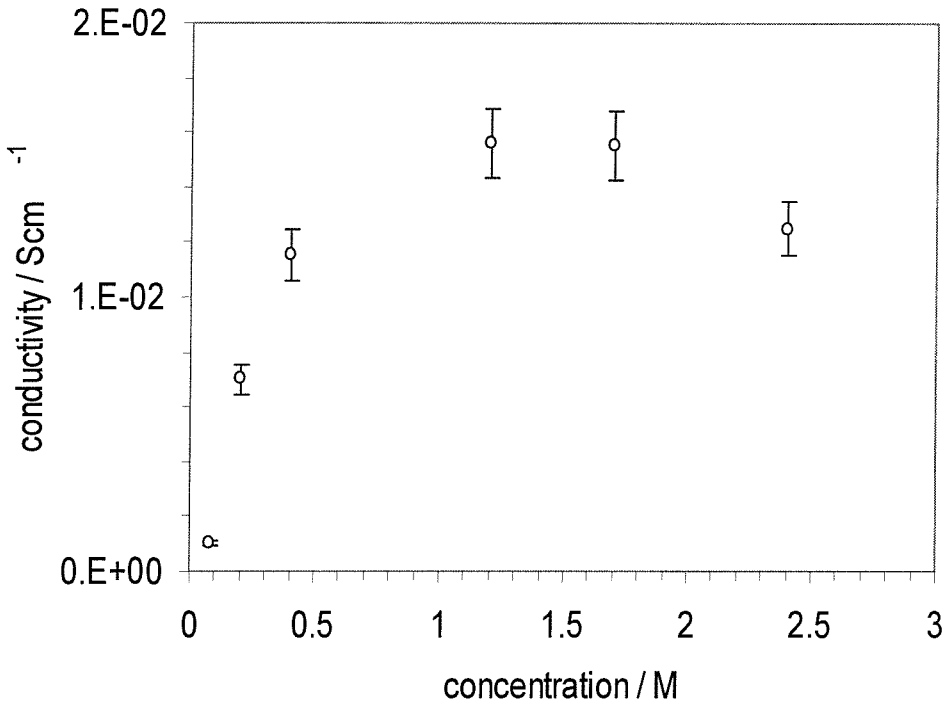

Figure (3.3): A plot of the conductivity of various IMI:PC solutions

3.2.2 Conductivity studies on the polymer films

3.2.2.1 PVdF-HFP:IMI:PC polymer films

As can be deduced from figure (3.3) 1.2 M IMI:PC solution has one of the highest measured conductivities. Therefore, it has been chosen for optimisation of the conductivity of PVdF-HFP:IMI:PC films. Films incorporating 1.2 M IMI:PC solution in various weight ratios (10-70 w.t.% IMI content) were prepared with a typical thickness of 0.20 mm (± 0.01). All the films had good mechanical properties with the exception of the 70% sample which was fragile and easily torn. Room temperature conductivity of the films was measured using the cylindrical cell. Figure (3.4) shows the logarithm of the measured conductivities against the 1.2 M IMI:PC liquid weight content. It can be observed that the logarithm of the conductivity increases linearly with the amount of added solution. A break in the conductivity was observed at the 40 % content. Similar behaviour was reported by Tsunemi *et al* [5] for $LiClO_4$/PC/PVdF films at a constant $LiClO_4$/PC weight percentage. They have attributed that behaviour to the state of $LiClO_4$ dispersion before and after the break point. MacFarlane *et al* [6] have studied free volume as a function of salt concentration in the PAN:LiTFSI polymer-in-salt system. They observed that the mean free volume cavity size increased as a function of w.t. % content of LiTFSI up to 45 w.t.% at which point it levelled off. They suggested a percolation threshold phenomenon to explain the observation.

The linear increase is in accordance with what is expected for ionic liquid/polymer gels as has been discussed in the introduction. However, the break in the conductivity could be attributed to a percolation threshold. Before the break point the system can be thought of as separate IMI:PC domains distributed randomly within the PVdF-HFP matrix. As the content increases domains interconnect with each other up to the break point where they form a continuous conduction path showing a behaviour similar to the neat liquid. Figure (3.5) shows a schematic diagram of the proposed model.

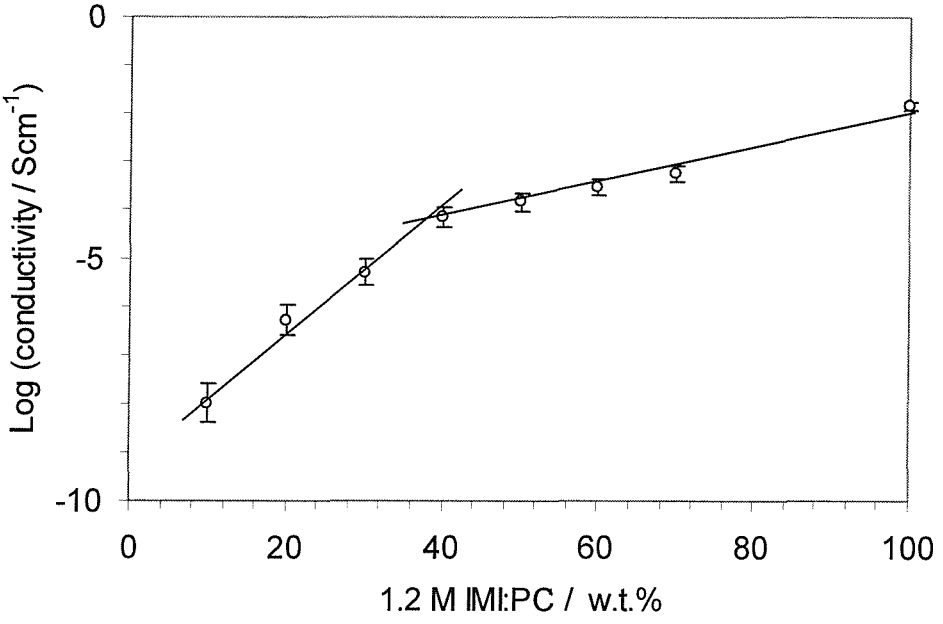

Figure (3.4): Plot of the logarithm of the room temperature conductivity of various (1.2 M IMI:PC):PVdF-HFP polymer films as a function of the liquid weight content.

As mentioned in the introduction the linear relationship of Log(conductivity)-composition of polymeric gels was explained by considering that the liquid itself is highly conductive in its own right and the polymer chains do not influence the liquid conductivity. [7] The purpose of the polymer is thus to work as a stiffener for the liquid to give free standing films

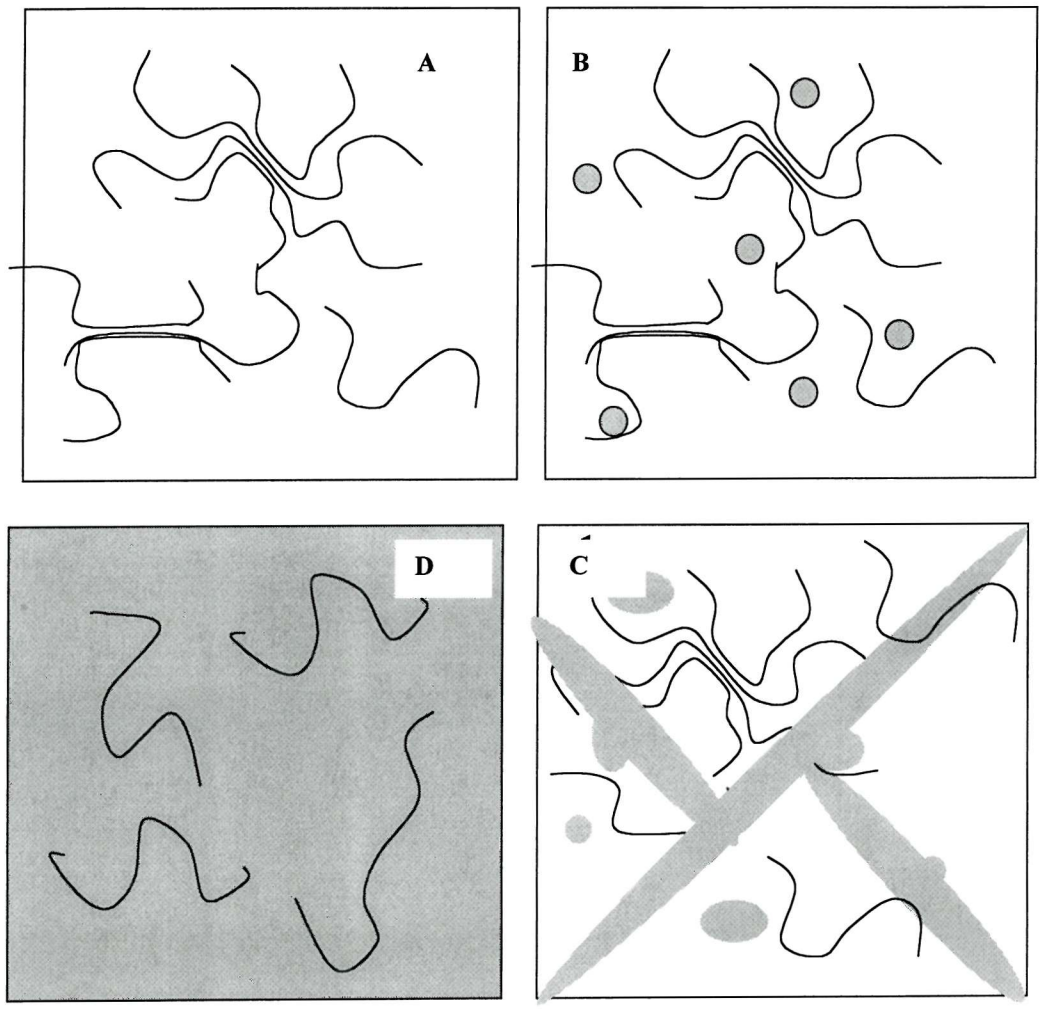

Figure (3.5) A schematic diagram of the proposed percolation threshold mechanism for the conductivity of PVdF-HFP:IMI:PC polymers.

3.2.2.2 PEE:IMI polymer films

Figure (3.6) shows the logarithm of the room temperature conductivity of PEE:IMI films as a function of IMI content. The plot showed a linear relationship. This results are in agreement with Watanabe's findings that molten salt-polymer systems shows a linear dependence of their conductivity as a function of salt content as the conductivity does not involve any polymeric chain movement and it is only arising from the neat liquid itself. [8]

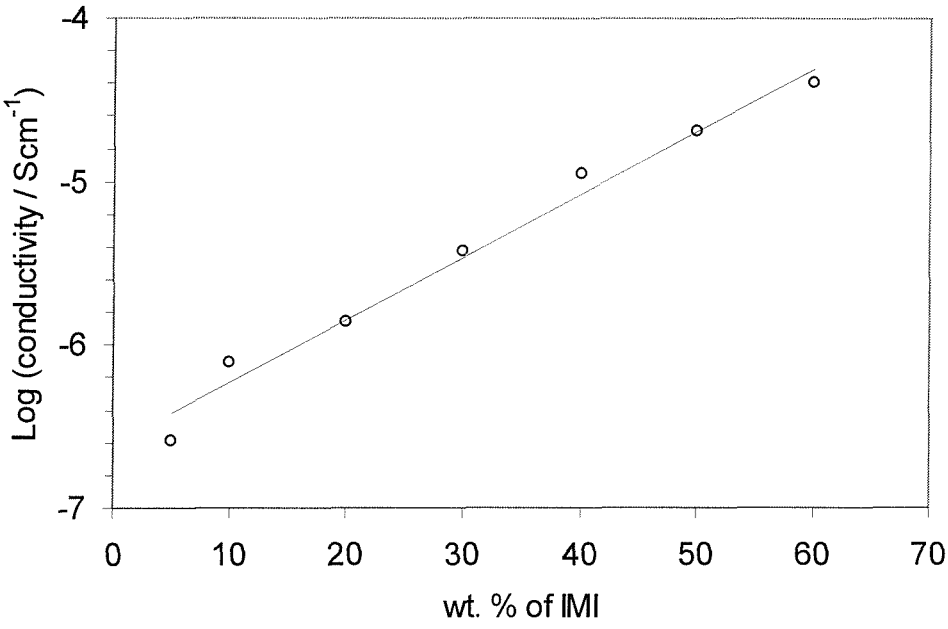

Figure (3.6): Concentration dependence of the logarithm of the room temperature conductivity of PEE:IMI films,

3.2.2.3 (PMMA:PVdF-HFP):IMI polymer films:

Ionic conductivity of (PMMA:PVdF-HFP):IMI films was measured as a function of IMI weight content and the results are shown in figure (3.7):

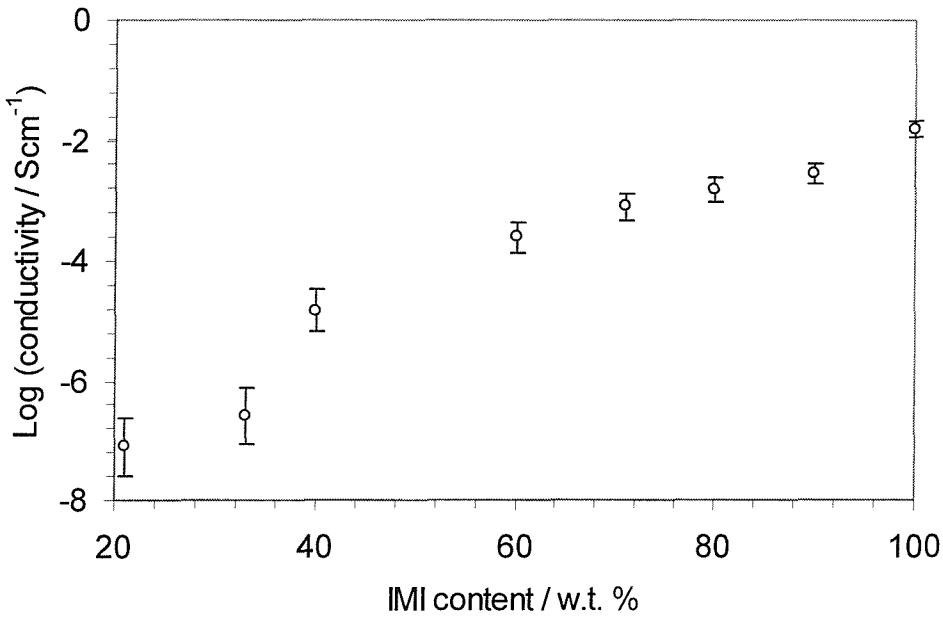

Figure (3.7): Plot of the logarithm of the room temperature of the conductivity of (PMMA:PVdF-HFP):IMI films as a function of IMI content.

From the graph it can observed that the log of the ionic conductivity of the films increases almost linearly as the amount of IMI was increased. The conductivity showed a sharp increase above the 33% composition, which corresponds closely with the mechanical strength of the film, since at that content mechanical properties go from a stiff-rubbery to a rubbery behaviour. This also indicates a possible percolation threshold at that composition. Samples with weight ratios between 71-90 could be treated as liquids as mentioned in table 3.1. The highest obtained conductivity of the latter is still one order of magnitude less than that of the IMI.

As discussed in the introduction a dual phase architecture has been suggested for polymer films incorporating the polymer blend/liquid.[9] This allows for the formation of ion-conducting pathways of IMI:PMMA in an inert polymer matrix of PVdF-HFP/PMMA to provide the mechanical integrity.

3.2.3 Temperature-dependence of the conductivity of the films

3.2.3.1 50% IMI:PC:PVdF-HFP polymer films

Figure (3.8) shows the temperature dependance of ionic conductivity of IMI, 2.5 M IMI:PC solution and the EF1 polymer film. The plots were curved and were fitted to the VTF equation by selecting the best straight lines according to a linear least squares analysis. Values of σ_0, B and T_0 resulting from the fit are shown in Table (3.2).

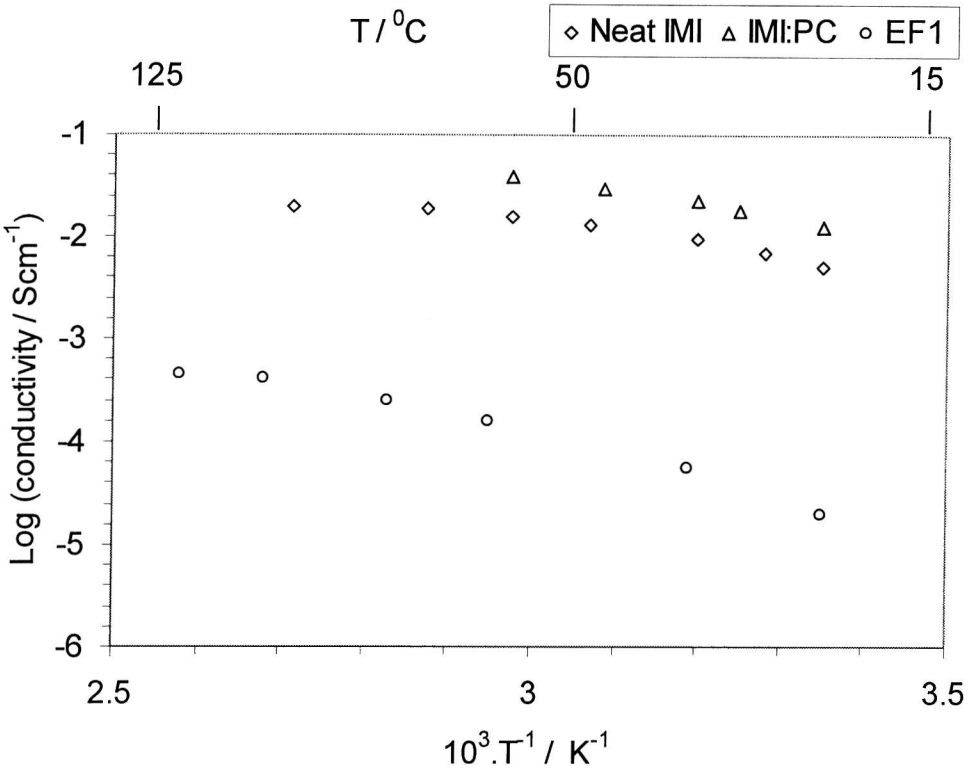

Figure (3.8): Temperature dependence of ionic conductivity of IMI, 2.5 M IMI:PC and EF1.

Table (3.2): VTF analysis results for IMI, its PC solution and its PVdF-HFP polymer.

	σ_0	B / kJ mol^{-1}	T_0 / K
IMI	2.9	0.9	245
IMI:PC	1.3	2.1	210
EF1	4.9	3.9	216-220

The B values have increased from 0.98 kJ mol^{-1} for the IMI liquid to 2.10 for the solution to 3.96 for the polymeric gel. Such an increase implies an increase in the activation energy for ionic conduction. As for the polymer film, such a value is in the same order with the reported values for PEO:salt:solvent polymers. [10]

3.2.3.2 PEE:IMI polymer films:

Figure (3.9) shows the temperature dependence of the conductivity of the films. The plots showed a gradual increase in conductivity as temperature was increased with an overall curved trend. This indicates a VTF behaviour and therefore the data were fitted by linear then non-linear least squares regression analysis to the VTF equation. The results of the analysis are shown in tables (3.3) and (3.4), respectively.

Table (3.3): Results of VTF analysis for 10, 40 and 60% IMI:PEE films. The IMI data are shown for comparison.

	A	B / kJ mol^{-1}	T_0 / K
10%	7.7	3.6	232-237
40%	2.9	9.1	168-177
60%	4.6	3.4	220-223
IMI	2.8	0.9	245

Table (3.4): Non-linear VTF analysis results for different PEE:IMI films.

	A	% error	B / kJ mol^{-1}	% error	T_0 / K	% error
10%	7.92	0.22	3.27	41.38	234	10.86
40%	3.02	1.40	8.73	460.14	172	78.57
60%	4.72	0.22	3.39	51.52	221	15.27

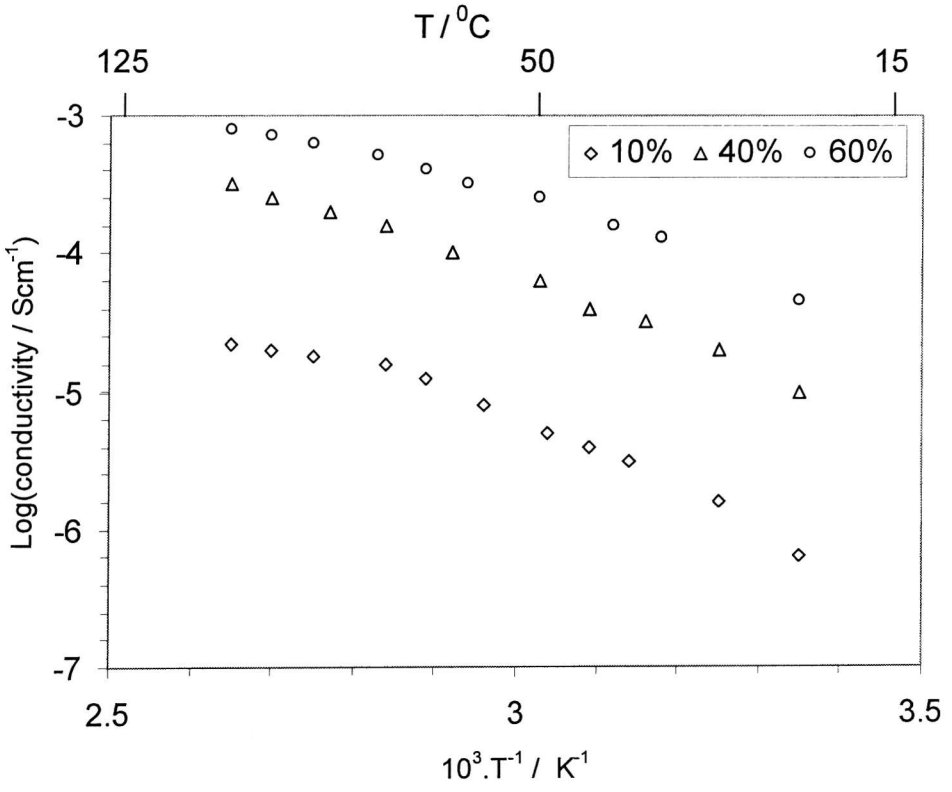

Figure (3.9): Temperature dependence of conductivity of 10, 40 and 60% IMI:PEE samples.

analysis it is difficult to estimate the errors because the B values can vary significantly with small variations in the choice of T_0 to give a straight line plot. The non-linear analysis package gave computed error, which as seen in table (3.4) can be very large indeed. In the case of very large errors it may be questioned whether the VTF analysis itself is an appropriate model for the temperature dependence analysis.

However, the results of the two analyses are very close. The B parameter showed an expected larger value for the films as compared to the IMI liquid indicating a higher activation barrier for the films. Tg is usually 50 K below the T_0,[11] The fitting gives an estimate of 271 K for the Tg of the 60% sample. It is the same as the measured value of 221 K which suggests that T_0 is actually equal to Tg.

The data for the 40% sample showed a large percentage error and therefore have been ignored in the discussion.

3.3 Characterisation of the polymer films:

3.3.1 IMI:PC:PVdF-HFP films:

To study the properties of the films, three polymer films of IMI:PC-50% PVdF-HFP with different compositions, table (3.5), have been prepared.

Table 3.5: Composition of three 50% IMI:PC-PVdF-HFP films

IMI:PC solution (M)	IMI:PC weight ratio	Polymer sample
2.5	1:1	EF1
0.83	1:3	EF2
7.48	3:1	EF3

Figure (3.10) shows the X-ray diffraction patterns of pure PVdF-HFP, EF1, EF2 and EF3. All the films have shown poor crystallinity. Pure PVdF-HFP, EF1 and

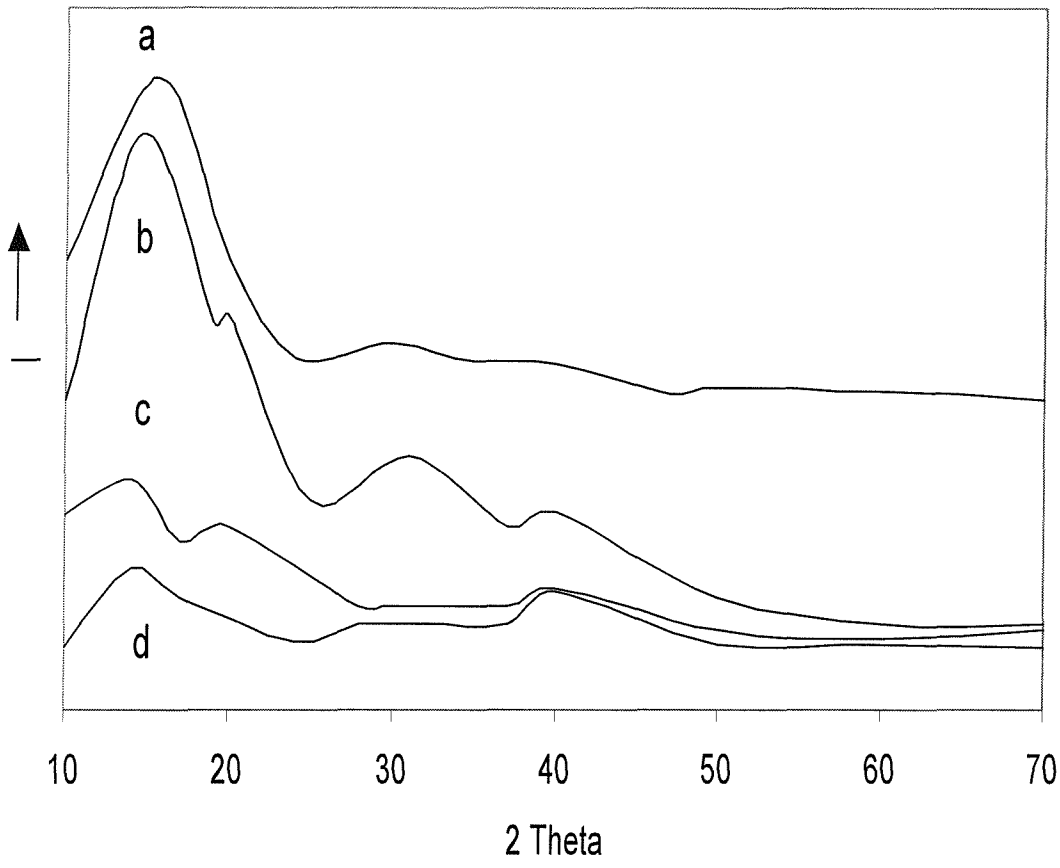

Figure (3.10): Smoothed X-ray diffractions of (a) EF2, (b) EF1, (c) EF3 and (d) pure PVdF-HFP. Values of the intensity are arbitrary.

EF2 samples have exhibited similar pattern. They have shown a parent peak at 14° (2θ) and two smaller ones at 30° and 40° corresponding to the crystalline structure of the PVdF-HFP polymer, whereas EF3 has shown an extra peak at 20°. This might have originated from a different crystalline structure of the parent polymer, or from PVdF moieties in the polymer sample [5]

Figure (3.11) display DSC plots for EF1 and EF2 films. Both showed a single sharp peak at about 95 °C. The peak corresponds to the melting of the pure PVdF-HFP polymer. In the case of EF3 film the peak was slightly shifted to a lower temperature. The fact that no other peaks has been observed suggests that no hybrid polymer of any kind has been formed between IMI and PVdF-HFP and also no melting or freezing of the IMI:PC liquid had occurred within the tested temperatures.

The DSC curves did not show any glass transition behaviour despite the use of slow and fast scan rates. This has not been investigated any further and could be attributed to technical problems.

Thermal stability of the films was checked by Thermogravimetric analysis technique. Plots for the mass loss as a function of temperature for EF1 and EF2 films are shown in figure (3.12). Both samples show a similar pattern of two step degradation process. The first step occurred up to 225 °C which is mainly due to a possible evaporation of PC and imidazole from IMI. The second step which occured at about 300 °C involved evaporation of the fused salt in the IMI and the start of PVdF-HFP degradation. Generally, the two samples have shown a good thermal stability up to 130 °C with weight loss less than 5% and 10% for the EF3 and EF1 samples respectively.

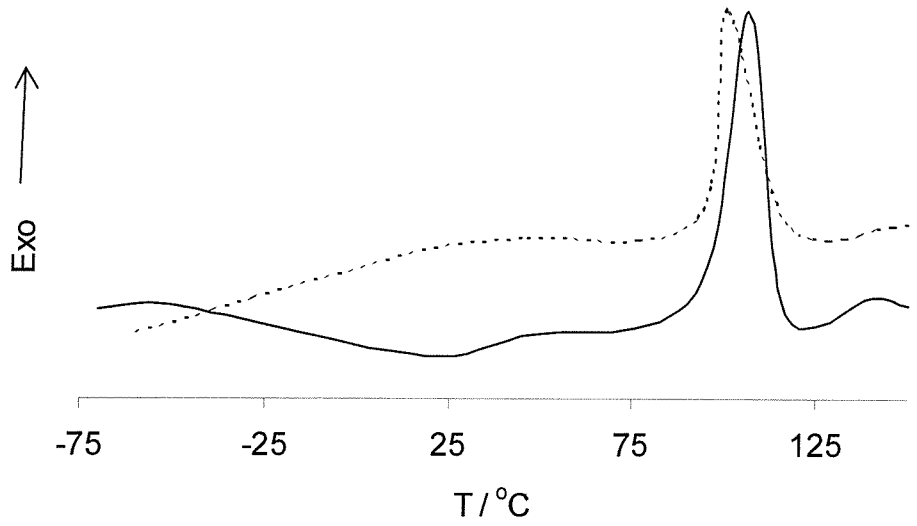

Figure (3.11): DSC curves for EF1 and EF3, (--).

3.3.2 IMI:PEE films:

Figure (3.13) shows the differential scanning calorimetry curves of the 20% and 30% samples. The DSC curves show no peaks, indicating that no polymer-IMI complex, with any defined stoichiometry, has been formed. However, the curve showed a glass transition, which can be clearly seen in figure (3.14) for many films. The obtained Tg values of the films are summarised in table (3.6). Tg of the pure PEE is –43, this has been shifted to lower values as the amount of IMI content in the films was increased. Such shift was not very profound. Others have observed similar behaviour. [12] The decrease can mainly be ascribed to the plasticising effect of the IMI liquid on the polymer chains, this has also been noticed visually by the deterioration in the mechanical strength of the films.

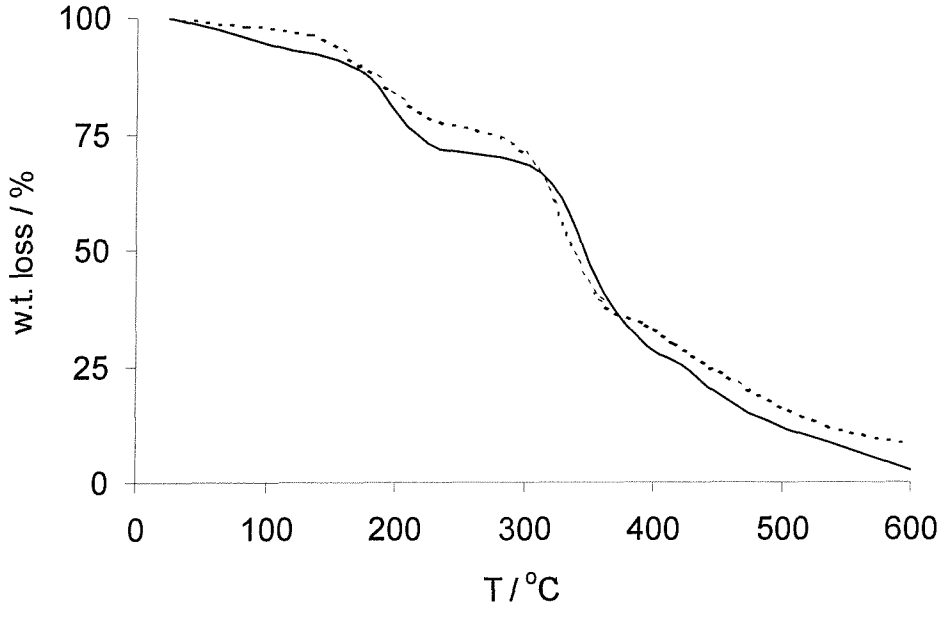

Figure (3.12) TGA curves for EF1 and EF3, (--), films..

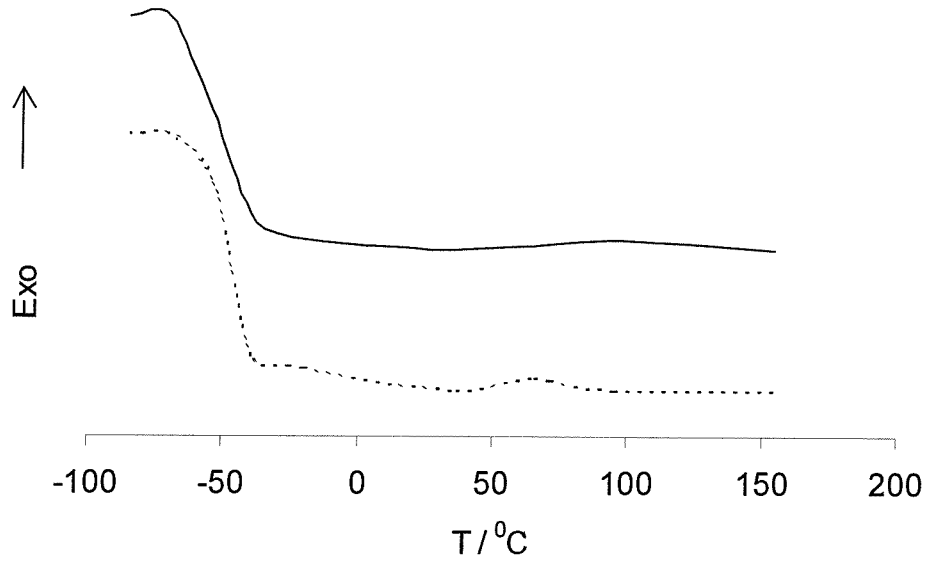

Figure (3.13): DSC curves for 20%, (...), and 30% samples.

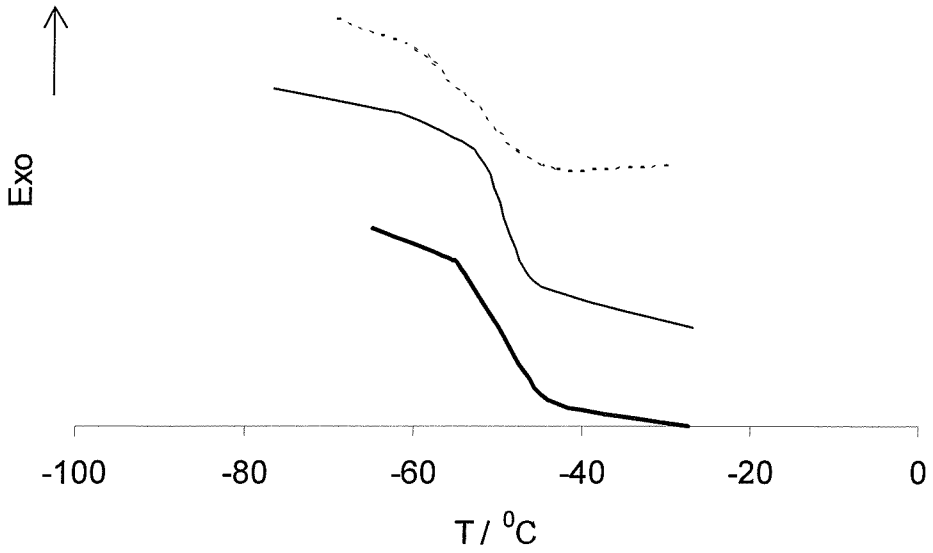

Figure (3.14): DSC curves for 20%, 30%, (—), and 60%, (...), samples.

Table (3.6): Glass transition temperatures of PEE:IMI as a function of added IMI.

IMI content / w.t. %	Tg / °C
0	-43
20	-47
30	-49
60	-52

The thermal stability of the films was checked by TGA. Plots for the mass loss as a function of temperature for a 50% sample is shown in figure (3.15). The plot shows a two-step degradation process; one starts at 175 °C due to the evaporation of imidazole from IMI and a second at 300 °C due to the PEE degradation. Silva *et al* reported that the degradation of PEE occurs in a single step at 350 °C. [12] The discrepancy might be attributed to the different source of the PEE as well as the state of the sample at the time of taking the measurements as the level of moisture in the sample affect can affect the degradation mechanism.

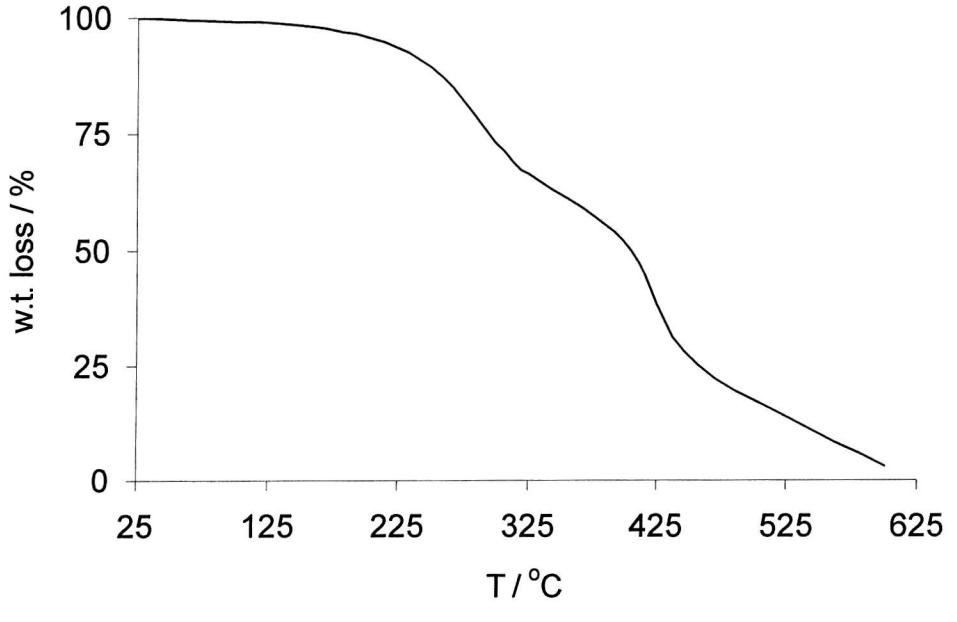

Figure (3.15): TGA curve for a 60% IMI:PEE film.

Figure (3.16) presents IR spectra registered for pure IMI, pure PEE and various PEE:IMI polymer films. The intensity of the vibration characteristics of the IMI bonds increases with an increase in IMI content of the films. However, the position of the peaks does not change. This can be clearly seen in the spectrum of the 60% sample, which mainly showed a similar pattern to the IMI. The fact that the spectra of the PEE:IMI films have shown no new peaks indicates that no interaction has taken place between the two.

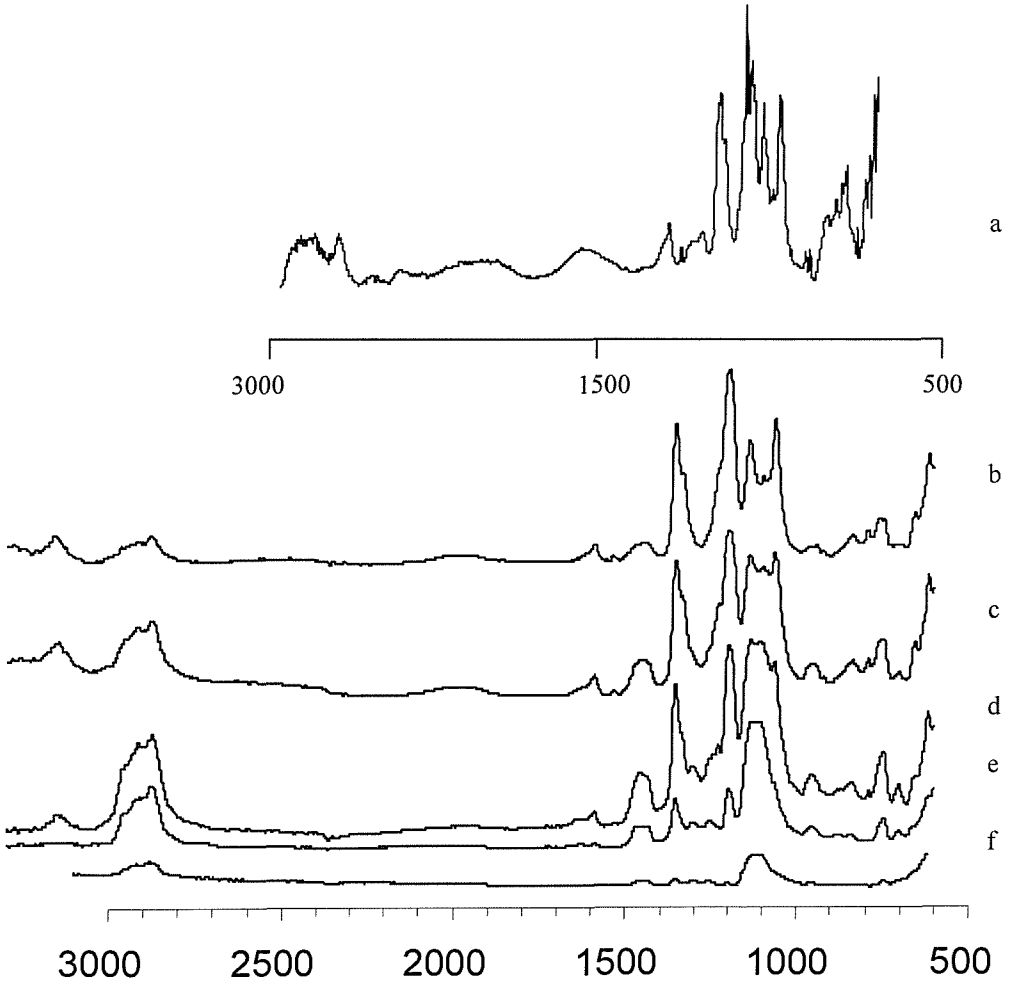

Figure (3.16) Infrared spectra of the neat IMI liquid ,a, pure PEE, f, 10, e, 20, d, 40 c, and 60% PEE, b.

3.3.3 IMI:(PMMA:PVdF-HFP) films:

Thermal stability of the films was checked by TGA. The plots of the mass loss as a function of temperature for 40% and 70% samples are shown in figure (3.17). Losses less than 4% of the total weight was observed up to 130 °C. A second large mass loss was observed at 280 °C due to the degradation of the two polymers. Generally, the two sample have shown good thermal stabilities.

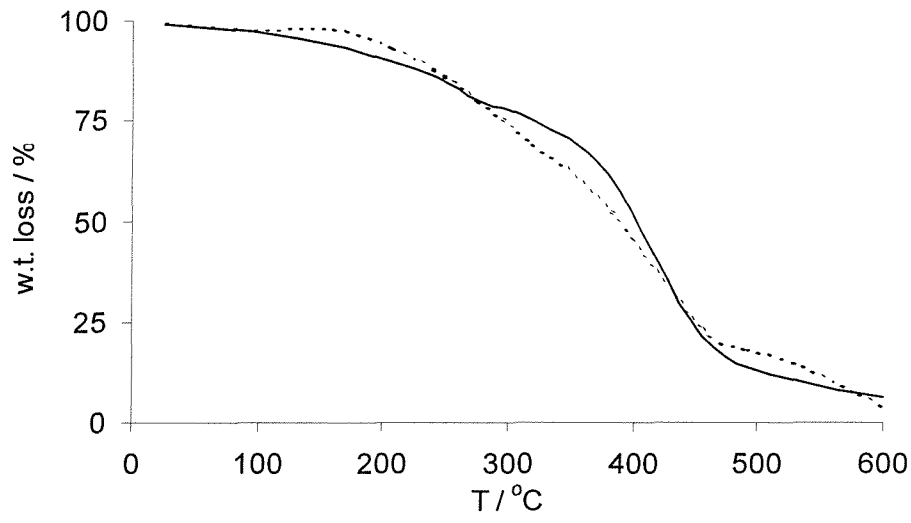

Figure (3.17): Thermogravimetric curves for (...) 40% and 70% samples.

References

1 K. Abraham, Z. Jiang and B. Carroll, *Chem. Mater.*, **9** (1997) 1978.

2 B. Oh and Y. Kim, *Solid State Ionics,* **124** (1999) 83.

3 "Ionic Liquids", Ed. By D. Inman and D. Lovering, Plenum Press 1981, New York, P 296.

4 "Comprehensive Treaties of Electrochemistry", Ed. By B. Conway, J. Bookris and E. Yeager, Plenum Press 1983, New York, vol. 5, P 223.

5 K. Tsunemi, H. Ohno and E. Tsuchida. *Electrochimica. Acta*, **28 (6)** (1983) 833.

6 D. Macfarlane, J. Sun, P. Meakin, P. Fasoulopoulos, J. Hey, M. Forsyth, *Electrochimica. Acta*, **40 (13)** (1995) 2131.

7 J. Fuller, A. Breda and R. Carlin, *J. Electrochem. Soc.*, **459** (1998) 29.

8 M. Watanabe, S. Yamada and N Ogata, *Electrochimica. Acta*, **40 (13)** (1995) 2285.

9 M. Matsumoto, *Polymer*, **36 (16)** (1995) 3243.

10 M. Armand, J. Chabagno and M. Daclot, in " Fast ion transport in solids ", Ed. By P. Vashista, J. Mundy and G. Shenoy, Elsevier, New York, 1979, P. 1319.

11 "Polymer electrolyte reviews 1", Ed. By 0. J. MacCallum and C. Vincent, Elsevier Applied Science, 1997, P. 193.

12 G. Silva, N. Lemes, C. Fonseca and M. De Poli, *Solid State Ionics*, **93** (1997) 105.

Chapter Four

Results and discussion

Amperometric CO sensors using polymer electrolyte

4.1 CO sensors incorporating IMI:PC:PVDF-HFP films:

A planar CO sensor was fabricated as described in chapter two using an EF1 polymer film, see chapter three. The sensor was then loaded into the CO sensing rig. A bias voltage of 0 vs the Pt/air reference electrode was applied on the working electrode. The response of the sensor was recorded as a function of CO concentration as well as relative humidity.

Figure (4.1) shows the response of a sensor, at various CO concentrations: (100, 200, 400 and 600 ppm) for relative humidity less than 5%. The measurements were taken in sequence and the sensor was allowed to go back to the background level after each measurement. The response is generally sluggish and noisy. The t_{90}, the response time for 90% of the signal, is about 4-5 minutes for the 600 ppm concentration. It can also be observed that the lower the concentration the longer the t_{90}.

Figures (4.2), (4.3) and (4.4) shows the sensor response at 42, 70 and 100 % relative humidities. The signal response is less noisy than at less than 5% and the t_{90} is shorter.

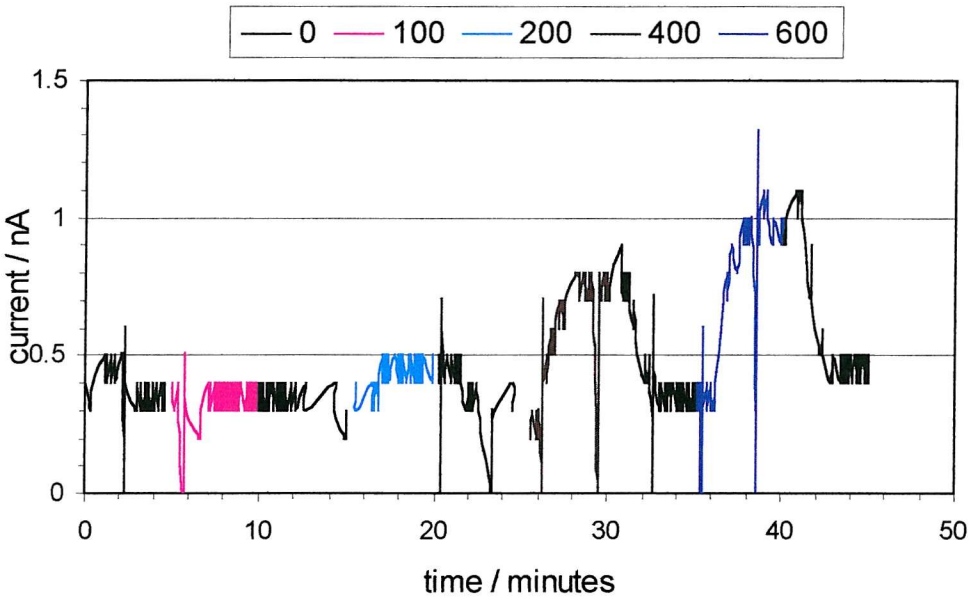

Figure (4.1) Response of the sensor exposed for various CO concentrations at relative humidity less than 5%. The numbers in the top represent the concentrations in ppm.

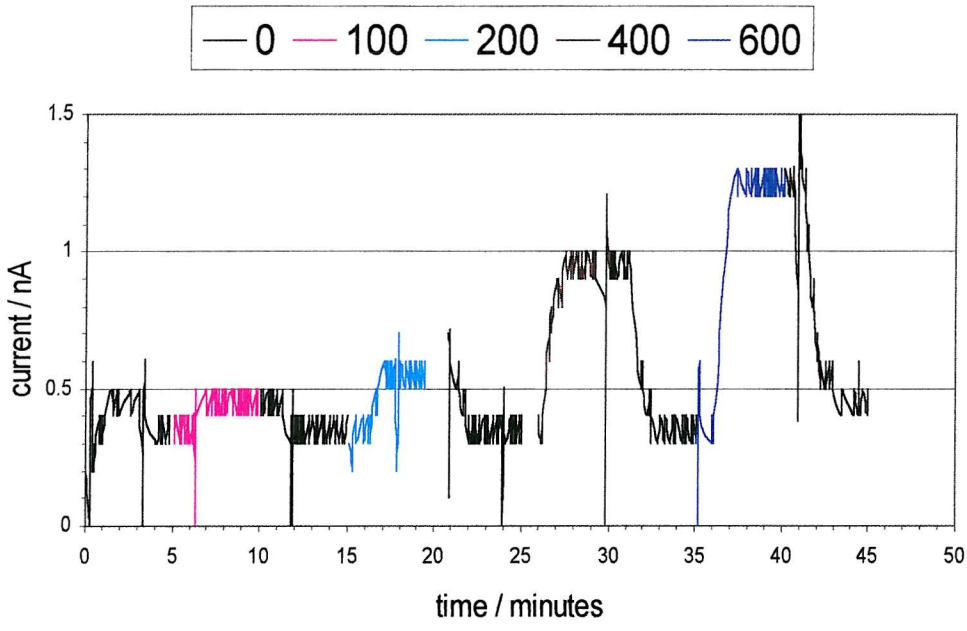

Figure (4.2) Response of the sensor at 42% relative humidity.

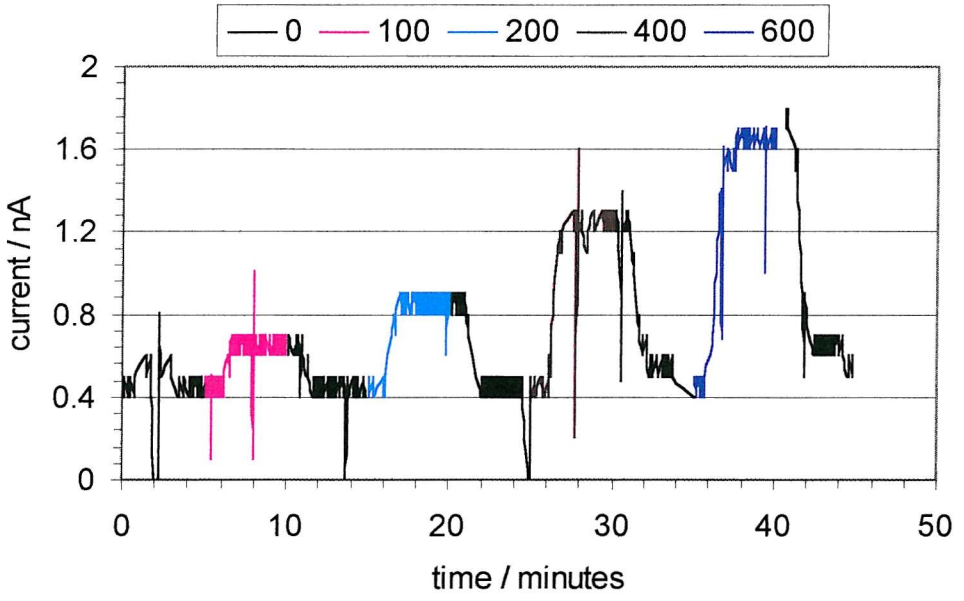

Figure (4.3) Response of the sensor at 70% relative humidity.

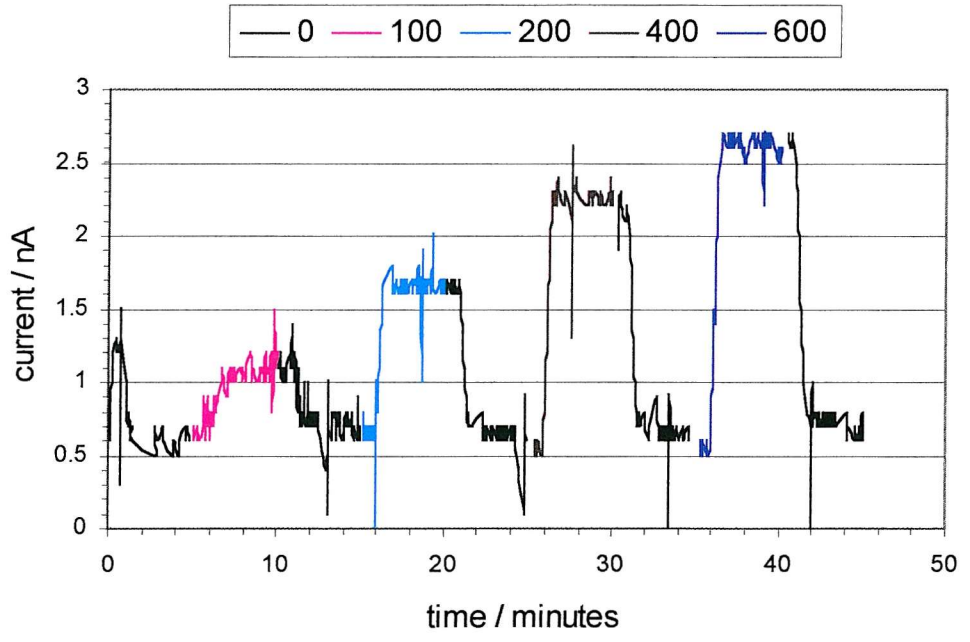

Figure (4.4) Response of the sensor at 100% relative humidity.

The CO oxidation current was measured as the difference in current when the sensor is exposed to CO and the background current when its exposed to air. Figure (4.5) shows the measured CO oxidation currents at the applied relative humidities. The oxidation current was a linear function of the relative humidity. Similar dependence has been observed by other research groups for sensors using NAFION or other proton conducting polymers as the solid polymer electrolyte. [1] We can also observe that a slight deviation from linearity at 100 % relative humidity.

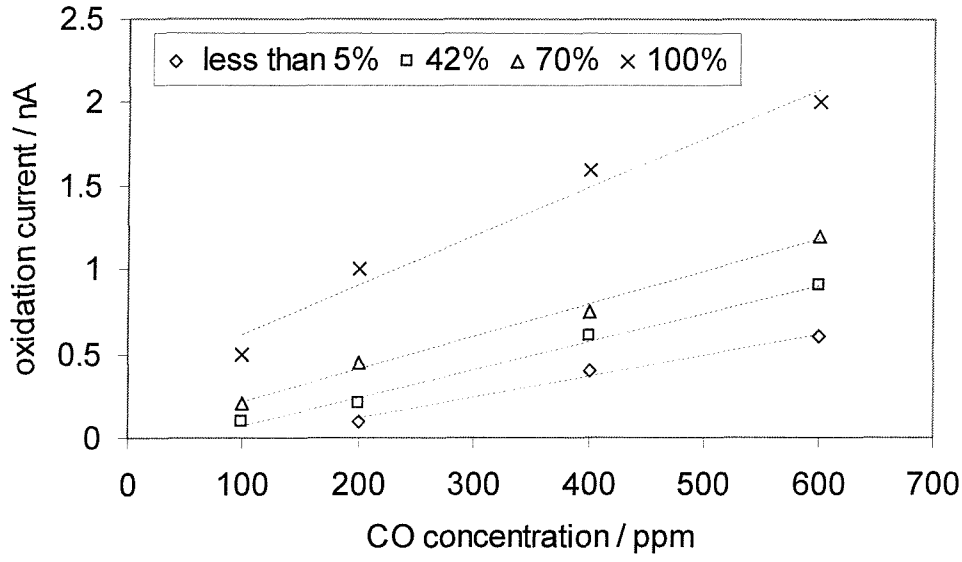

Figure (4.5) Measured CO oxidation currents vs CO concentrations at different relative humidities.

The background current, the current when the sensor is exposed to air, was also found to be a function of relative humidity as shown in figure (4.6). Background currents are a familiar behavior in most amperometric CO sensors. The origin of such current is ambiguous. In NAFION-based sensors it was attributed to a drift in protons in the polymer film originating from water reduction at the working electrode.[2] In PVA/H_3PO_4-based sensors the current was attributed to the possible oxidation of H_2O_2 and other species in the polymer film. [3] In the case of EF1 sensor, it is more possible to attribute it to water reduction as it was stated in the beginning of this section that the sensor showed no response and background current when dry. Figure (4.7) shows the t_{90} of the sensor at 100 % as a function of CO concentration. It can be observed that the time became shorter as the concentration was increased.

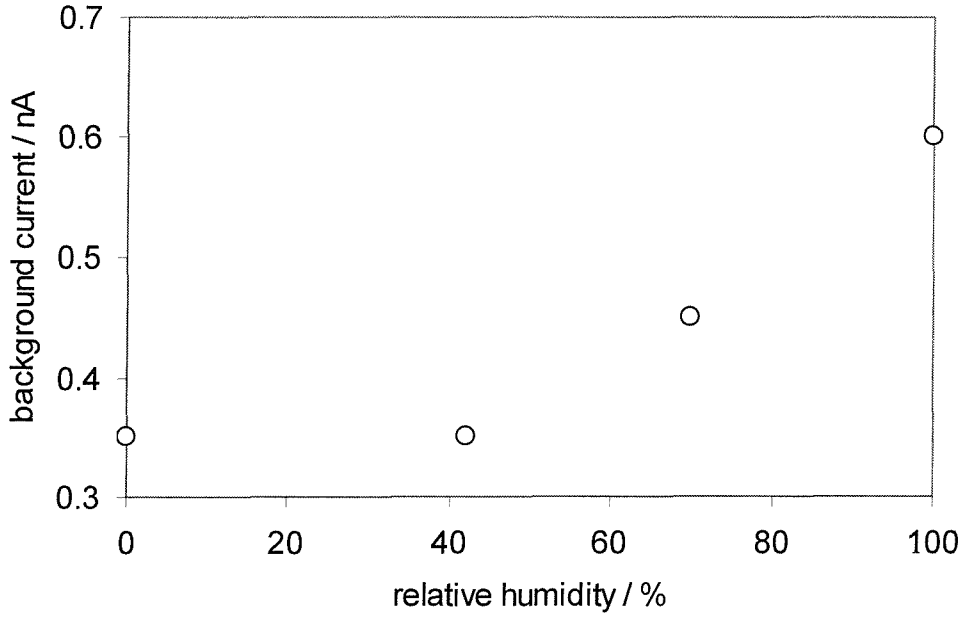

Figure (4.6) Background current as a function of gas humidity.

Figure (4.8) shows a plot of the logarithm of sensitivity, defined as the slope of the current-CO concentration curve, of the sensors as a function of logarithm of relative humidity. Altough it would not be appropriate to conclude an order of the reaction from the plot. It may be said that the evidence here points to an effective order much less than the values close to one as found for Nafion-based sensors where the slope varied between 1 and 2.[4]

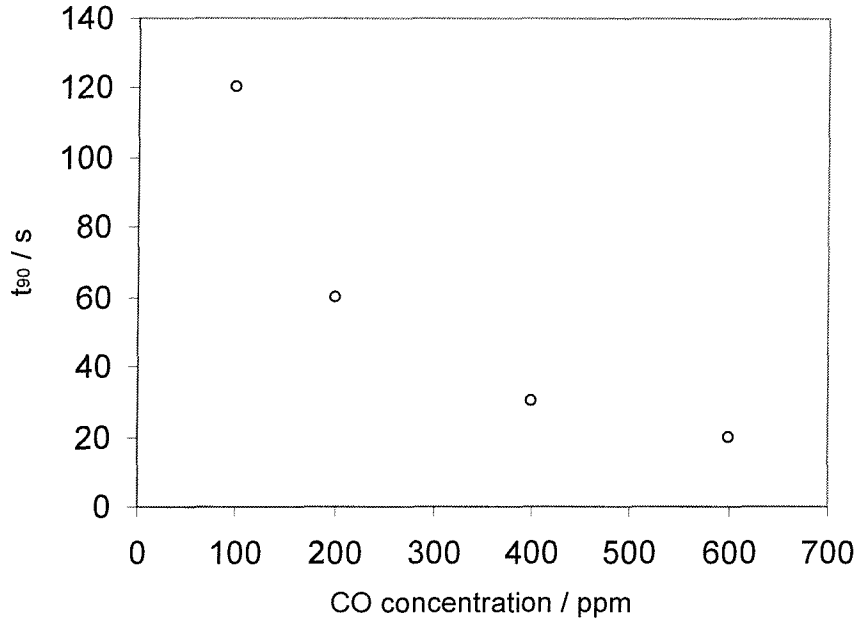

Figure (4.7) Plot of the decrease in t_{90} as a function of CO concentration.

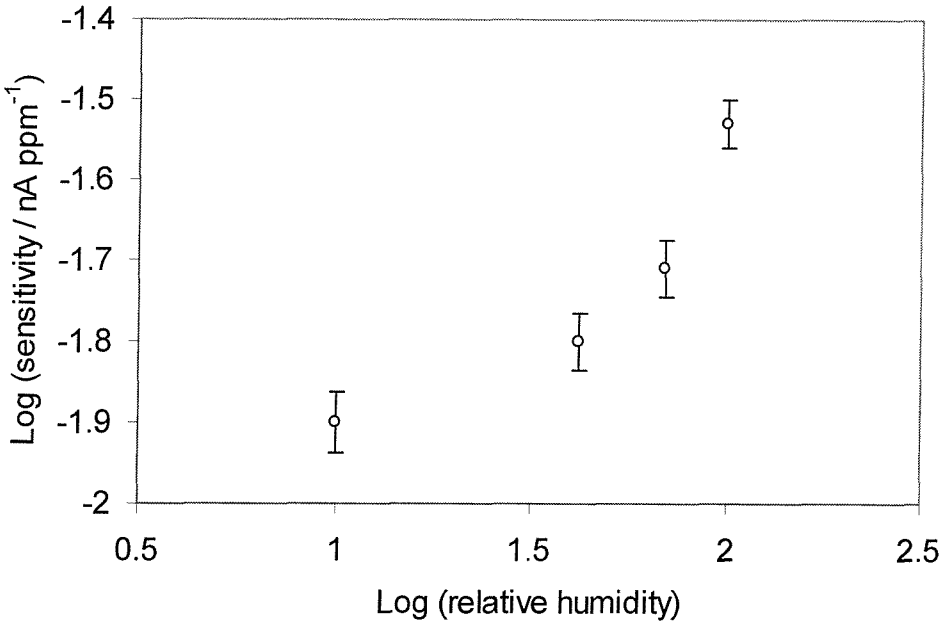

Figure (4.8) Log of the sensitivity of the sensor with the Log of the relative humidity.

The sensor showed a common feature at all relative humidities, there was always a lag time between the moment CO set to be injected to the sensor by the computer and the first response. This lag time was nearly one minute at low CO concentrations, became shorter to few seconds at higher concentrations. This can be ascribed to the longer time required, at low concentrations, for CO to make a

maximum coverage. This can also be explained by the need to increase the density of CO_{ads}/OH_{ads} neighboring sites. [5,6]

4.1.1 Reproducibility of the sensor:

During the fabrication of the sensor many processes are involved which might have contributed to the variation in the current values from the three sensors used. Most important of all was the casting of the polymer film on top of the electrodes, which would have given a variation in the film thickness as well as to a contact resistance due to the difference in the adherence of the film to the electrodes from a sensor to another. Another source of error might have been sensor environment. A lot of effort was made to keep similar operating conditions for sensors.

4.2 Electrochemical investigation of a Pt electrode in the IMI/PC liquid:

The purpose of this set of experiments is to understand the behavior of the Pt electrode in IMI:PC solution using a three-electrode-cell using standard calomel electrode as a reference electrode, a Platinum gauze as a counter electrode, a 0.05 mm diameter Pt electrode as a working electrode. Figure (4.9) shows the response of the Pt electrode in 1 M sulphuric acid. The CV showed typically two regions of hydrogen adsorption/desorption and oxide formation/stripping peaks.[7] The hydrogen adsorption region has two peaks; the first peak appears at the most positive potential (-0.15 V) which is assigned to strongly adsorbed hydrogen atoms on Pt surface the second peak at –0.4 V is related to weakly adsorbed protons. On the reverse scan the desorption peaks are slightly shifted to a more negative potentials (-0.16 and –0.6 V).

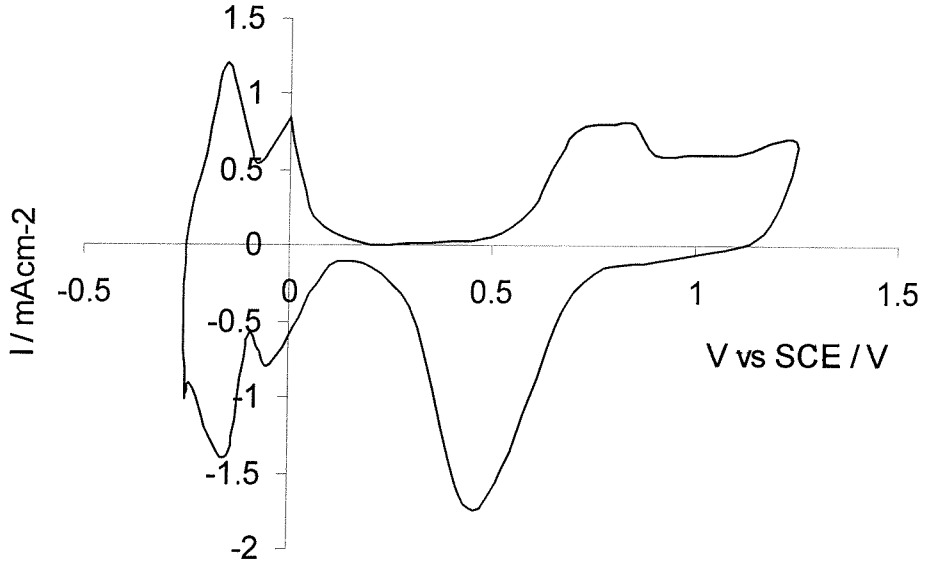

Figure (4.9) Cyclic voltammetry of a 0.5 mm Pt electrode with a Pt gauze counter electrode in 1 M sulphuric acid at a sweep rate of 200 mV/s.

The same electrode was polished and then loaded into the cell but this time using 0.2M IMI:PC as an electrolyte and the CV is shown in figure (4.10). The CV showed a different behaviour to the sulphuric acid solution. It showed a broad peak at –0.4 and a similar one in the reverse scan at –0.9. The first could be attributed to the proton or imidazolium ion adsorption on the surface of the electrode unlike the case in Pt/sulphuric acid, the peaks are not split. It can be noticed that the peaks corresponding to the oxide formation /stripping did not appear and this obviously is due to the absence of water in the system. To investigate the latter, the cell was exposed to air at approximately 50 % humidity for half an hour and cycled again. The obtained CV is shown in figure (4.11), and interestingly, the oxide formation/stripping peaks have re-appeared. This behavior has not been investigated

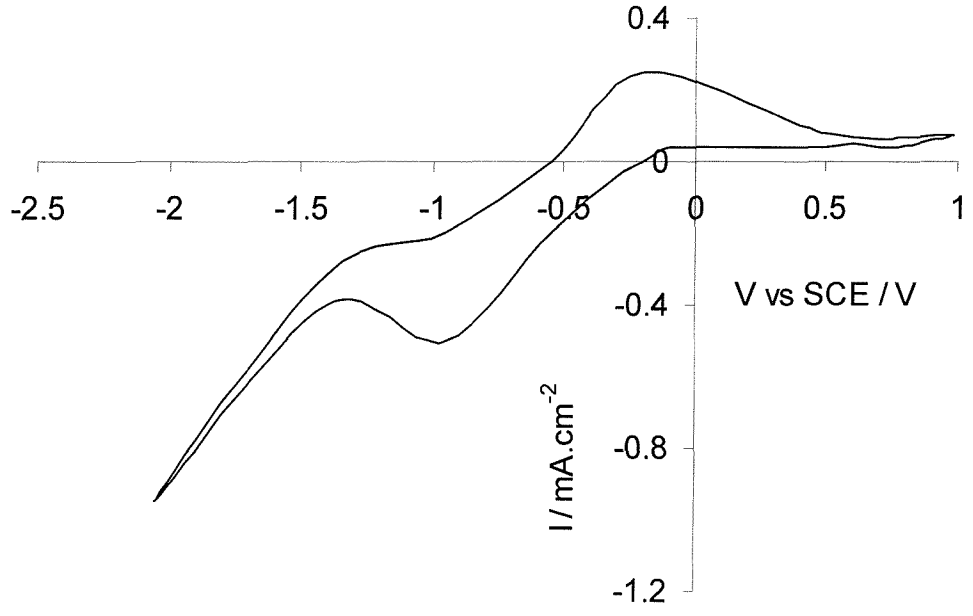

Figure (4.10) Cyclic voltammetry of a 0.5 mm Pt electrode with a Pt gauze counter electrode in 0.2 M IMI/PC solution at 200 mV/s.

further.

This experiment demonstrates the ability of the non-aqueous electrolyte to support the oxidation of platinum in the presence of a small amount of water introduced from the ambient air. This is a crucial step in the work of the overall sensor. [7] Therefore the experiment explains the earlier results obtained in the sensor in the previous section.

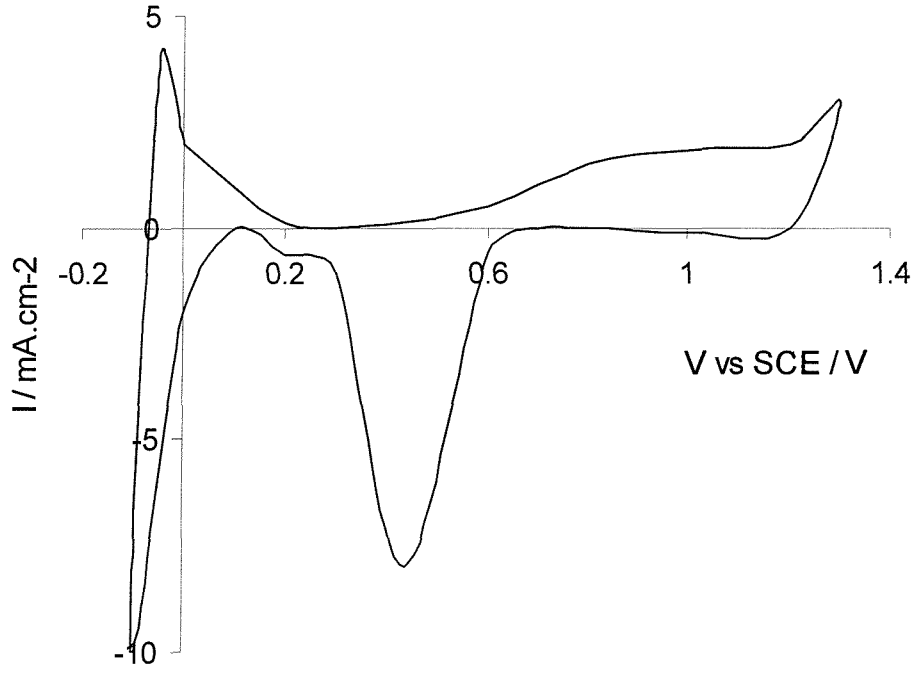

Figure (4.11) Cyclic voltammetry of the same cell as in figure (4.10). This time with the cell exposed to ambient conditions.

References

1 A. Yasuda, K.Doi, N. Yamago, T. Fujioka and S. Kusanogi, , *J. Electrchem. Soc.*, **139(11)** (1992) 3224.

2 S. Lee, A. Cocco, D. Keyvani and G. Maclay, *J. Electrchem. Soc.*, **142(1)** (1995) 157.

3 L. Lemoine, Department Of Chemistry, University Of Southampton, MPhil thesis, **1997**, P. 54.

4 Ref 3, P. 57.

5 R. Bellows, E. Marucchi-Soos and T. Buckley, *Ind. Eng. Chem. Res.*, **35** (1996) 1235.

6 M. Koper, A. Jansen, A. Santen, J Lukkien and P. Hilbers, *J. Chem. Phys.*, **109 (14)** (1998) 6051

7 Southampton Electrochemistry Group, "*Instrumental methods in electrochemistry*", John Wiley and Sons, 1985, P 234.

Chapter Five

Results and discussion
Development of a gap cell technique for conductivity measurements of polymer electrolytes

5.1 Measurements of the dimensions of GC 160 and GC 161 gap cells

The dimensions of the two cell designs GC 161 and GC 160 have been measured using the optical microscope and confirmed by SEM. The results are shown in table (5.1)

Table (5.1): measurements of the dimensions of the gap cell. Numbers are quoted in microns with a 95% confidence limit. Where b and d are the length and the width of the electrodes respectively, and w is the gap width between the two electrodes.

b	578.9 ± 1.3
d	197.2 ± 0.5
w	
200	198.3 ± 1.5
100	101.1 ± 0.6
50	50.6 ± 0.6
20	21.5 ± 0.6
10	11.8 ± 0.2
5	7.4 ± 0.4

It is observed that the small gaps have higher error in their fabrication as compared with the larger ones. All calculations were made using the experimentally determined dimensions but for simplicity the manufacturer's dimensions [1] will be quoted throughout the chapter.

5.2 Cyclic Voltammetry of GC 160 and GC 161 cells in sulphuric acid

Cyclic voltammetry, CV, was used to check the quality of fabrication and the lifetime of the cells.

Figure (5.1) shows CVs for 50 and 5 μm gaps of a GC 160 cell in 1 M sulphuric acid before and after use (see next paragraph). Figure (5.2) shows similar CV characteristics for a GC 161 cell. All CVs show a typical CV of Pt in sulphuric acid. It shows the two distinct regions of adsorbed and desorbed hydrogen peaks. The first region appears at the positive potentials, which is assigned to strongly adsorbed hydrogen atoms on Pt surface. The second one is for the weakly adsorbed protons. When going higher in the positive potential oxide formation and oxide stripping are observed.[2] The fact that no extra peaks has been observed indicates that after the fabrication there were no impurities left on the surface of the electrodes.

To obtain some knowledge about the recyclability of the cells, a CV was run on a GC 161 cell after it had been used with a polymer and washed with a solvent. The C.V showed a decrease in the peak currents. However their shape and position have not been affected. As for the GC 160 cells, a similar effect was observed but in this case there was a less profound decrease in the peak currents.

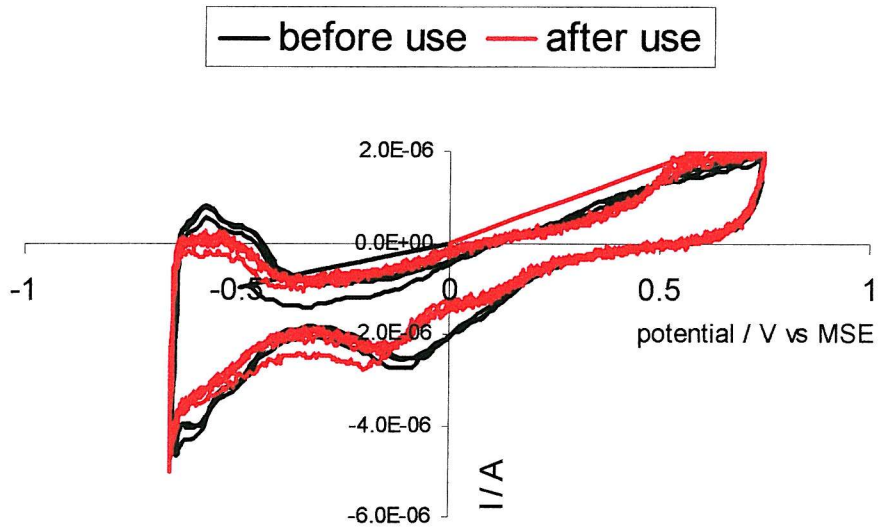

Figure (5.1 A) Cyclic voltammograms of a 50 μm gap of a GC 161 cell in 1 M sulphuric acid. The scan rate was 50 mV/s. The CV in red is for the cell after it had been used with a polymer and washed with a solvent.

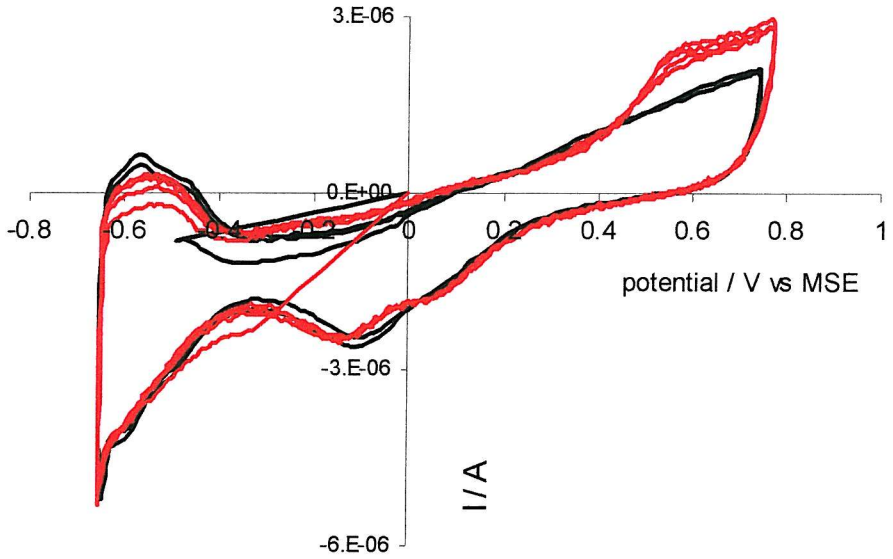

Figure (5.1 B) Cyclic voltammograms of a 5 μm gap of a GC 161 cell in 1 M sulphuric acid. The scan rate was 50 mV/s. The CV in red is for the cell after it had been used with a polymer and washed with a solvent.

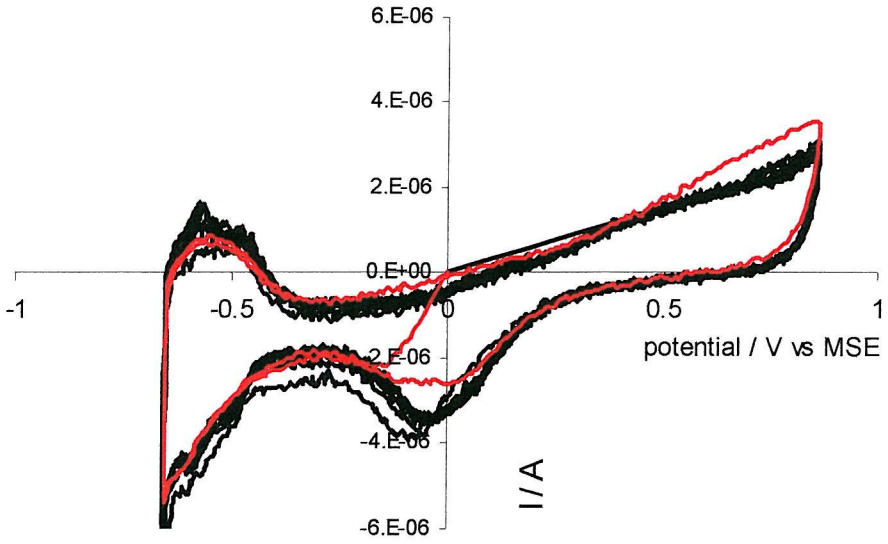

Figure (5.2 A) Cyclic voltammograms of a 50 μm gap of a GC 161 cell in 1 M sulphuric acid. The scan rate was 50 mV/s. The CV in red is for the cell after it had been used with a polymer and washed with a solvent.

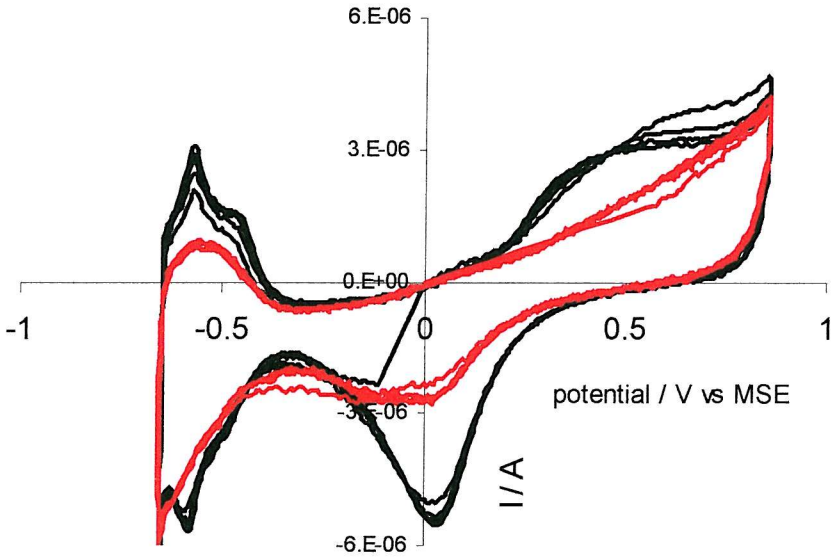

Figure (5.2 B) Cyclic voltammograms of a 5 μm gap of a GC 161 cell in 1 M sulphuric acid. The scan rate was 50 mV/s. The CV in red is for the cell after it had been used with a polymer and washed with a solvent.

5.3 A Gap cell using a 0.1 M KCl solution

Complex impedance diagrams of a GC 160 device, in a 0.1 M KCl solution, on all gaps sizes have been obtained. A similar behavior has been seen for all the gaps and figure (5.3) shows a typical plot for the case for a 200 μm gap. The plot showed a semi-circle at the high frequency range corresponds to the bulk electrolyte response, *i.e.*, R_bC_b in the equivalent circuit, (see chapter 1).[3]

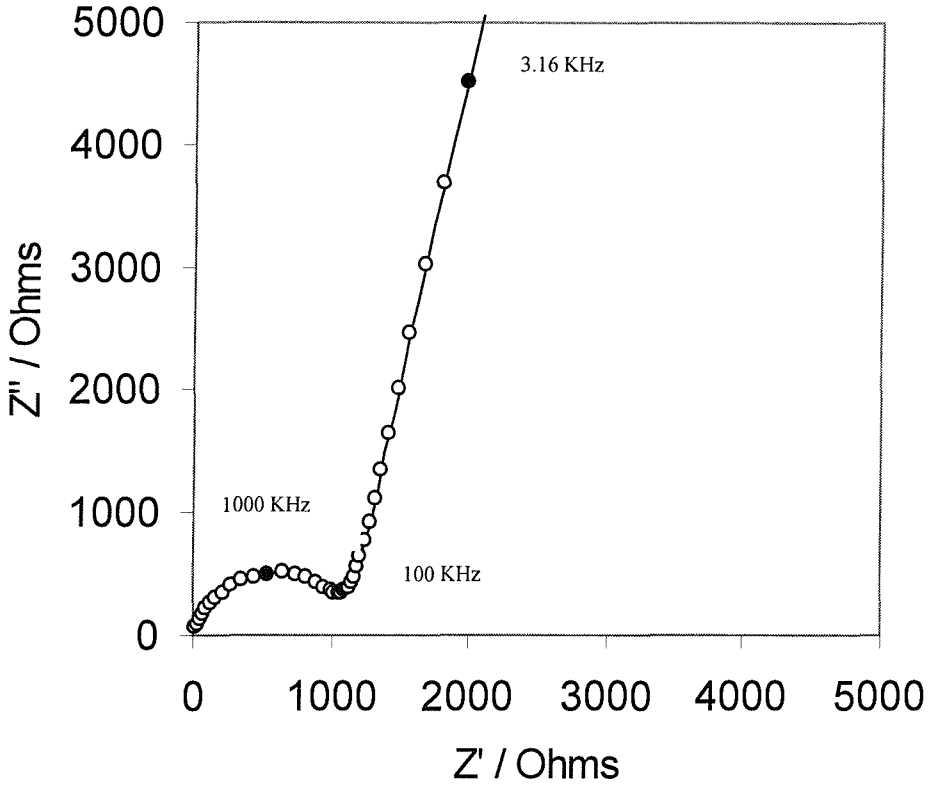

Figure (5.3): A typical example of a complex impedance plots observed on all the gap sizes. The plot is for a 200 μm gap in a GC 160 cell in 0.1 M KCl solution. The frequency values correspond to the black circles.

5.3.1 Measurement of the resistance:

$R_{b,,}$ which is in this case the KCl solution resistance, was obtained by extrapolating the low frequency end of the semi-circle. However since the semi-circle looked slightly depressed, which introduced a slight error in the values of R_b, an extrapolation of the spike was performed. Table (5.2) shows values of R_{bc}, obtained from the extrapolation the semicircle and R_{bl} obtained from the extrapolation of the spike.

Table 5.2: Resistance values from the extrapolation of the complex impedance plot for 0.1 M KCl solution.

w / μm	R_{bc} / Ω	R_{bl} / Ω
5	800	650
10	850	700
20	900	750
50	1000	850
100	1200	950
200	1250	1100

Figure (5.4) shows a bode plot for the 200 μm gap. In the plot a plateau, which is taken to be due to the solution resistance, is noticed in the frequency range 4.5-5.8 log (Hz), below and above which the cell showed a capacitve behavior.

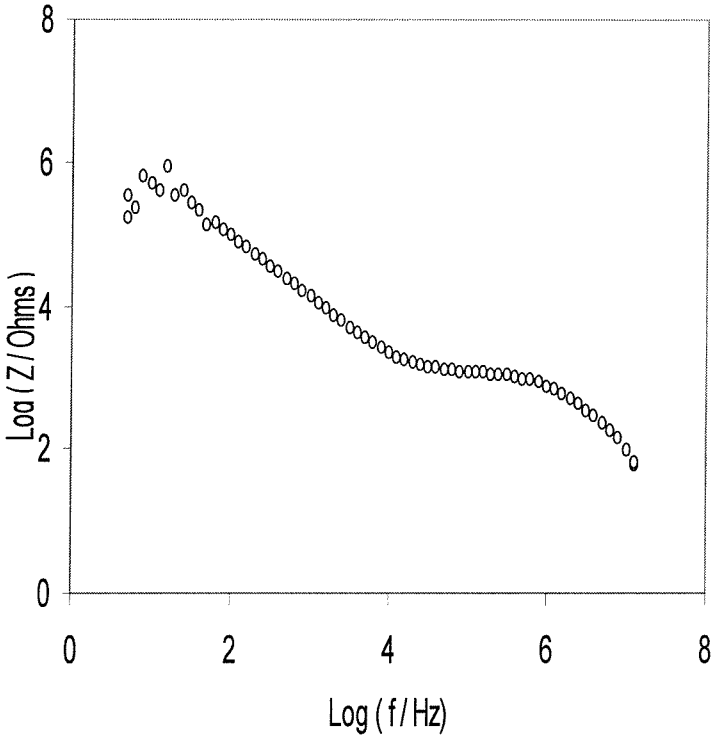

Figure (5.4): Plot of the modulus of the impedance against frequency for a 200 μm.

Figure (5.5) shows a plot of the logarithm of each of the individual components of the impedance, *i.e.*, Z', Z'', against the logarithm of the frequency

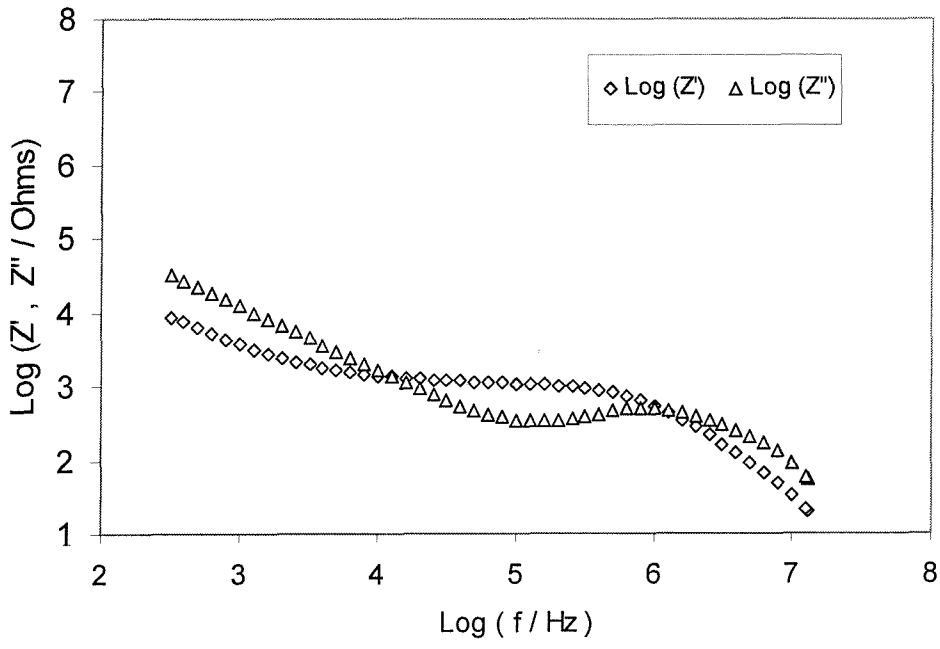

Figure (5.5): Plot of log (Z') and log (-Z'') against log (frequency) for the data in figure (5.4).

5.3.2 Cell constant calculations

The Cell constant of the cell, K, was calculated for each gap width using $K = \sigma_{KCl} \times R_b$, where σ_{KCl} is the conductivity of the 0.1 M KCl solution at 25 °C (2.9×10^{-2} S/cm). Using the R_b values stated in table (5.1) the calculated cell constants are shown in table (5.3).

Table (5.3): Calculated cell constants as a function of gap width.

w / μm	K using R_{bc} / cm^{-1}	K using R_{bl} / cm^{-1}
5	10.32	8.38
10	10.96	9.03
20	11.61	9.67
50	12.90	10.96
100	15.48	12.25
200	16.12	14.19

The cells represent a case of coplanar electrodes (see chapter 1). Therefore equation (36) was used to calculate the theoretical cell constant. [4] All details of the calculations of the integrals involved are stated in Appendix 1. The theoretical cell constant was calculated using a value of 1 cm for the thickness to simulate the real case.

It is observed from the graph that the simulation and the experimental results have the same shape but the experimental values were lower. The calculated K values using R_{bc} gave closer results to the simulated values at low gap widths. One possibility for the observed decrease in the resistance at high gap widths might be due to the presence of other metallic tracks in the region of the electric field.

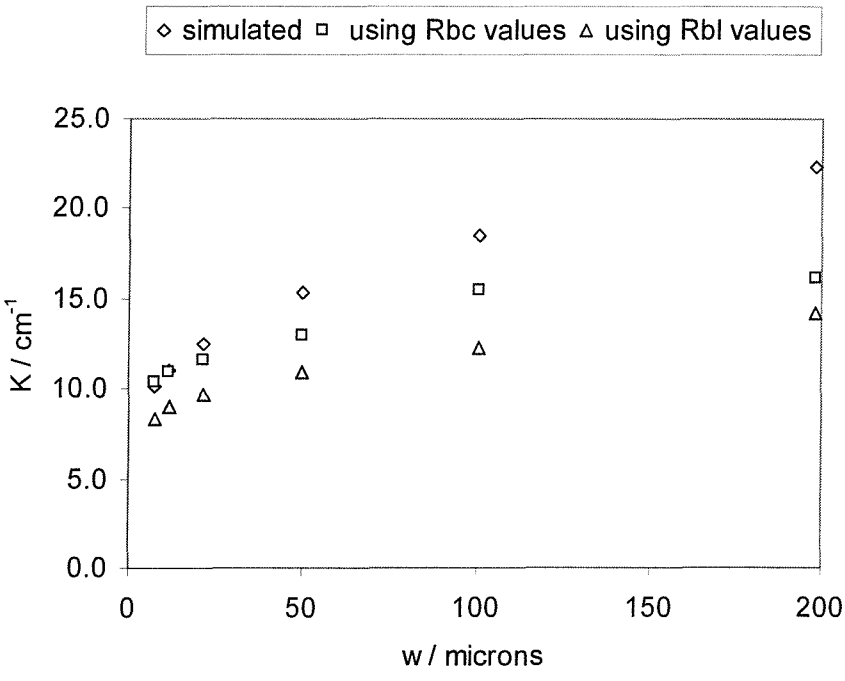

Figure (5.6): Simulated and experimental values of the cell constant versus the gap width.

5.4 Gap cells using Polymer electrolytes

5.4.1 Simulation Results

Figure (5.7) shows a plot of the simulated values of the cell constant, K_{sim}, as a function of gap width for many film thicknesses. It can be observed from the graph that there are two regimes, one is when the gap width is the same order of magnitude as the film thickness, then the cell constant values varies approximately linearly with gap width as expected from increasing the length of the current path. The extrapolation to zero gap width gives a positive intercept, which probably corresponds to the spreading resistance from the inner paths of the electrodes.

In the case where the gap width is much less than the film thickness the above assumption breaks down and the line becomes curved in order to approach the origin as required to produce zero resistance at zero gap width.

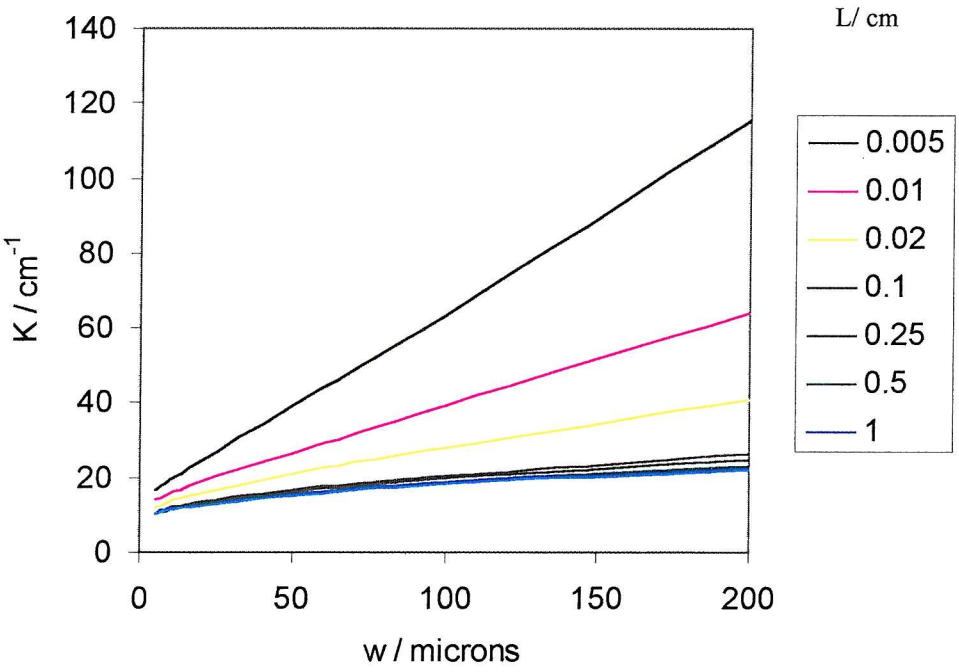

Figure (5.7) Plot of the simulated cell constant, K_{sim}, against the gap width for many polymer film thicknesses. The film thicknesses shown in the legend are in centimeters. b and d were 578.9 and 197.2 μm, respectively.

In a normalized plot, figure (5.8), which is a plot of the ratio of the resistance of one gap to the largest gap against the gap width, the transition from the linear behavior to the curve behavior was more emphatic. This is because comparisons can be made over the whole range of gap widths.

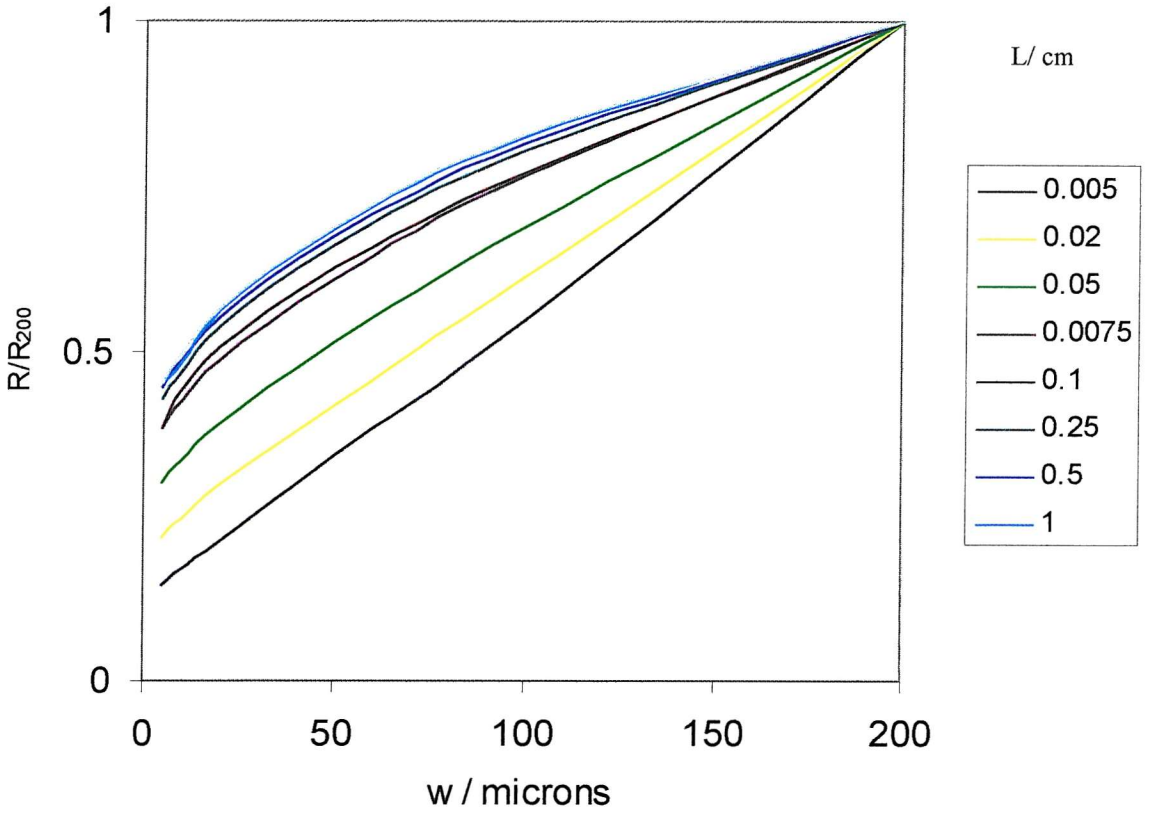

Figure (5.8) Plot of the normalized resistance against the gap width for many film thicknesses. The film thicknesses shown in the legend are in centimetres. b and d were 578.9 and 197.2 μm, respectively.

When the film thickness was much less than the gap width a linear behavior is observed, whereas the curvature begins to change as soon as the film thickness becomes significantly larger than the gap size.

5.4.2 Experimental results

Three types of ionically conducting polymers were used to check the validity of the gap technique. Two of which, PEE:IMI, and 60% (1.2 M IMI/PC):PVdF-HFP, were investigated in chapter three and their conductivities were obtained using the cylindrical cell. The third polymer was NAFION, which has been chosen because of its well-reported conductivities.

5.4.1 PEE:IMI and 60% (1.2 M IMI/PC):PVdF-HFP polymers results

Complex impedance plots were first obtained for the polymers on a GC 160 cell, figure (5.9). It is observed from the plot that the semi-circle is not complete and any extrapolation would lead to high errors in the value of the resistance. Therefore admittance plots were obtained instead, as the semi-circle transforms to a spike which is much easier and more explicit to extrapolate than the semi-circle.

AC admittance measurements were performed on all of the gaps for the two polymers. All gaps have shown a general behavior and figure (5.10) shows an admittance plot for a 5 μm gap. The graphs were fitted in order to find the conductance value from the extrapolation of the spike for each gap.

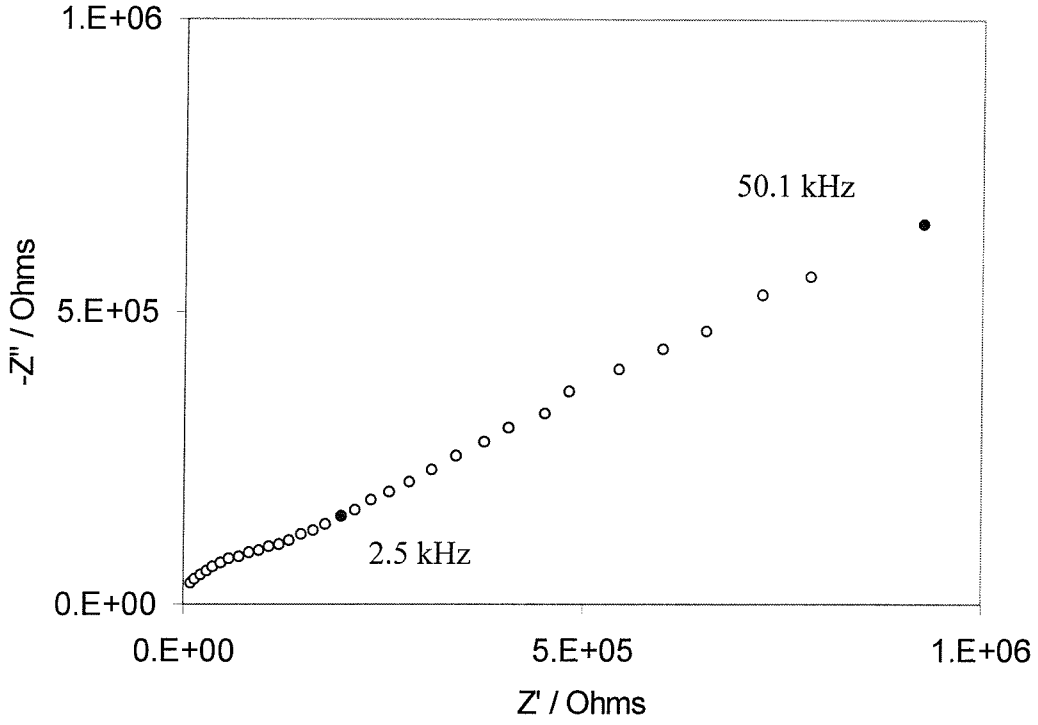

Figure (5.9) A complex impedance plot of 60% IMI/PEE on a GC 161 device for a 5 μm gap.

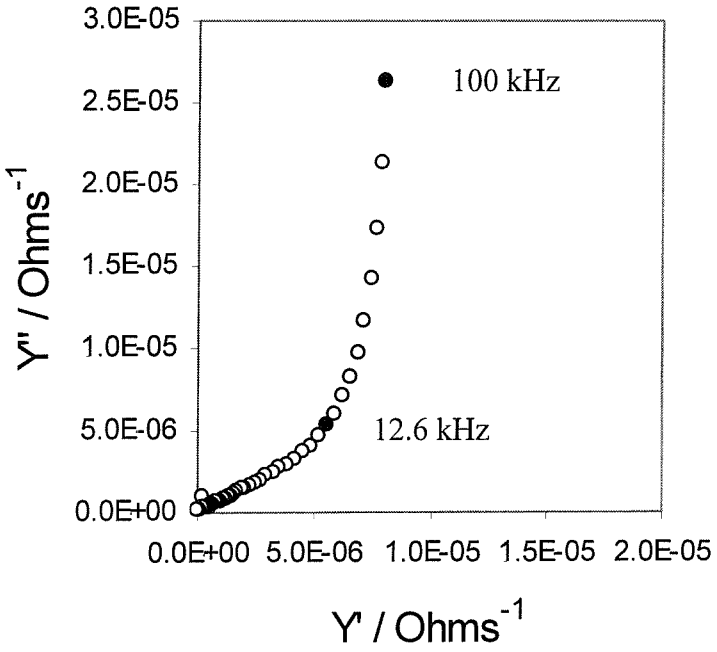

Figure (5.10) A complex admittance plot for a 60% IMI/PEE on a GC 161 device for a 5 μm gap.

5.4.2 Nafion:

Measurements have been performed in this experiment to demonstrate the change in the conductance as a function of the film thickness. This has been achieved for all the gaps by building up the film in five stages as described in chapter two.

Admittance diagrams were obtained after each stage of polymer casting. Figures (5.11) and (5.12) show the results for a few gaps to show that all the results fall

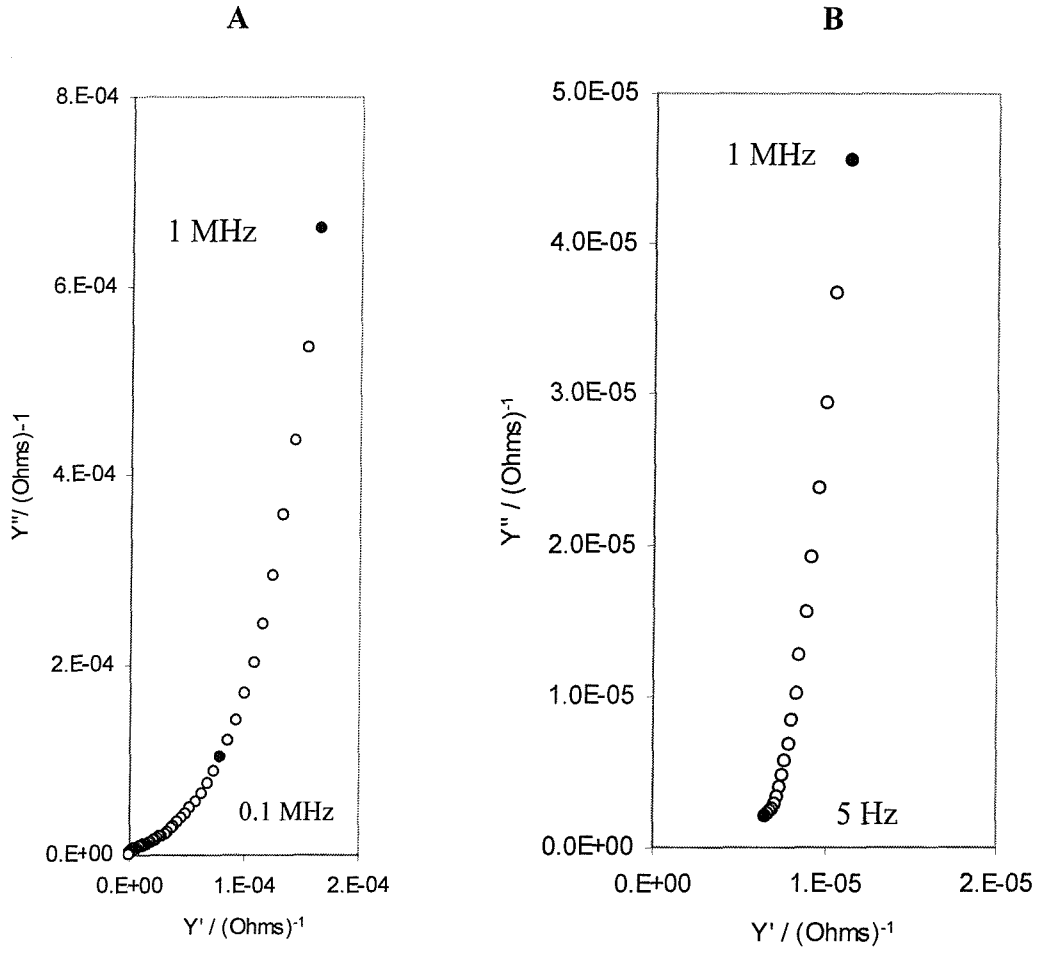

Figure (5.11): Complex admittance plots for a NAFION film on a GC160 device at stage two. On a 5 μm gap (A), and a 200 μm (B).

approximately into the general pattern shown in Figure (5.13). The same general behavior is obtained.

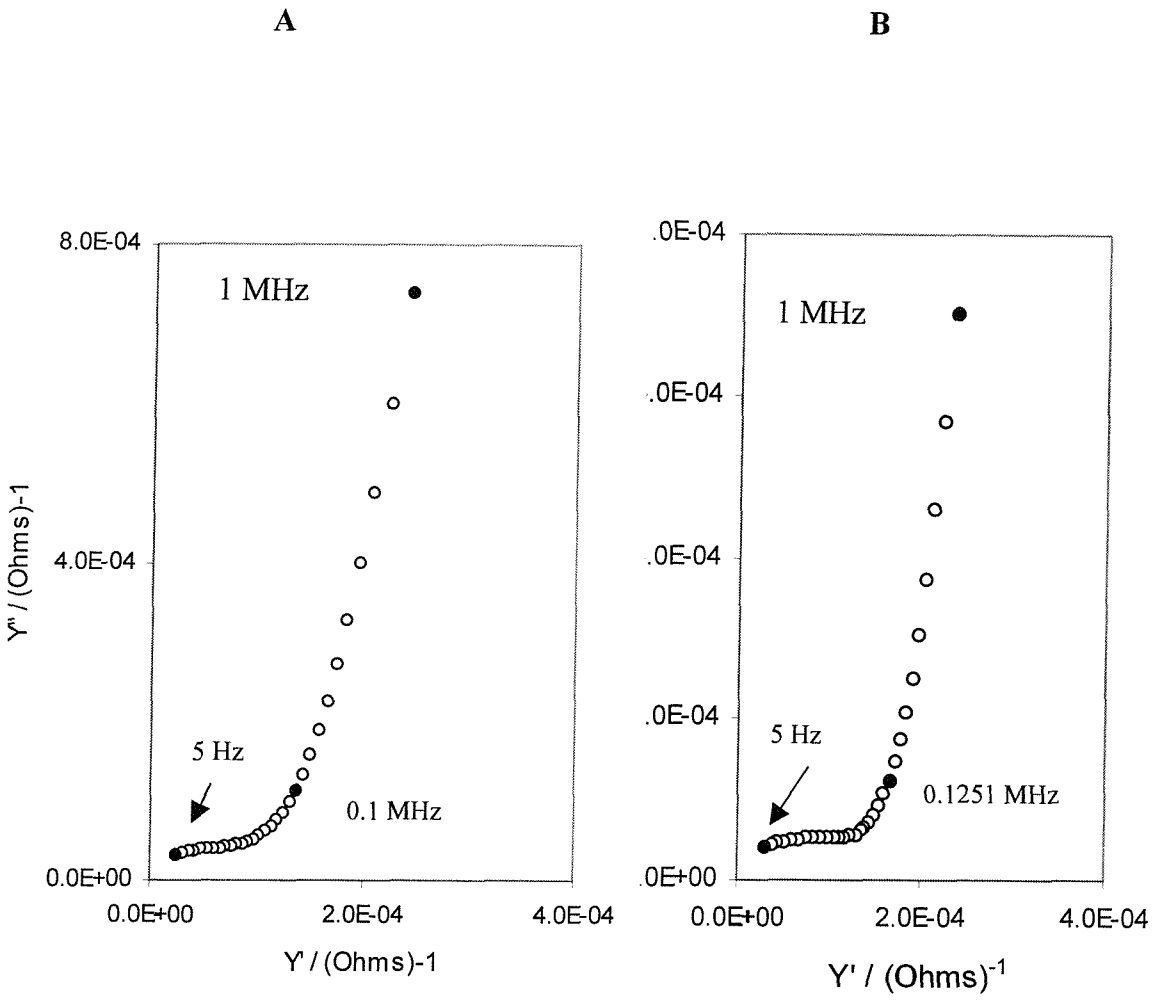

Figure (12): Complex admittance plots for a NAFION film on a GC160 device at stage four on a 50 μm gap (A), and a 200 μm (B).

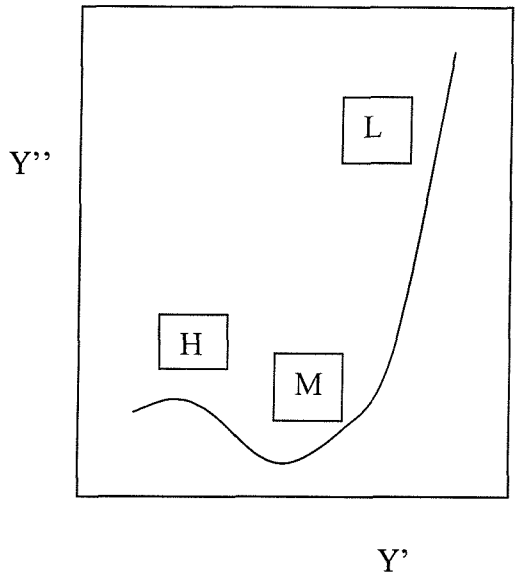

Figure (5.13) A schematic diagram showing a general complex admittance plot for the NAFION experiment.

The results fall into three frequency regions as follows

1. Low frequency (L)

Here a resistance is observed as evaluated by the Schwartz Kristoffel transformation placed in parallel with the dielectric capacitance and the instrumental capacitance, showing a straight line.

2. Medium frequency (M)

Here a Warburg behavior is observed as suggested by the finite element analysis.

3. High frequency (H)

This is represented by a semicircle through the origin.

Two types of analysis may be made. The high frequency G which can be obtained by extrapolation of the vertical admittance spur. Alternatively, the medium and low frequency portions may be analysed by fitting to the finite element analysis. Only the former has been done

5.4.5 Calculation of the conductivity

After obtaining the G values for each gap width, two approaches were used in order to find a value for the conductivity.

1- The normalization method

Herein the G values were converted to R/R_{200}, by dividing the resistance of each gap by the resistance of the largest gap (200 μm). After that the obtained (R/R_{200} vs w) set of values for each polymer were matched to the simulated curve.

Then a value for the film thickness was obtained from the best match as can be seen in figure (5.14) The K_{sim} values at that film thickness were used to calculate the conductivity,

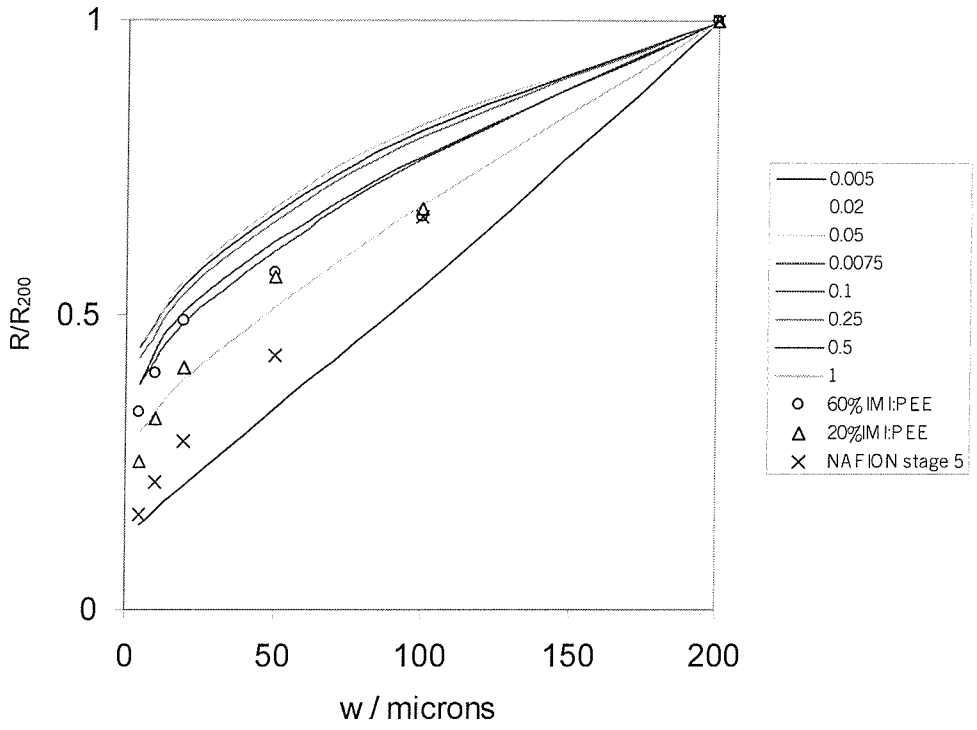

Figure (5.14) Plot of R/R_{200} vs the gap width showing the fitting as well as some experimental results.

where $\sigma = K_s * G$.

Two observations can be made regarding the normalization method:

A-The effective thickness sensed by the gap, i.e., the obtained value from the fit in the (R/R_{200} vs w) plot, are larger than the thickness measured by SEM as can be seen in table (5.4)

Table (5.4) The film thickness of the polymers as obtained from the fitting and SEM.

Polymer	Thickness from the fit / cm	Thickness from the SEM / cm
20% PEE:IMI	0.01	0.002
60 % PEE:IMI	0.05	0.003
60% (1.2 M IMI/PC):PVdF-HFP	0.075	0.005
NAFION	0.02	0.001 for each stage

A possible reason why the two do not agree is that the film has decreased in the SEM due to the evaporation of the liquid content of the films at the very high vacuum applied in the SEM chamber.

B- The calculated conductivity values were not consistent over the whole range of the gap widths. This is a more serious problem with the method.

2- The iteration method

This method is similar to the normalization method but here the obtained film thickness from matching the experimental results in the (R/R_{200} vs w) plot was iterated until the conductivity values were consistent over the whole range of the gap widths. Figure (5.15) shows an example for the case of the 20% PEE:IMI.

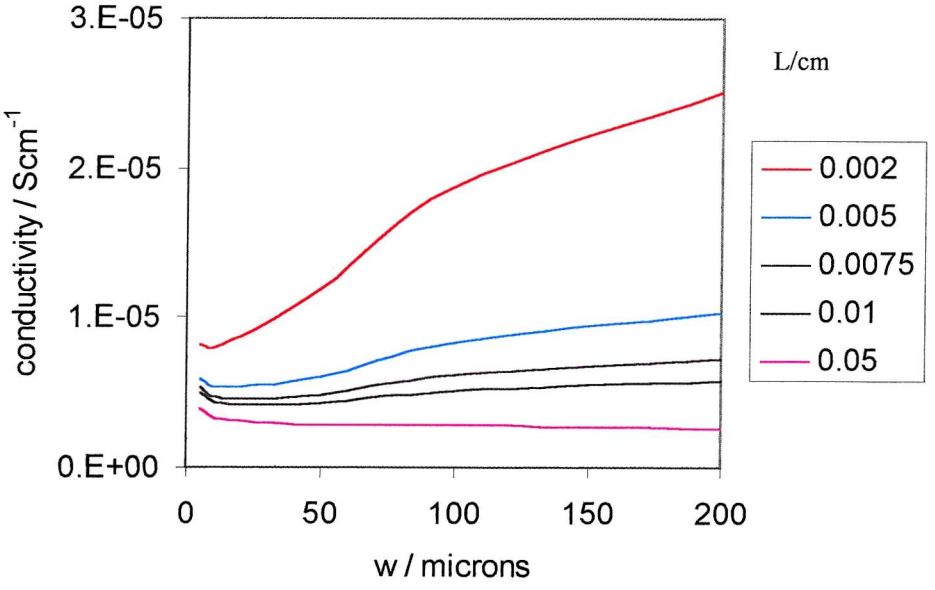

Figure (5.15): A plot of conductivity versus the gap width for the 20% PEE:IMI polymer at many film thicknesses (in centimeters).

The obtained conductivity values of all the polymers are shown in table (5.5)

Table (5.5) Comparison of the conductivity obtained from the gap electrode method and the cylindrical method.

Polymer	Conductivity from the cylindrical method / Scm^{-1}	Conductivity from the gap electrode method / Scm^{-1}	The film thickness at which K_{sim} was used / cm
20% PEE:IMI	$1.4x10^{-6}$	$5.2x10^{-6}$	0.05
60 % PEE:IMI	$4.2x10^{-5}$	$5.5x10^{-5}$	0.1
60% (1.2 M IMI/PC):PVdF-HFP	$3.0x10^{-4}$	$1.5x10^{-4}$	0.1
NAFION [5] stage 1	$1.0x10^{-2}$	$1.6x10^{-3}$	0.02
NAFION stage 2		$1.4x10^{-3}$	0.01
NAFION stage 3		-	-
NAFION stage 4		-	-
NAFION stage 5		$5.1x10^{-3}$	0.02

It is observed from the table that the that gap electrode method gave acceptable conductivity values as compared to the cylindrical method. In the case of NAFION on increasing the film thickness from 0.001 to 0.002 cm (stage 1 to stage 2) the conductivity remained the same. This was not the case for the 0.005 cm thick film

which showed five times greater conductivity. Values for the conductivity could not be obtained for stages 3 and 4 because the experimental results could not be fitted into the normalized plot.

5.5 Simulation results from a finite element analysis

Theoretical modeling was performed by Prof. A. Fitt of the mathematics department. The problem was summarized as follows: a cuboid shaped polymer is placed symmetrically on top of two electrodes with a gap in between. A potential difference is applied on the polymer through the electrodes. The objective of the modelling is to determine the resistivity of the polymer. A commercial finite element PDE solver package, FASTFLO was used to numerically solve the problem.

The results of the analysis have verified the experimentally observed Warburg impedance. This approach opens a new method of interpretation, which unfortunately is outside the scope of this thesis and remains a topic of further work.

References:

1 Warwick centre for microelectronics, University of Warwick.

2 Southampton Electrochemistry Group, "*Instrumental methods in electrochemistry*", John Wiley and Sons, 1985, P 234.

3 P. G. Bruce in "Polymer electrolyte reviews 1", Ed. J. R. MacCallum and C. A. Vincent, Elsevier Applied Science, London, 1987, chapter 8 , P. 237.

4 J. Gardner, P. Bartlett and K. Pratt, *IEE proc. Circuits devices sys.*, **5** (1995) 321.

5 P. Alsebert, F. Novel-Cattin, M. Pincri, C. Doumain and R. Durand, *Solid State Ionics*, **35** (1989) 3.

Chapter Six

Summary and conclusions

A novel non-aqueous proton conducting ionic-liquid based on imidazole was prepared. It consisted of a 1:1 molar ratio of imidazole to imidazolium (bistrifluoromethanesulphonyl) imide salt. This liquid was used to prepare proton conducting polymeric gel films. Many polymeric hosts have been investigated to make films. Firstly, PVdF and PVdF-HFP were used. Direct addition of the IMI liquid to either of the two gave phase-segregated films. Hence, PC was incorporated into the system to help solubilise the IMI in the polymeric matrix. A three-component-composition diagram was constructed to optimise the ratio of the three in order to give a homogeneous, free-standing and highly conducting films. The conductivity of the IMI:PC liqiuds were also measured to find the highest conductivity of the IMI:PC solution. The 1.2 M solution was found to have one of the highest conductivities and thus has been used to make films with PVdF-HFP. The conductivity of films was found to be dependant on the amount of added 1.2 M IMI:PC liquid. The Log (conductivity)-composition plot showed a linear relationship similar to ionic liqiud-polymer and salt-solvent-polymer systems but with a break point at 40% liquid content. The film with the highest content showed a room temperature conductivity of $6x10^{-4}$ S/cm.

Thermal and X-ray studies were performed on many of the films. DSC experiments on the films have shown a melting peak of PVdF-HFP but no glass transition nor the formation of other hybrid films as confirmed by the IR spectra. The thermal stability of the films was checked by TGA which showed that the films are stable up to 130 °C.

XRD experiments showed that the films have a similar pattern to that of the PVdF-HFP.

Secondly, PEE was used as a polymeric host. It was compatible with IMI and polymer films were obtained. DSC curves showed a glass transition with Tg values decreasing with increasing IMI content in the films. Moreover, the system did not show any melting peaks. The films were thermally stable up to 170 °C as observed by TGA. Ionic conductivity of the films was measured as a function of IMI content. The conductivity had shown a similar logarithmic dependence as in the (1.2 M IMI:PC):PVdF-HFP films. The film with the highest IMI content showed a room temperature conductivity of $4x10^{-5}$ S/cm.

Finally, a polymer blend of PVdF-HFP and PMMA was used. Films of the two polymers and IMI were prepared and their conductivity was investigated as a function of IMI content. The conductivity showed a logarithmic dependence. The high room temperature conductivity of $2.8x10^{-3}$ S/cm was obtained for the highest IMI content film. The films showed a higher thermal stability up to 280 °C as observed by TGA.

A planar amperometric CO sensor was fabricated using a IMI:PC:PVdF-HFP film as the solid polymer electrolyte. The sensor showed no response without being pre-equilibrated with water. The sensor response was linear in CO concentration and t_{90} was found to decrease with increasing CO concentration. The response was also found to be dependent on the relative humidity. The dependence in this case is less than the reported values in the literature.

To understand more about the mechanism of CO oxidation on Pt. CVs were taken for a Pt electrode in IMI:PC and sulphuric acid solutions. The absence of metal oxidation reaction confirmed that the surface adsorbed OH_{ads} species required for the CO oxidation was not present at low humidity.

A novel gap electrode technique was investigated as an alternative to the traditional method of measuring the conductivity of polymer electrolytes. The devices were characterized experimentally using 0.1 M KCl solution for the calculation of cell constants. The technique was also used for many polymers such as NAFION, PEE:IMI and IMI:PC:PVdF-HFP.

The technique was intended to remove the uncertainty in the polymer thickness from the conductivity calculations. The principle of the method was that the polymer thickness could be calculated from the variation in resistance with gap width. However, the results showed that uncontrollable variations in either the polymer conductivity, the geometry, or both made it difficult to fit the experimental values systematically to the theoretical model. Under these circumstances the gap electrode technique, as originally specified, failed to give consistent results. Nevertheless, acceptable conductivity values were obtained for the polymers by an iteration method, and the technique should still be applicable given better control of polymer uniformity and thickness.

Appendix 1

Equations (35) and (36) involves the determination of two integrals A* and F, where F is the integral in equation (36) which becomes G=(σ b/2A*L)*F. Excel program was recorded to numerically solve the integrals. The geometrical modulus, M, in equations 35 and 36 was calculated using equation 34 and the results are shown below in table (A.1).

Table (A.1): The geometrical modulus of all the gaps

w /microns	M
7.4	$1.8x10^{-2}$
11.8	$2.9x10^{-2}$
21.5	$5.2x10^{-2}$
50	$11.3x10^{-2}$
101	$20.4x10^{-2}$
198	$33.4x10^{-2}$

The calculated values of A* are shown in the table (A.2) below:

Table (A.2): Calculated values of A* for each gap width.

w/microns	A*
7.4	4245
11.8	2662
21.5	1462
50	630
101	314
198	163

These values of A* allow for the calculation of the F integral which in turns was used to calculate the cell constant as a function of film thickness and gap width. To simulate the experimentally obtained results on KCl solutions, calculations were made using a 1 cm value for the film thickness.